

GIANNINI CONTROLS CORPORATION
Control/Nucleonics Division
Duarte, California

ER-80194

VENT QUALITY METER STUDY,

FINAL REPORT

VOLUME I

In Support of
Contract No. NAS8-11814

Prepared for

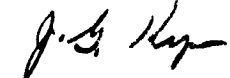
NATIONAL AERONAUTICS AND SPACE ADMINISTRATION
Marshall Space Flight Center
Huntsville, Alabama

W. J. McKinney, Contracting Officer
C. D. Arnett, Contracting Officer's Representative
Fluids Mechanics Section
Fluids Mechanic and Thermodynamics Branch
Propulsion Division
Propulsion and Vehicle Engineering Laboratory
Research Operation

7 December 1964

Giannini Controls Corporation

Prepared by:

J. G. Kyser
Project Engineer

Approved by:

D. E. Wright
Manager, Advance Systems
Control/Nucleonics Division

TABLE OF CONTENTS

	<u>Page</u>
1.0 INTRODUCTION	1
2.0 DENSITY DETERMINATION BY GAMMA SCATTER	3
2.1 Description of Scattering	3
2.2 Vent Quality Meter Analysis	9
3.0 DENSITY MEASUREMENT BY GAMMA RAY ABSORPTION	26
4.0 DENSITY MEASUREMENT BY NEUTRONS	39
4.1 Neutron Interactions with Matter	39
4.2 Thermalization of Fast Neutrons by Hydrogen	39
4.3 Shielding	41
4.4 Conclusion	41
5.0 DENSITY MEASUREMENT WITH BETA PARTICLES	42
5.1 Beta Absorption	42
5.2 Beta Scattering	48
6.0 CAPACITANCE MEASUREMENT METHOD	53
6.1 Matrix Capacitors	56
6.2 Description of Cryogenic Quality Meter	57
6.3 Advantages and Disadvantages of Matrix Capacitor	58
7.0 DENSITY MEASUREMENT BY SOUND VELOCITY	60
8.0 VIBRATION PADDLE SENSOR	61
9.0 OPTICAL ABSORPTION	63
9.1 Description of Method	63
10.0 DENSITY MEASUREMENT USING MICROWAVE TECHNIQUES	66

TABLE OF CONTENTS

	<u>Page</u>
<u>LIST OF FIGURES</u>	
Figure 2-1 Compton Scattering	4
Figure 2-2 Loss of Photon Energy in Compton Scattering	5
Figure 2-3 Compton Scattering Cross Section	6
Figure 2-3(b) Photon Energy Mev	
Figure 2-4 Compton Scattering	8
Figure 2-5 Solid Angle Subtended by Concentric Detector	11
Figure 2-6 Source-Detector Geometry	14
Figure 2-7 ρ from 0 to .1	19
Figure 2-8 ρ from 0 to .5	20
Figure 2-9 Count Rate Characteristic for Error Analysis of LH ₂	21
Figure 3-1a Mass Absorption Coefficients vs Energy	27
Figure 3-1b Dose Building Factor as a Function of Density and Energy	27
Figure 3-2 One Arrangement for γ -Ray Transmission Liquid Density Sensor	29
Figure 3-3 Geometry Used on Pipes less than 10 inches in Diameter to Maintain a Radiation Path Length of 10 Inches	30
Figure 3-4 Count Rate vs Density of Hydrogen for Hard and Soft γ Rays	31
Figure 3-5 Count Rate vs Density of Oxygen with and without Dose Buildup Factor for hard and soft γ Rays	32
Figure 3-6 Placement of Pulse Height Window Discriminator for "Viewing" Photopeak Energies Only	33
Figure 3-7 Possible Orientations of Elemental Mass Volume Illustrating Need for a Linear Relationship between Count Rate and Density	34

TABLE OF CONTENTS

	<u>Page</u>
<u>LIST OF FIGURES - Continued</u>	
Figure 3-8 Anticipated Count Rate vs Density of Oxygen with Window Discriminator Property Placed	36
Figure 3-9 Experimental γ -Photon Count Rate vs Simulated Oxygen Density for 10 inch Diameter Pipe	37
Figure 5-1 Beta Particle Spectrum for Radium E	43
Figure 5-2 Source-Detector Geometry Considered for Beta Absorption Technique	46
Figure 5-3 Source Detector Configuration for Beta Scatter	49
Figure 6-1 Illustration Showing Effect of Geometry on Capacitance Measurements	54
Figure 8-1 Vibrating Paddle Point Level Sensor	62
Figure 9-1 Optical Gas Line Absorption Method	65
<u>LIST OF TABLES</u>	
Table 1 Explanation of Symbols	22
Table 5.1-1 Sources of Beta Radiation Used for Density Measurement	45
<u>LIST OF APPENDICES</u>	
APPENDIX I Experimental Verification of Backscatter Calculations	I-1
Figure I-A Geometrical Nomenclature for Experimental Setup	I-2
Figure I-B 10-inch Diameter Comparison of Equation (12) with Experimental Data	I-5
APPENDIX II Standard Deviation of DC Output	II-1
APPENDIX III Conversion of Average Density to Quality	III-1

iv

TABLE OF CONTENTS

	<u>Page</u>
APPENDIX IV Preliminary Consideration of Wall Wetting problem	IV-1

1.0 INTRODUCTION

This is the Final Report under Contract No. NAS8-11814. The report presents the results of a study of ten techniques which seemed to have applicability to the problem of determining the relative amounts of liquid and vapor present in a two phase flow through pipes of from 1.0 to 10 inch diameter. It was concluded that only one of the methods could cover the full range of requirements.

The report is presented in three volumes.

In the subsequent sections of Volume I each of the methods studied is described in detail.

In Volume II, a comparison of all methods studied is carried out. From this comparison, it is seen that the technique of gamma ray absorption covers the full range of requirements. This method has several distinct advantages.

- (1) All components are external to the pipe.
- (2) All requirements can be met with identical hardware.
- (3) System is simple, reliable, and easy to calibrate.
- (4) System has reasonable weight and power requirements.

The remainder of Volume II is devoted to detail design considerations of the hardware required to implement the gamma absorption technique.

One of the methods studied was to try to determine the fluid density by measuring the velocity of sound in the fluid. In the course of study a method, which measures both the velocity of sound and the velocity of fluid transport, was discovered. Inasmuch as the contractor had been directed by NASA to include a discussion of the feasibility of developing the vent quality system into a mass flow meter, this technique was investigated in detail by the Powertron Division of Giannini Controls. The results of this investigation are presented in Volume II. It was found that the ultrasonic velocity technique combined with the gamma ray absorption method of density measurement is feasible for flow meter applications in which the vapor content does not exceed 20%.

As a result of the NASA review of the preliminary draft of this report, two additional questions were raised. One question was "How is the average density information to be turned into fluid quality?" A discussion of the techniques for doing this has been added as Appendix III to Volume I. In Appendix III, it is shown that the volumetric quality is given directly by the average density. In addition, a method of obtaining the mass quality is described.

The second question had to do with the effects of liquid collection on the pipe walls. This problem is discussed in Appendix IV of Volume I.

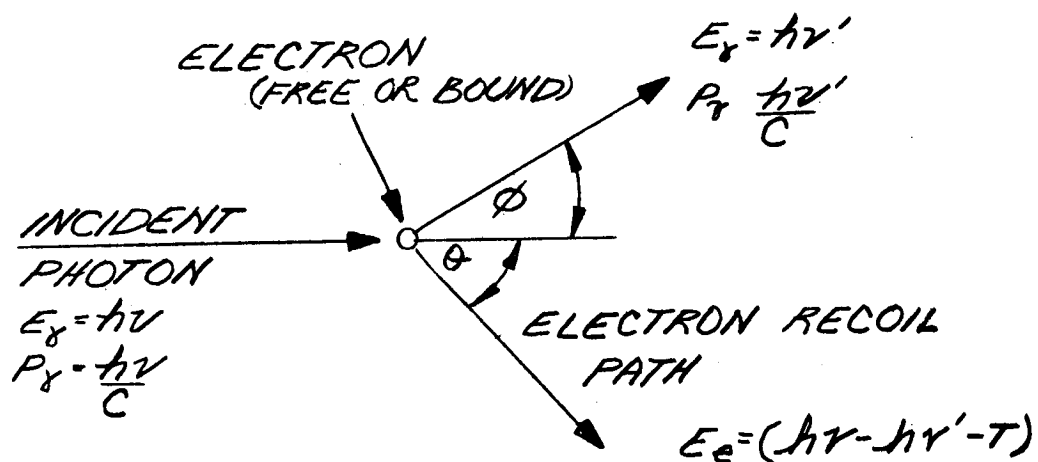
2.0 DENSITY DETERMINATION BY GAMMA SCATTER

2.1 Description of Scattering

The system to be described depends upon Compton scattering of low energy gamma rays. The system description will be preceded by a brief description of the Compton process. Briefly, a Compton event is a collision between a gamma photon and an electron. Energy and momentum are conserved in Compton events.

2.1.1 Loss of Energy in Scattering: Since the usual laws of energy and momentum conservation apply, the quantum hypothesis assigning energy and momentum to the photons is needed. Furthermore, the momentum and energy of the photon must change as a result of the collision. This means the wavelength of the radiation is increased. Figure 2-1 depicts the situation in a Compton event. The energy exchange between the photon and the electron depends upon the initial photon energy and the angle of scattering. The relation between photon energy, energy loss, and scattering angle is given in Figure 2-2.

2.1.2 Scattering Cross Section: The curves of Figure 2-2 result from consideration of the conservation of energy and momentum in a Compton event. To predict the amount of scattering which will occur in a given direction, a knowledge of the probability of occurrence of a Compton event is needed. It has been shown by the quantum mechanical calculations of Klein and Nishina that the required probability can be expressed as a cross section per electron. The cross section depends upon the initial photon energy. Figure 2-3 displays the cross section



P_γ = PHOTON MOMENTUM
 E_γ = PHOTON ENERGY
 h = PLANCK'S CONSTANT
 ν = RADIATION FREQUENCY
 C = VELOCITY OF LIGHT
 E_e = ELECTRON ENERGY

COMPTON SCATTERING

FIG. 2-1

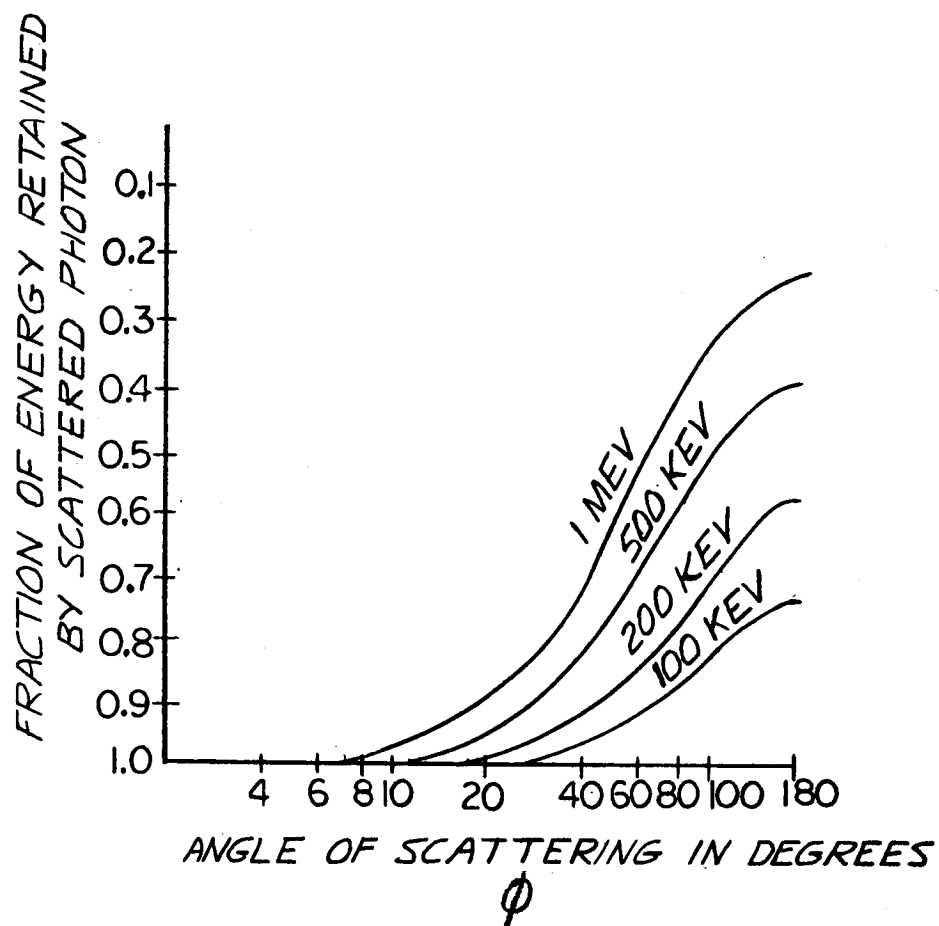
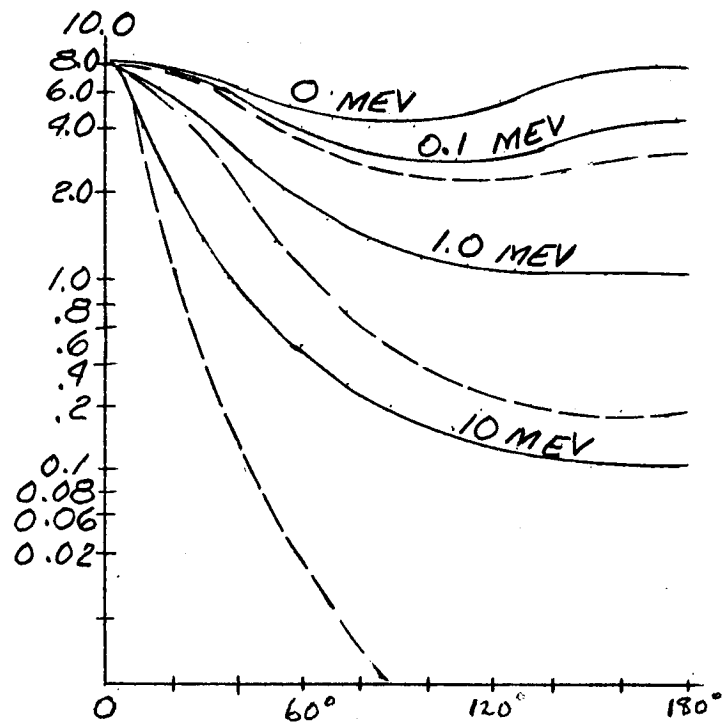


FIGURE 2-2
LOSS OF PHOTON ENERGY IN COMPTON
SCATTERING

C(W) CROSS SECTION IN CM⁻²ELECTRON⁻¹ STERADIAN⁻¹
(X10²⁶)



ANGLE OF PHOTON SCATTERING IN DEGREES

COMPTON SCATTERING CROSS SECTION

FIG 2-3(a)

per electron for photons of various energies in cm^2 per electron per steradian. The dashed lines of Figure 2-3 combine the information of Figure 2-2 with the cross sections to show the energy scattered. In particular, it should be noted that the cross sections for scattering through large angles decrease very rapidly with energy. At 100 kev and below, the scattering cross sections are not a strong function of the scattering angle, i.e., the scattering is nearly isotropic. It should also be noted that the increase in scattering cross section which can be obtained by going lower than 100 kev is small. On the other hand, the absorption cross section rises rapidly. See Figure 2-3(b). Therefore, for backscattering, a source of 100 to 200 kev is optimum. The detector can be placed outside the pipe since the 100 to 200 kev will penetrate the medium Z (steel) pipe walls fairly well. In addition, 100 to 200 kev can be easily shielded and collimated with high Z shields, and yet still has high scattering cross section. Good detector efficiency can also be obtained if scintillation detectors are used. If Geiger tube, ion chamber, or solid state detectors are considered, a lower source quantum energy might be chosen to increase detector efficiency. Even so, the ability to penetrate the pipe wall would be severely reduced and detector efficiency would still be low.

2.1.3 Macroscopic Discussion of Compton Scattering:

Figure 2-4 depicts an element of volume dv . It is supposed that dv is filled with matter of atomic number Z and atomic weight A . Then, the Number N_e of electrons in dv is:

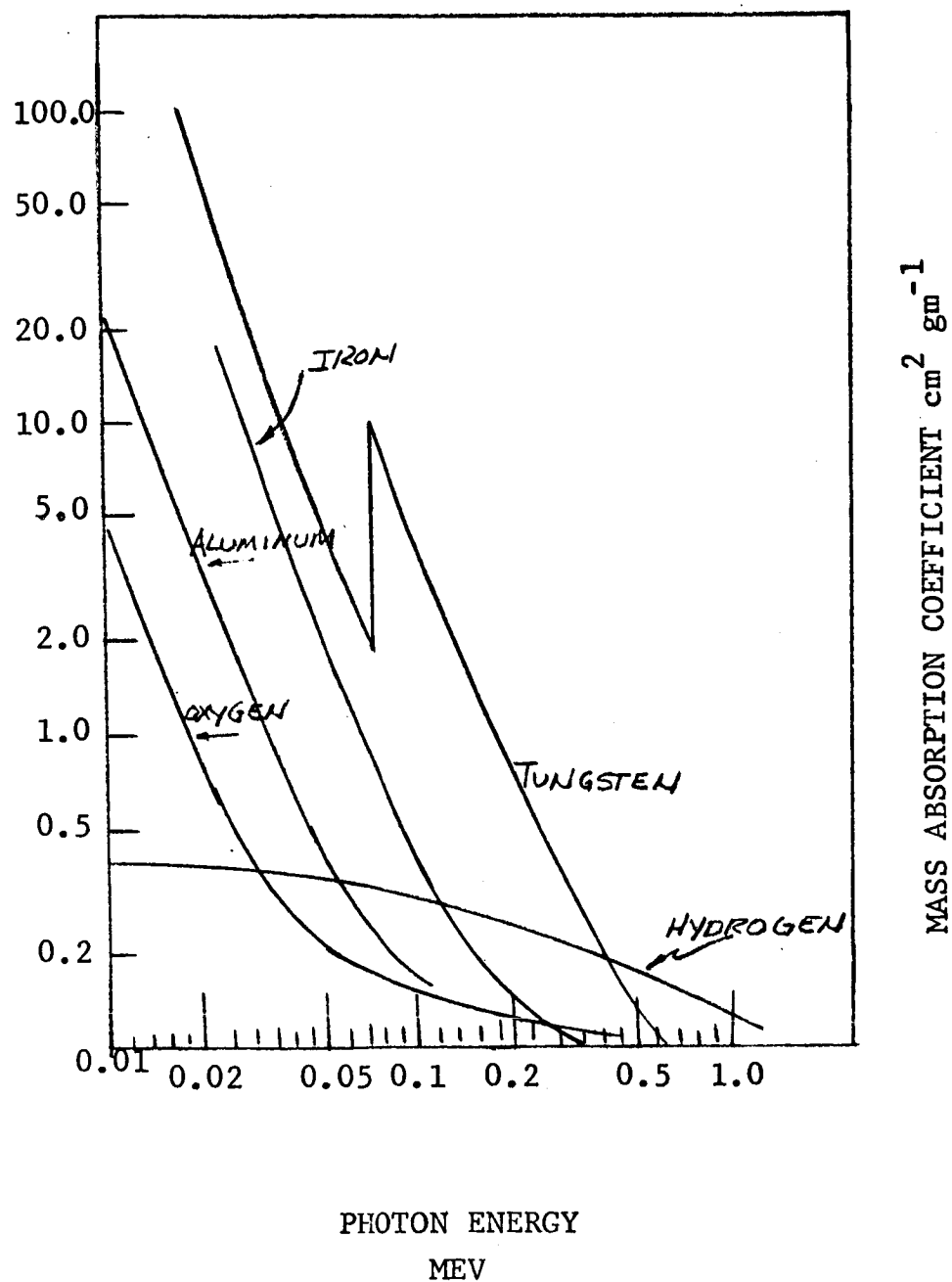
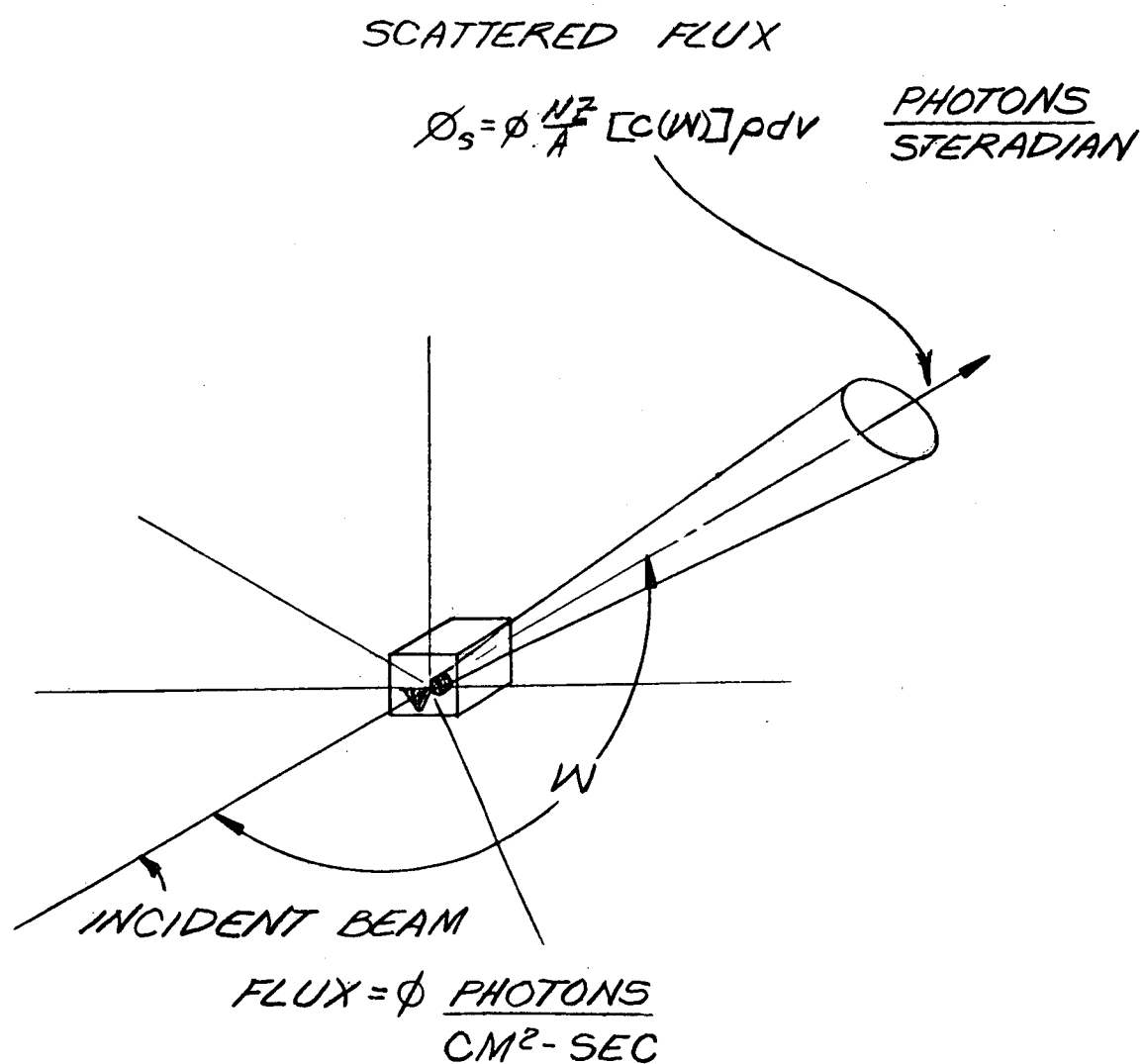


FIGURE 2-3(b)



COMPTON SCATTERING

FIG. 2-4

$$N_e = \frac{NZ}{A} \rho \, dv \quad (N = \text{Avogadro's Number}) \quad (1)$$

where N_e is the density in dv . Let the flux in the incident beam of radiation be denoted by ϕ . If ϕ is given in photons $\text{cm}^{-2}\text{sec}^{-1}$, the number N_p of photons scattered into the small solid angle dw is given by:

$$N_p = \frac{NZ}{A} \rho [C(w)] \phi \, dv \quad (2)$$

where $C(w)$ is given in Figure 2-3 for photons of various energies. Equation (2) is the basis for the vent quality meter design to be discussed in the remainder of this section. Note that the number of photons scattered from unit volume is just proportional to the number of electrons in the volume and the flux which threads the volume. This in turn is proportional to the density, since N , Z , and A are constant for a given material. The distribution of flux within the volume must be controlled according to the detector geometry, so that the detector senses the same change for each mass element regardless of the position of the mass element in the pipe.

2.2 Vent Quality Meter Analysis

2.2.1 Detector Solid Angle: Equation (2) enables one to compute the number of photons scattered from a small element of volume into a given solid angle at any angle. Thus, in order to find the effect on a detector of scattering from dv , one must know the solid angle subtended at dv by the detector. In the vent quality meter, the effect of a given volume element on the detector must be dependent only on the density in the element and not on the position of the element. Furthermore, the

detector must cover the entire pipe cross section uniformly. The second requirement can be met by making the detector concentric with the pipe. However, when this is done, the solid angle subtended by the detector varies with the radial position of the volume element under consideration. First, the way in which the detector solid angle varies will be determined. Then, it will be shown that the source can be designed to compensate.

In Figure 2-5, the geometrical relations are shown. Let the axial dimension of the detector be l_D . Then the element of detector area dA is:

$$dA = l_D R_D d\theta \quad (3)$$

The solid angle subtended by dA is:

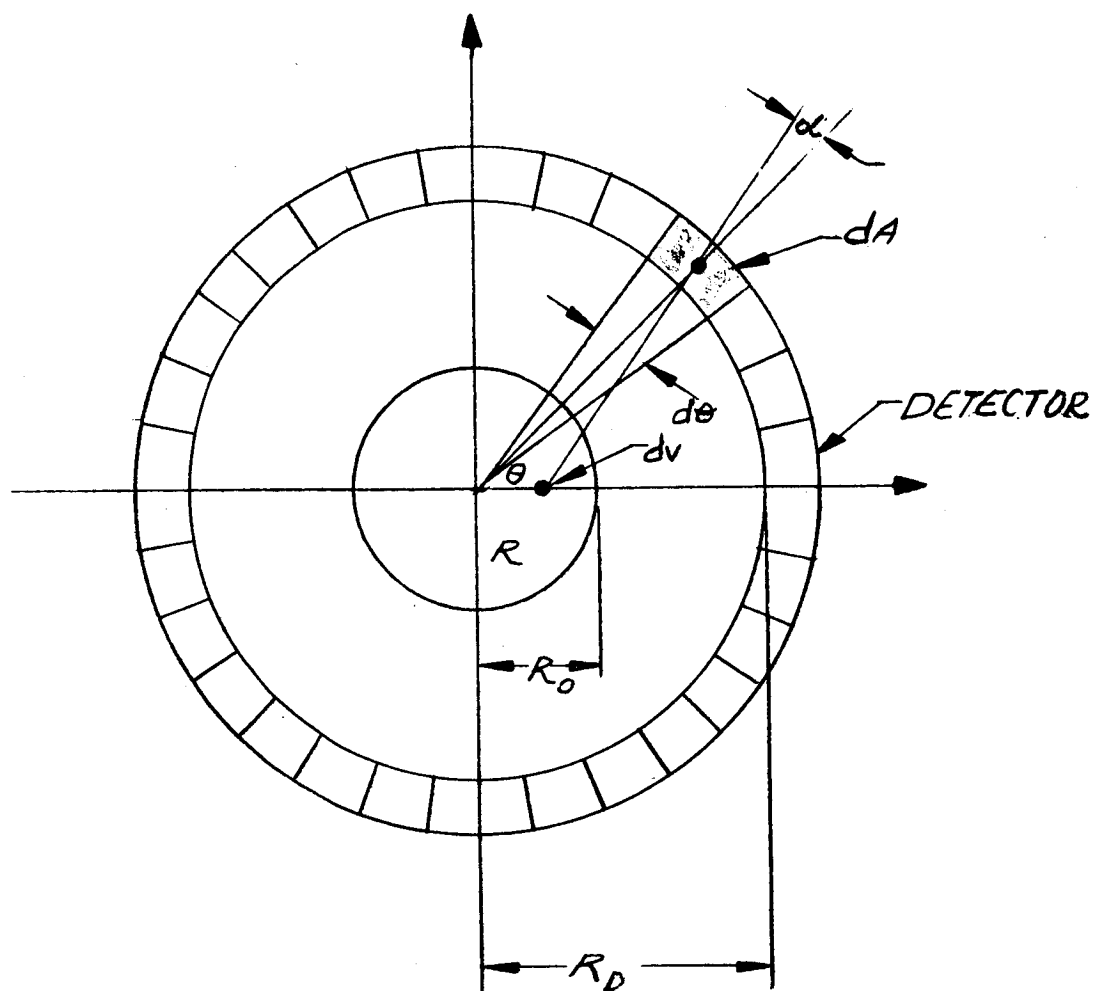
$$dw = \frac{l_D R_D \cos \alpha d\theta}{R_D^2 + R^2 - 2R_D R \cos \theta} \quad (4)$$

One other fact must be noted in connection with the solid angle. The detector will be a plastic scintillator. The detector absorption efficiency will vary almost directly as the thickness. Thus, flux arriving at the detector at angle α with the normal to the detector will traverse a thickness $t_0 \sec \alpha$ rather than t_0 where t_0 is the detector thickness. Therefore, the effective solid angle is given by:

$$dw = \frac{l_D R_D d\theta}{R_D^2 + R^2 - 2R_D R \cos \theta} \quad (5)$$

Integration of equation (5) gives the total solid angle as:

$$w = \frac{l_D}{R_D} \frac{2\pi}{1 - \frac{R^2}{R_D^2}} \quad (6)$$



SOLID ANGLE SUBTENDED BY
CONCENTRIC DETECTOR

FIG 2-5

The meaning of equation (6) is just that a unit mass situated distance R from the center of the pipe will have a greater effect on the detector than the same mass located at the center. To correct this difficulty, one could either design the detector with R_D sufficiently greater than R_o , or design the source so that the flux within the pipe decreases with R according to:

$$\phi_R = \phi_C \left(1 - \frac{R^2}{R_D^2}\right) \quad (7)$$

where ϕ_R denotes the flux at R centimeters from the center and ϕ_C that at the center. The latter method is preferable, particularly in the larger pipes, since the detector dimensions will have to be quite large to reduce the variations described by equation (6) to tolerable values.

2.2.2 Source Considerations: The source must be designed to give the flux distribution required by equation (7). In addition, the source must be collimated so as to minimize the flux which is directly incident on the detector, and must minimize the flux incident on the pipe walls within the field of view of the detector. The source radiation should be in an energy range that scatters well. In addition, it is desirable that the source radiation penetrate the pipe wall easily so as to permit external installation of the detector.

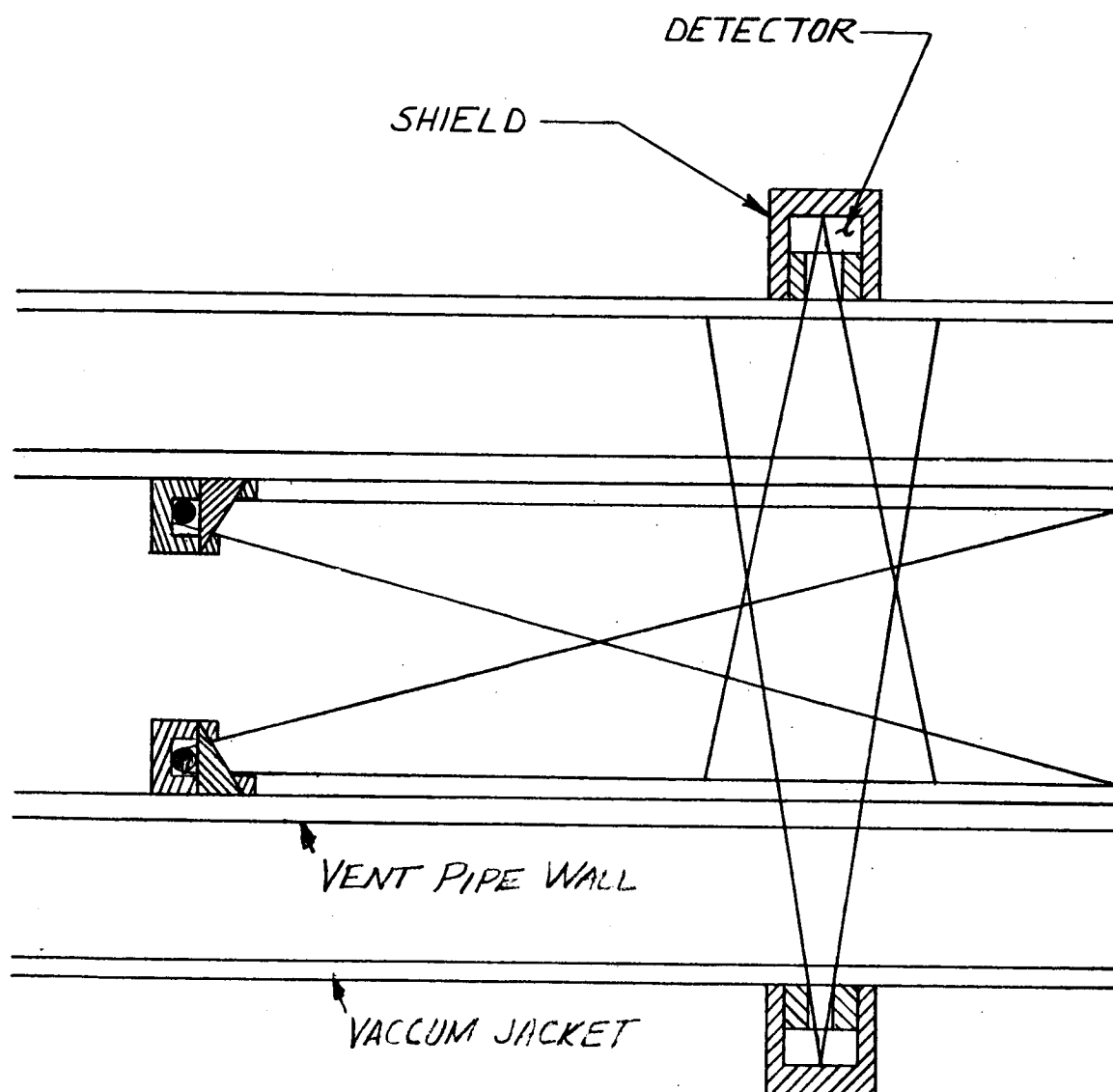
As previously noted, the optimum energy range is between 100 and 200 kev. This range of energies is highly attenuated by high Z material such as lead and tungsten. It will

penetrate short paths in medium Z materials such as steel and aluminum, and will scatter almost as well as longer wavelength radiation.

Unfortunately, it does not seem feasible to keep the source outside the pipe. The reason for this is that the mass of pipe wall material, particularly in small pipes, is large compared with the mass of fluid. Therefore, the scattering from the pipe wall increases the system noise. The source, however, can be made extremely small, and is not in any way affected by contact with the fluid. Therefore, this disadvantage does not seem to be severe.

Figure 2-6 illustrates a method of installing the source to meet all the requirements discussed. A shaped absorber serves to give the required radial variation of flux. The shape of this absorber will have to be determined empirically, since scattering in the absorber itself will render accurate calculation next to impossible. However, it is obvious that the correct shape can be obtained.

In addition, the source can be collimated so that no flux is directly incident on the pipe walls within the viewing angle of the detector. The only scatter from the pipe walls will be from photons which have first scattered from the fluid, or from those photons which become incident on the walls because of imperfection in the shielding. Those in the first category contribute to the information, since this number will be dependent on the density. Good shield design will reduce the number of photons in the second category to tolerable values.



SOURCE-DETECTOR GEOMETRY

FIGURE 2-6

This point will be discussed in more detail in the next section.

2.2.3 Count Rate versus Density Characteristic: In Section 2.1.3 it was shown that the flux scattered from volume dv through angle θ into unit solid angle $d\Omega$ is given by equation (2) which is rewritten here for convenience:

$$\phi(\theta, d\Omega) = \frac{NZ}{A} [C(\theta)] \rho dv$$

In Section 2.2.1 it was shown that the total solid angle of the concentric detector at dv is given by equation (6) which is also rewritten:

$$\Omega = 2\pi \frac{l_D}{R_D} \left(\frac{1}{1 - \frac{R^2}{R_D^2}} \right)$$

where R_D , l_D , and R are respectively, the radius and width of the concentric detector and the distance of dv from the pipe center line.

Assume that the source is designed as discussed in Section 2.2.2. The flux ϕ in an empty pipe is then:

$$\phi = \phi_c \left(1 - \frac{R^2}{R_o^2} \right)$$

where ϕ_c is the flux at the center of the cross section of pipe where the measurement is made.

Ignoring for the moment the effects of absorption, the number of photons per second incident on the detector is:

$$I = \phi_c 2\pi \frac{NZ}{A} [C(\theta)] \frac{l_D}{R_D} \rho dv \quad (8)$$

If the pipe is full and the density uniform, this becomes:

$$I = 2 \pi^2 \frac{NZ}{A} [C(\theta)] \frac{1_D^2}{R_D} \phi_c R_o^2 \rho \quad (9)$$

where R_o is the radius of the pipe filled with fluid. It should be noted that, since the detector response depends only upon ρ and dv , that if ρ is not uniform, but varies in the cross section visible to the detector, then ρv in the above equation will be replaced by an effective value $\bar{\rho} \bar{v}$ which is given by

$$\bar{\rho} \bar{v} = \sum_i (\rho_i dv_i) \quad (10)$$

The detector reading is then proportional to the mass in the cross section viewed by the detector. Since the volume of the cross section being sampled is constant, the detector reading is proportional to the average density.

Equation (9) is an ideal characteristic. Needless to say, strict conformance to this ideal is not to be expected in the real world. The two main factors which contribute to the anticipated departure from equation (9) are absorption and a certain amount of unavoidable fixed scatter from the walls. Experimentally, it has been determined that the scatter from the walls is about 0.7% of the flux at the section under consideration. There is no doubt that this can be improved with additional experimental work; however, this figure will be used as a worst case.

The effects of absorption can also be handled on a worst case basis. An element of volume at the pipe center will be affected most by absorption. Assume (referring to Figure 2-6)

that the source is located R_D cm upstream (or downstream) from the pipe section under consideration. This allows enough distance for effective collimation. A ray travelling to the volume element at the center of the section traverses a distance $\sqrt{R_D^2 + R_o^2}$. This ray is attenuated by the factor $e^{-\mu \rho \sqrt{R_D^2 + R_o^2}}$. The flux scattered from this element must traverse the distance R_o , suffering additional attenuation by the factor $e^{-\mu \rho R_o}$. Therefore, the attenuation factor will be

$$e^{-\mu \rho [\sqrt{R_o^2 + R_D^2} + R_o]}$$

The worst case detector incident flux rate versus density curve will then be given by:

$$I = \left[2\pi^2 \frac{NZ}{A} [C(\theta)] \frac{1^2 R_o^2}{R_D} \rho e^{-3\mu \rho R_o} + 7 \times 10^{-3} \pi R_D I_D \right] \phi_c \quad (11)$$

If the detector absorption efficiency is denoted by η , and it is noted that ϕ_c will be given by:

$$\phi_c = \frac{I_o}{4\pi(R_o^2 + R_D^2)} \quad (12)$$

where I_o is the source strength in counts per second, the final expression for the detector count rate I will be:

$$I = \frac{1.75 \times 10^{-3} \eta e^{-\mu^w \rho^w t^w} R_D I_D I_o}{(R_o^2 + R_D^2)} \left[2.86 \times 10^2 \pi \frac{NZ}{A} [C\theta] \frac{1^2 R_o^2}{R_D} \rho e^{-\left(\sqrt{R_D^2 + R_o^2} + R_o\right)} + 1 \right] \quad (13)$$

The factor $e^{-\mu^w \rho^w t^w}$ accounts for the pipe wall absorption.

2.2.4 Recapitulation: In the preceding paragraphs, equation (13) has been derived. Equation (13) expresses the count rate as a function of density for a concentric detector

and shaped source in terms of the pipe dimensions. The various symbols in equation (13) were defined as they were introduced, but are given again in Table 2-1 for convenience.

2.2.5 Error Analysis: Equation (13) is evaluated for LH_2 and LO_2 in 1.0 inch and 10.0 inch pipes. For LH_2 equation (13) becomes:

$$\frac{I}{I_0} = 1.1 \times 10^{-4} (10 \rho e^{-0.247 \rho} + 1) \quad (14)$$

for a 1.0 inch pipe, and:

$$\frac{I}{I_0} = 3.3 \times 10^{-5} (20 \rho e^{-1.6 \rho} + 1) \quad (15)$$

for a 10.0 inch pipe.

Equations (14) and (15) are plotted in Figure 2-7.

For liquid oxygen, equation (13) gives:

$$\frac{I}{I_0} = 1.1 \times 10^{-4} (5 \rho e^{-0.124 \rho} + 1) \quad (16)$$

for a 1.0 inch pipe, and

$$\frac{I}{I_0} = 3.3 \times 10^{-5} (10 \rho e^{-0.8} + 1) \quad (17)$$

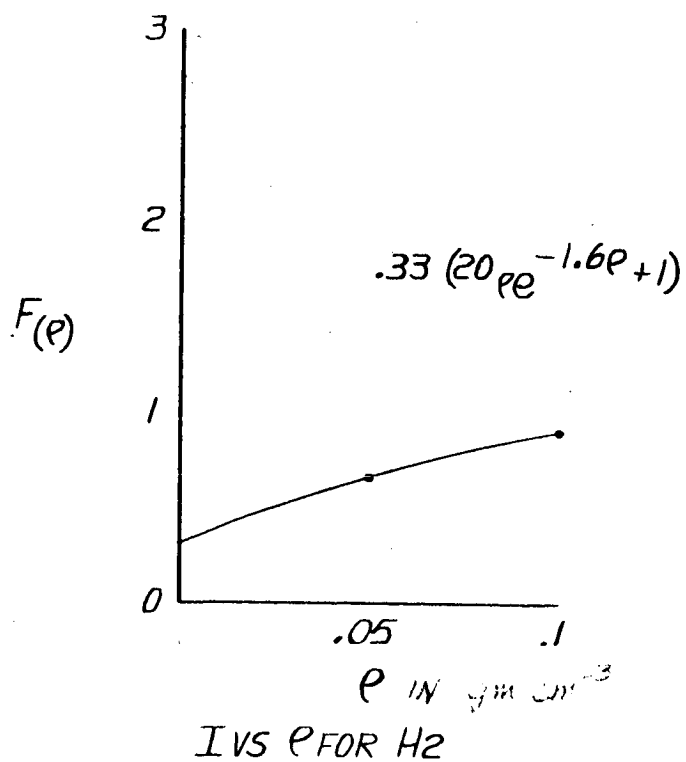
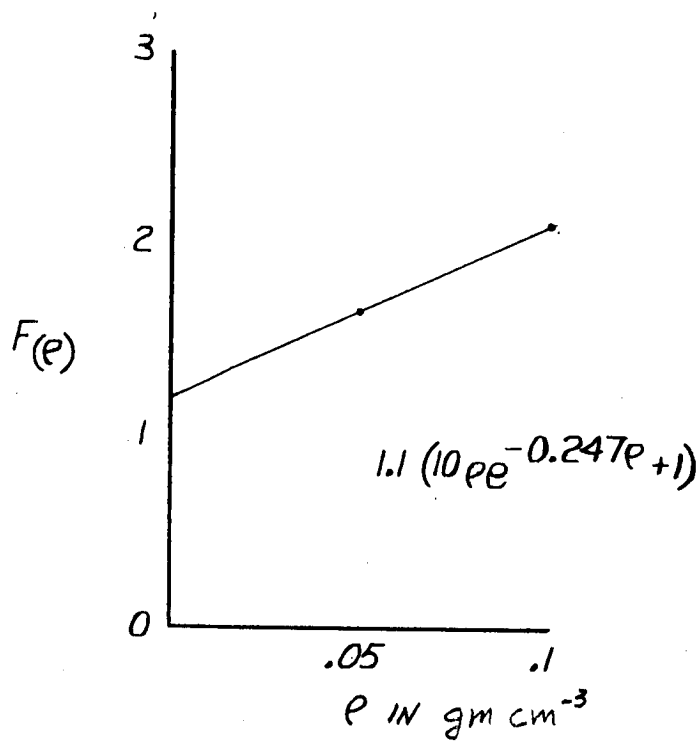
Equations (16) and (17) are plotted in Figure 2-8.

For the full range of liquid hydrogen densities (i.e., 0 to 0.07) equations (14) and (15) are linear for all practical purposes. The error analysis then can be based on a linear characteristic. Under this assumption, both cases are represented by:

$$I = K_1 I_0 (K_2 \rho + 1) \quad (18)$$

Equation (18) is plotted in Figure 2-9.

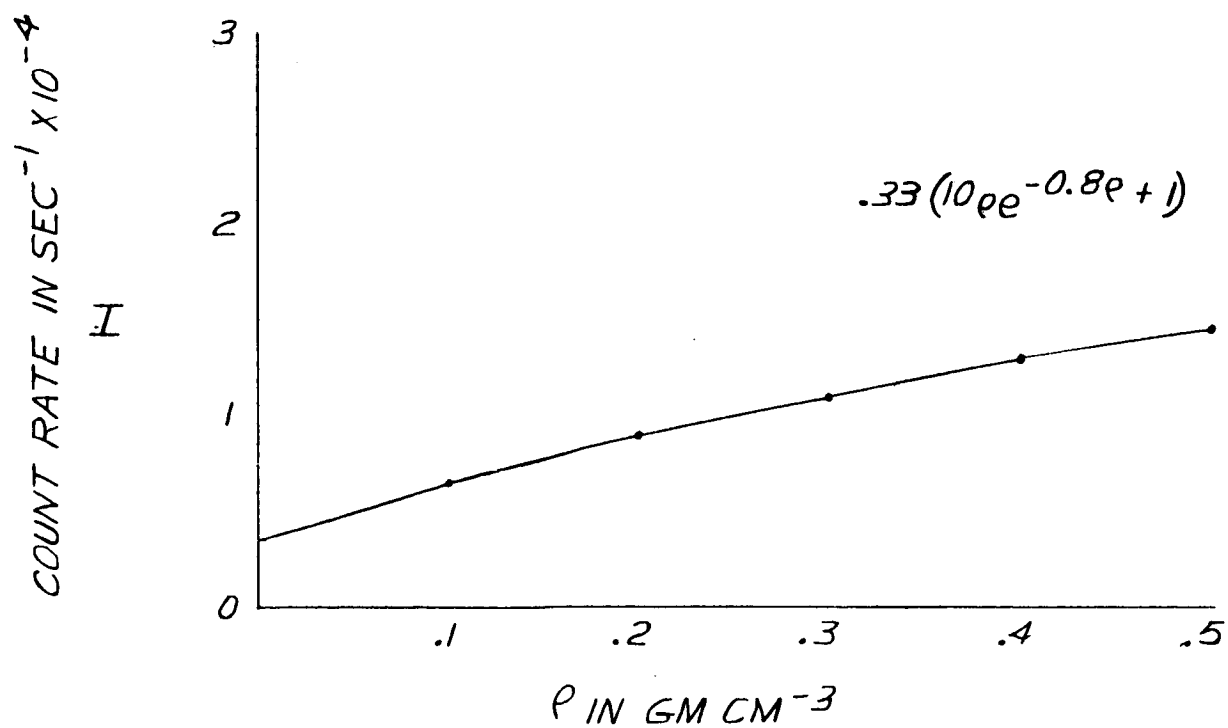
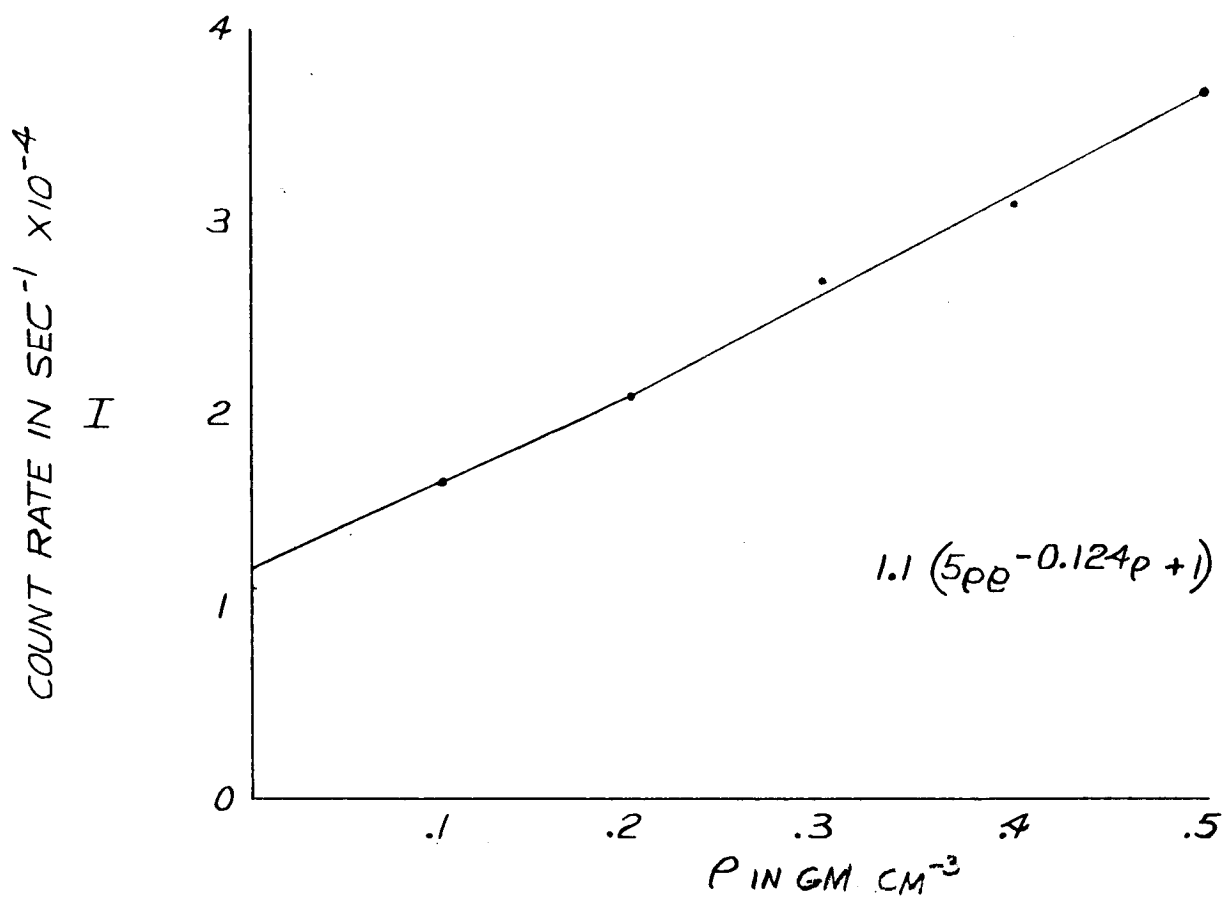
From Figure 2-9, the following relations can be seen:



IVS p FOR H_2

p FROM 0 TO .1

FIGURE 2-7



I VS ρ FOR O_2

ρ FROM 0 TO .5

FIGURE 2-8

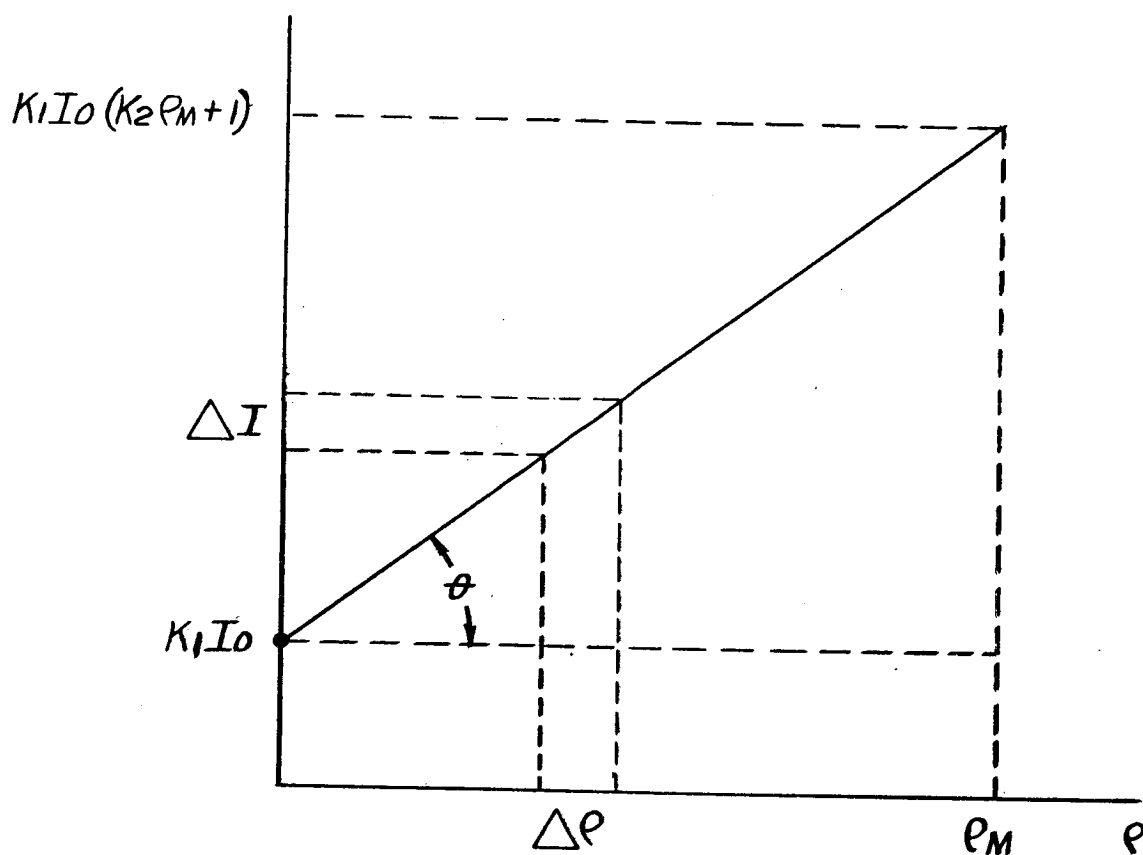


FIGURE 2-9
COUNT RATE CHARACTERISTIC FOR
ERROR ANALYSIS OF LH₂
SYSTEM

TABLE 1

EXPLANATION OF SYMBOLS

<u>Symbol</u>	<u>Quantity</u>	<u>Dimensions</u>	<u>Range of Values</u>
I	Detector count rate	sec^{-1}	0 - 5×10^4
N	Detector efficiency	unity	10%
R_D	Radius of concentric detector	cm	2.54 to 17.8
R_o	Radius of pipe carrying fluid	cm	1.27 to 12.7
l_D	Detector width	cm	2.5
N	Avogadro's number	atoms mole $^{-1}$	6×10^{23}
A	Atomic weight	GM mole $^{-1}$	1 for LH_2 ; 16 for LO_2
Z	Atomic number	electron atom $^{-1}$	1 for LH_2 ; 8 for LO_2
	Fluid density	GM CM $^{-3}$	0 to 0.5
$C(\theta)$	Compton Cross section	CM 2 electron $^{-1}$ steradian $^{-1}$	3×10^{-26} (for 100 Kev)
μ	Fluid mass energy absorption coefficient	CM 2 gm $^{-1}$	0.046 for LH_2 0.024 for LO_2
μ_w	Pipe wall mass energy absorption coefficient	CM 2 gm $^{-1}$	0.12 for 134 Kev 0.22 for 100 Kev
tw	Pipe wall thickness	CM	0.089
ρ_w	Pipe wall density	gm cm $^{-3}$	8.0
a	Number of times penetrate pipe wall	unity	

$$\Delta I = \Delta \rho \tan \theta \quad (19)$$

$$\tan \theta = \frac{K_1 (K_2 \rho_m)}{\rho_m} I_o = K_1 K_2 I_o \quad (20)$$

Therefore,

$$\Delta I = K_1 K_2 I_o \Delta \rho \quad (21)$$

In addition:

$$I = K_1 I_o + K_1 K_2 I_o \rho \quad (22)$$

Upon combining equations (21) and (22) one obtains

$$\begin{aligned} \frac{\Delta I}{I} &= \frac{K_2 \Delta \rho}{1 + K_2 \rho} \\ &= \frac{1}{\frac{1}{K_2 \rho} + 1} \frac{\Delta \rho}{\rho} \end{aligned} \quad (23)$$

Equation (23) gives the relative change of I for a given relative change in ρ . The relative value of I is subject to a statistical fluctuation whose standard deviation is given by:

$$\frac{\sigma_I}{I} = \frac{1}{\sqrt{N}} \quad (24)$$

where N is the number of counts from which I is computed.

From equation (23) it can be seen that the relative change in I for a 5% change in ρ where $\rho = \rho_m$ in a 1.0 inch pipe is:

$$\frac{\Delta I}{I} = \frac{.05}{1/.7 + 1} = 0.0203 \quad (25)$$

It should be numbered that the count rate I is to be integrated to obtain a 0 to 5 volt dc signal. The time constant of integration is to be 0.1 second. It is shown in Appendix II that the standard deviation of the dc signal will be the same as the standard deviation of the count rate based on a 0.2

second sample. Therefore, for a $\pm 5\%$ accuracy with 95% confidence, the count rate must be given by

$$\frac{1}{\sqrt{2I}} = 0.01 \quad (26)$$

In other words, if equation (26) is satisfied, the change of output for a 5% density change will be twice the standard deviation of the output. Moreover, this accuracy applies to an instantaneous reading of the output voltage. The time history of the density from a continuous record of the output can be obtained to much greater accuracy by curve fitting techniques.

Solving equation (26) for I gives:

$$\frac{5}{I} = 10^{-4} \quad (27)$$

or:

$$I = 5 \times 10^4 \text{ sec}^{-1}$$

The value of I_0 required can be found by substituting equation (27) in equation (14) which gives:

$$I_0 = 2.7 \times 10^8 \text{ sec}^{-1} \quad (28)$$

This in turn can be interpreted in terms of required source activity. Since one millicurie is 3.7×10^7 disintegration per second, assuming that a source which gives at least one photon per disintegration would have a strength of:

$$\begin{aligned} I_0 &= \frac{2.7 \times 10^8}{3.7 \times 10^7} \\ &= 7.3 \text{ millicuries} \end{aligned} \quad (29)$$

For the 10.0 inch pipe similar calculations show the source strength required is

$$\begin{aligned} I_0 &= 2.96 \times 10^8 \text{ sec}^{-1} \\ &= 8.0 \text{ millicuries} \end{aligned} \quad (30)$$

the others fall in between.

2.2.6 Radiation Safety: The radiation shielding problem will be discussed in detail under System Design. For the source strength required by equation (30) it is estimated that about 1.6 pounds of shielding is the most that would be required.

2.2.7 Use of Backscatter with Liquid Oxygen: Examination of equations (16) and (17) show that the backscatter technique cannot be used for liquid oxygen to obtain 5% accuracy under zero g conditions in larger pipes. The de-linearizing effects of absorption are too great. Thus for LO_2 pipes greater than 2-inch diameter, the gamma absorption technique described in Section 3.0 must be used to meet the stated requirements.

2.2.8: Experimental Results: The calculations given in the preceding section were verified experimentally. The results of the experiment are given in Appendix I.

3.0 DENSITY MEASUREMENT BY GAMMA RAY ABSORPTION

The absorption of gamma radiation by matter occurs as a combination of three processes; (1) The photoelectric absorption process in which direct collision of a gamma photon with one of the electrons of an atom results in the ejection of the electron from its shell; (2) Compton process in which the photon interacts with a free or loosely bound electron and gives up only a portion of its energy to the electron; (3) Pair production process in which the gamma photon interacts directly with a nucleus where the gamma photon disappears and a positive and a negative electron are set in motion. The effects of these processes are shown in Figure (3-1)a as the mass absorption coefficient for hydrogen and oxygen.

For the case when the density is sufficiently high, the transmission path is sufficiently long and the gamma-ray beam is broad, another factor appears. This is termed the dose build-up factor (B). The dose build-up factor is a result of Compton scattering. Figure (3-1)b shows the relationship of B with density and energy for a plane distributed source.

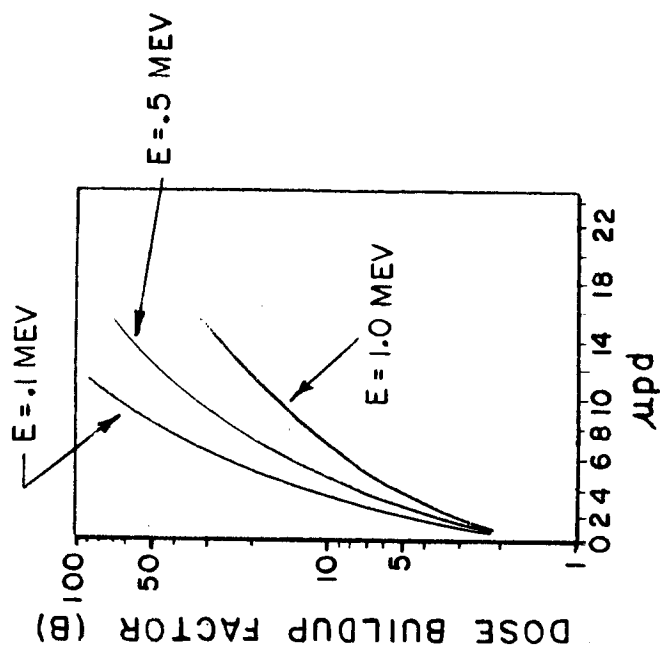
The relationship between the output gamma emission rate (I_o) and the detector count rate (I) is given below:

$$I = \frac{I_o A_d}{4\pi d^2} B e^{-\mu \rho d}$$

Where: A_d = Detector area

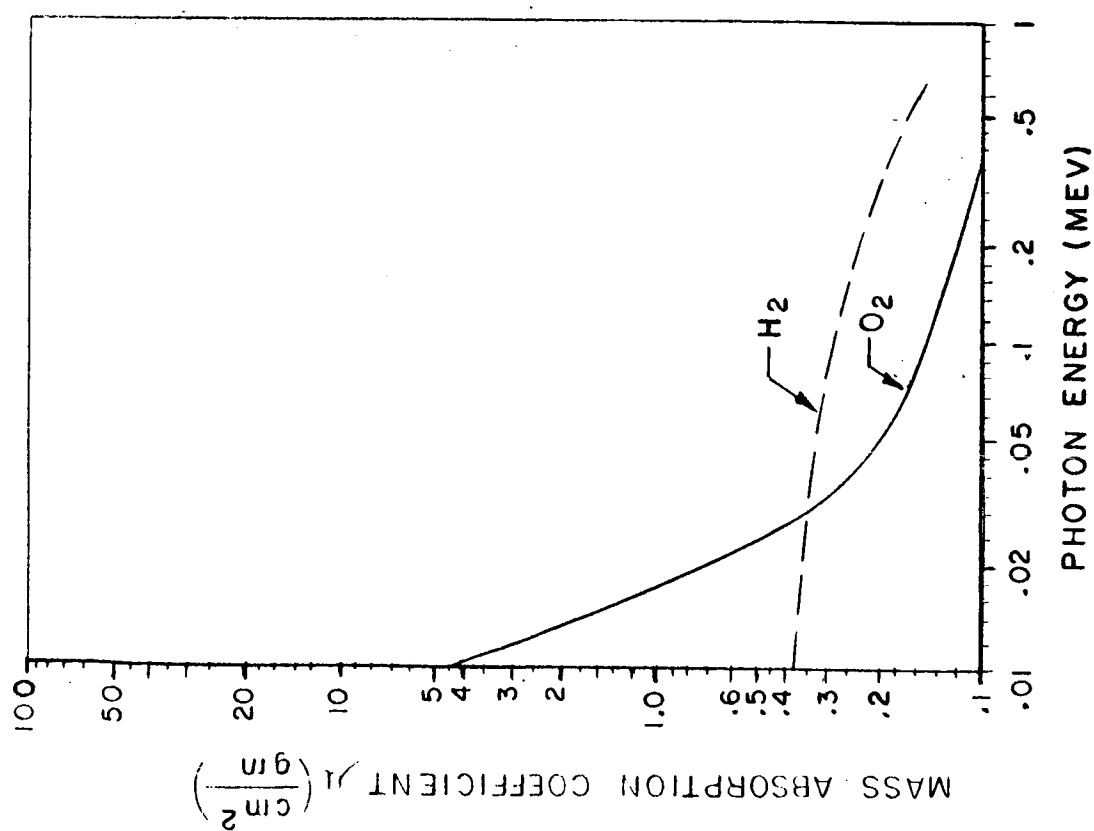
d = Pipe diameter

μ = Mass absorption coefficient



DOSE BUILDUP FACTOR
AS A FUNCTION OF DENSITY
AND ENERGY

FIGURE (3-1)b



MASS ABSORPTION COEFFICIENTS
VS ENERGY

FIGURE (3-1)c

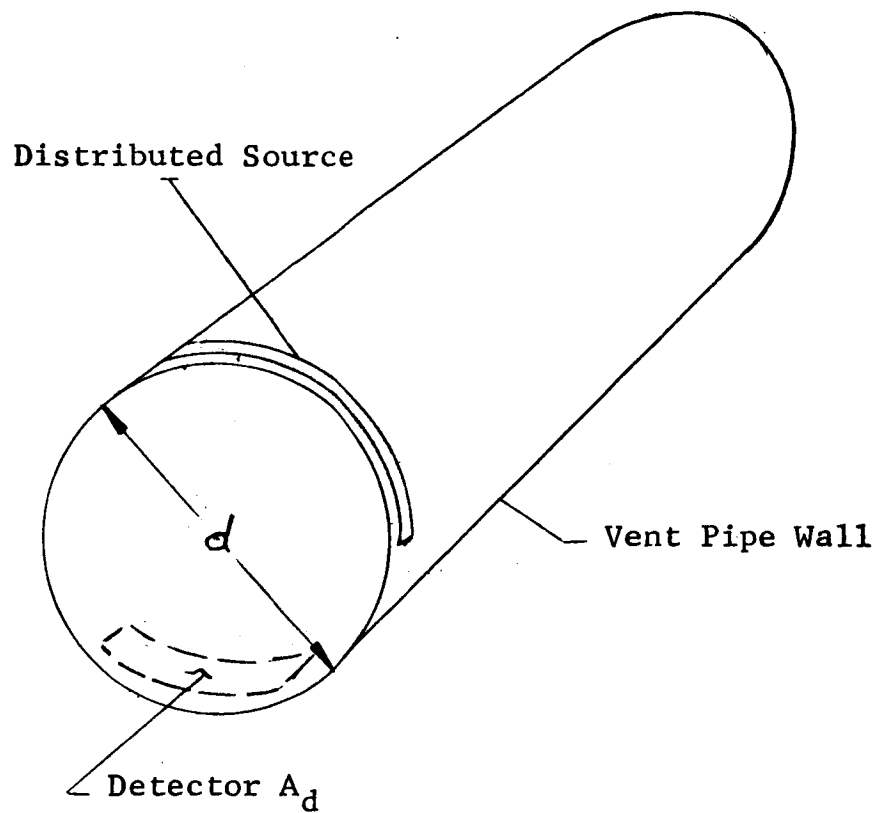
ρ = Density

W = Pipe wall absorption

B = Dose buildup factor

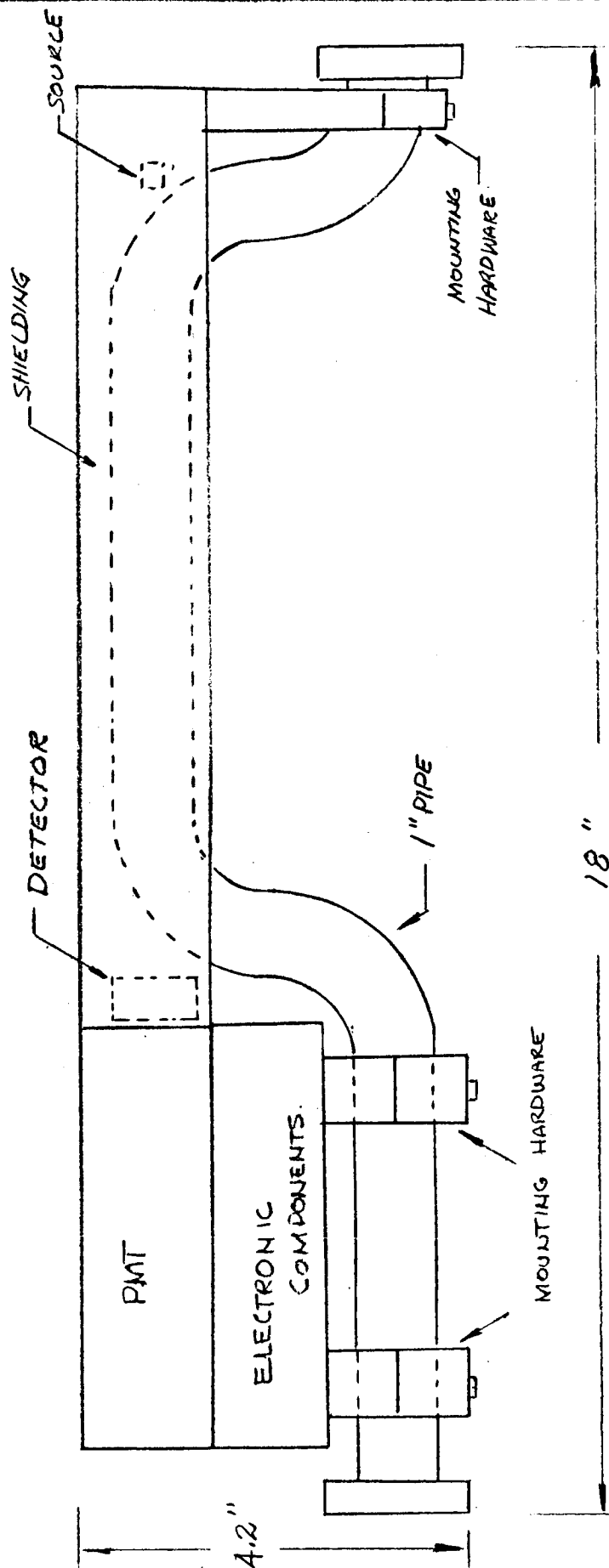
For a sensor arrangement as shown in Figure 3-2, all parameters are fixed except I_d and ρ . Pipe diameters from 1" to 10" are of interest. To achieve a maximum sensitivity, it is desirable to maintain the maximum radiation path length (assume 10 inches). This can be achieved for smaller diameter pipes by arranging the geometry as shown in Figure 3-3. Figure 3-4 illustrates the normalized count rate versus density for a narrow beam of hard and soft gamma-rays for hydrogen. Figure 3-5 gives the normalized count rate versus oxygen density for both hard and soft gamma-photons. The solid curves (in Figure 3-5) assume that the detector views only uncollided photons. This would be achieved by using a narrow window (pulse height) discriminator as shown in Figure 3-6. Without the window discriminator, the relationship between count rate and oxygen density is as given in the dashed curves of Figure 3-5.

Under "zero-g" conditions, measurement of a liquid mass regardless of position and orientation with a system exponentially related to mass thickness is difficult. For instance, an elemental liquid volume in the two orientations shown in Figure 3-7 would yield different count rates. Therefore, a count rate linearly related to mass is required. This can be achieved by using a window discriminator positioned not over the photopeak but rather below the photopeak energy. This yields a



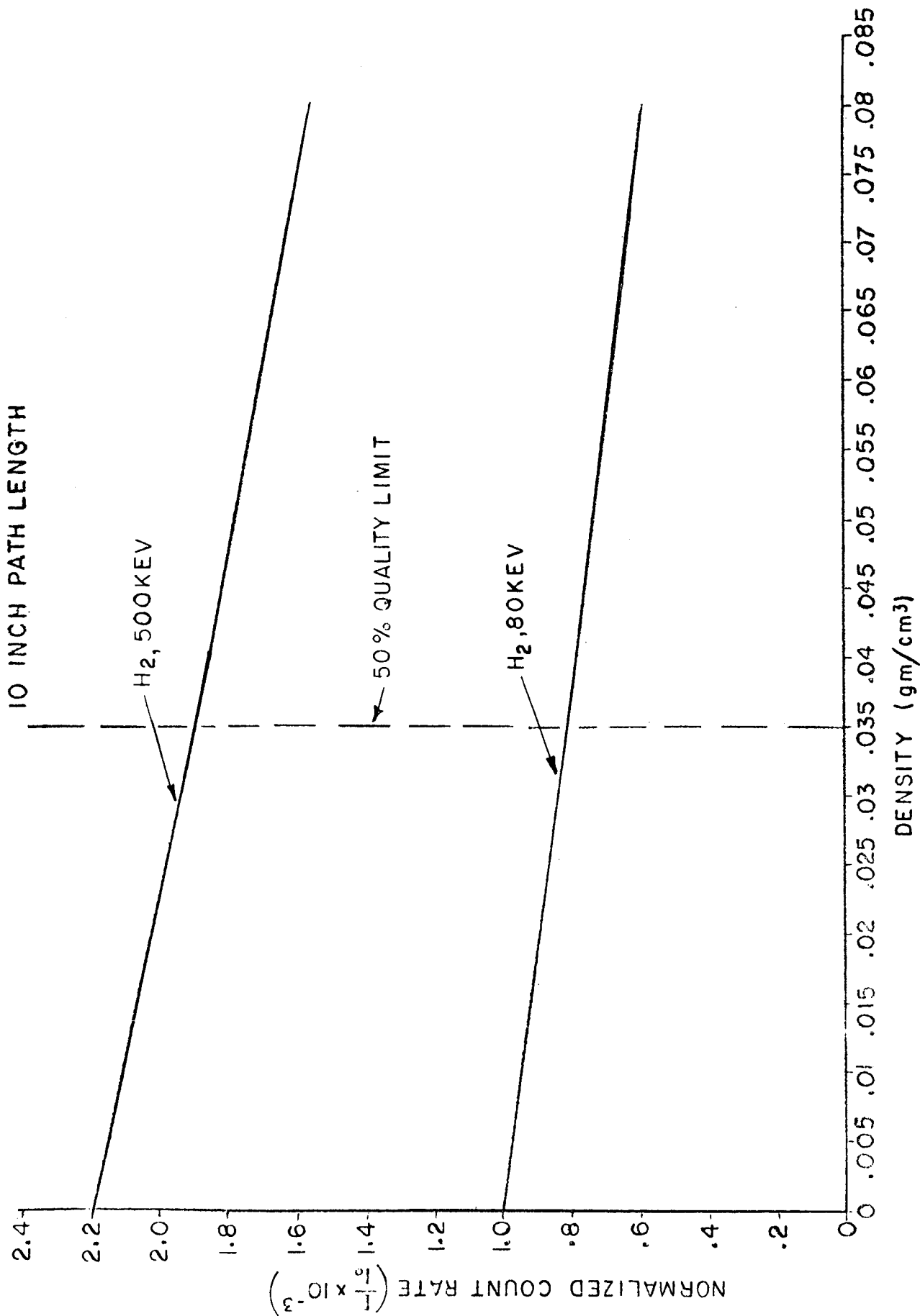
ONE ARRANGEMENT FOR γ -RAY TRANSMISSION
LIQUID DENSITY SENSOR

FIGURE 3-2



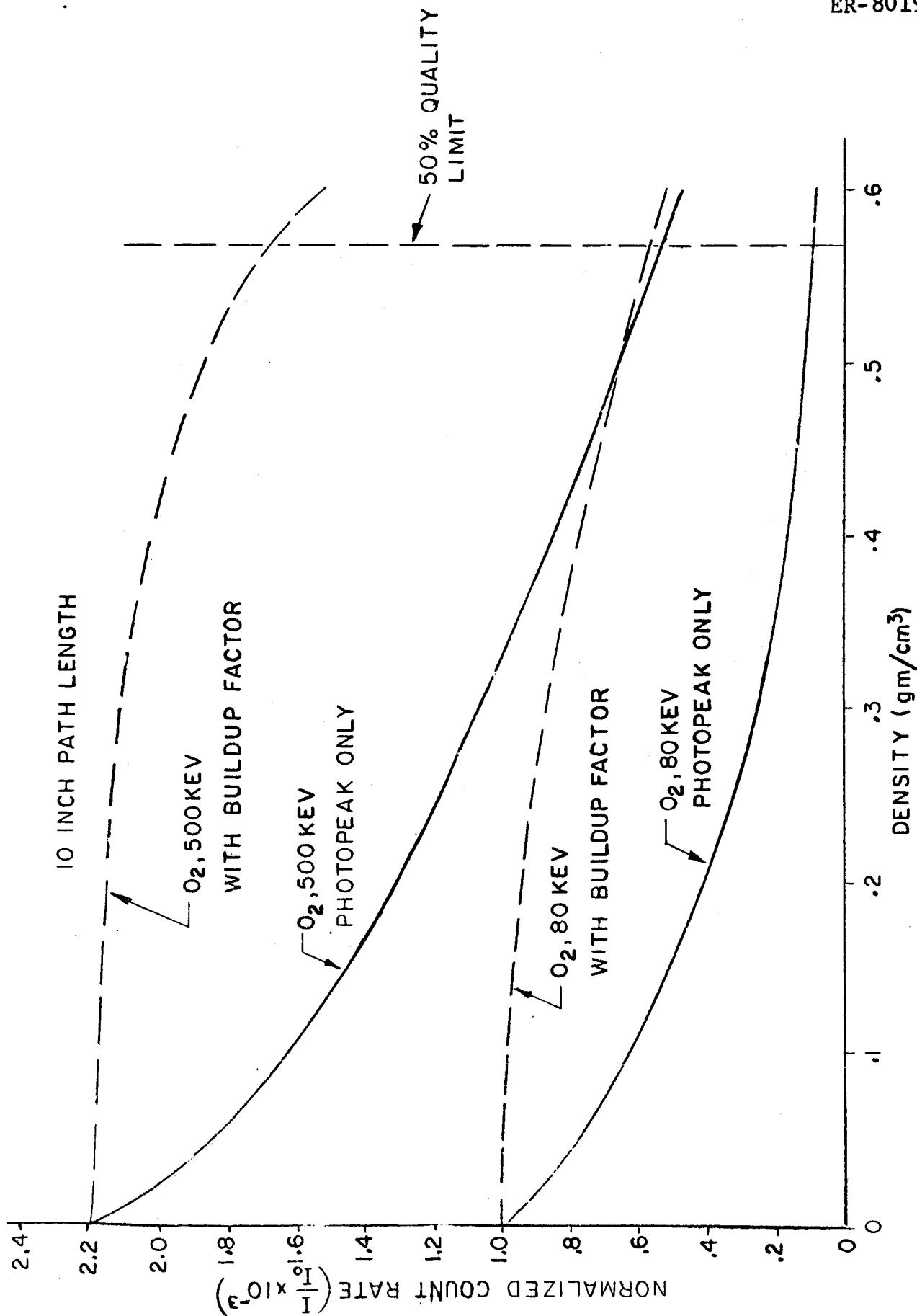
GEOMETRY USED ON PIPES LESS THAN 10 INCHES IN
DIAMETER TO MAINTAIN A RADIATION PATH LENGTH OF 10 INCHES

FIGURE 3-3



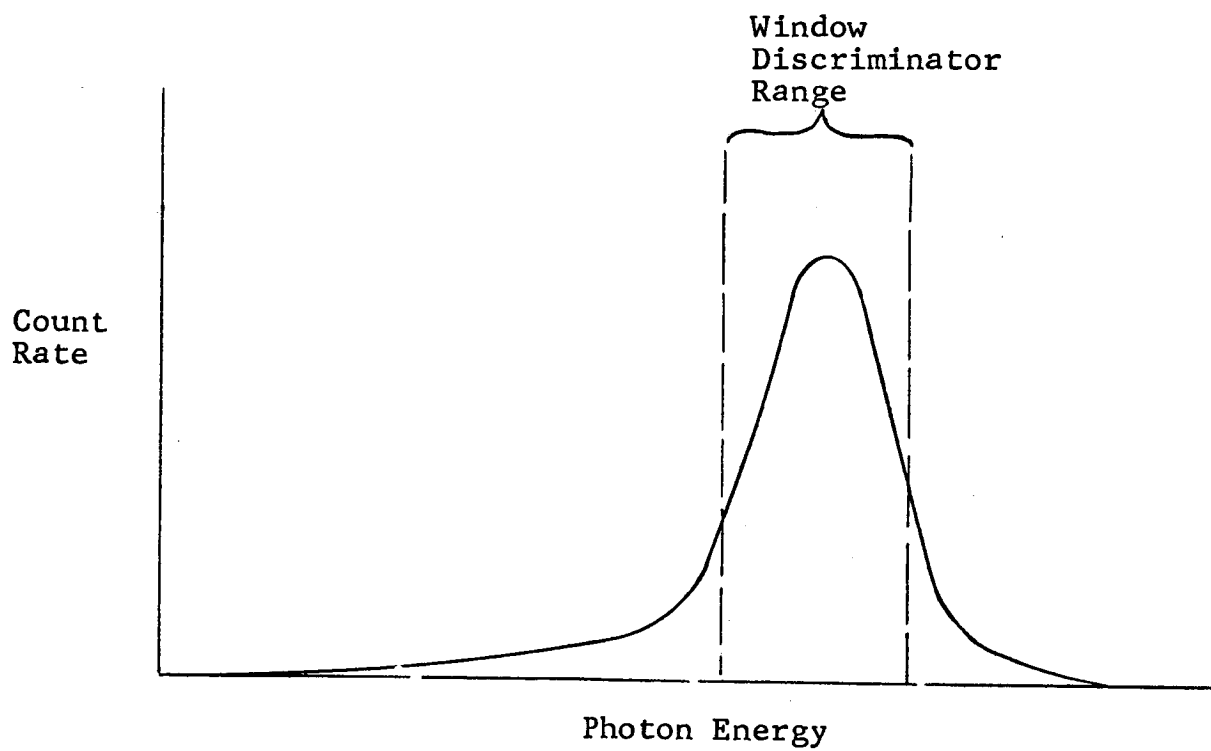
COUNT RATE VS DENSITY OF HYDROGEN FOR HARD AND SOFT γ RAYS

FIGURE 3-4



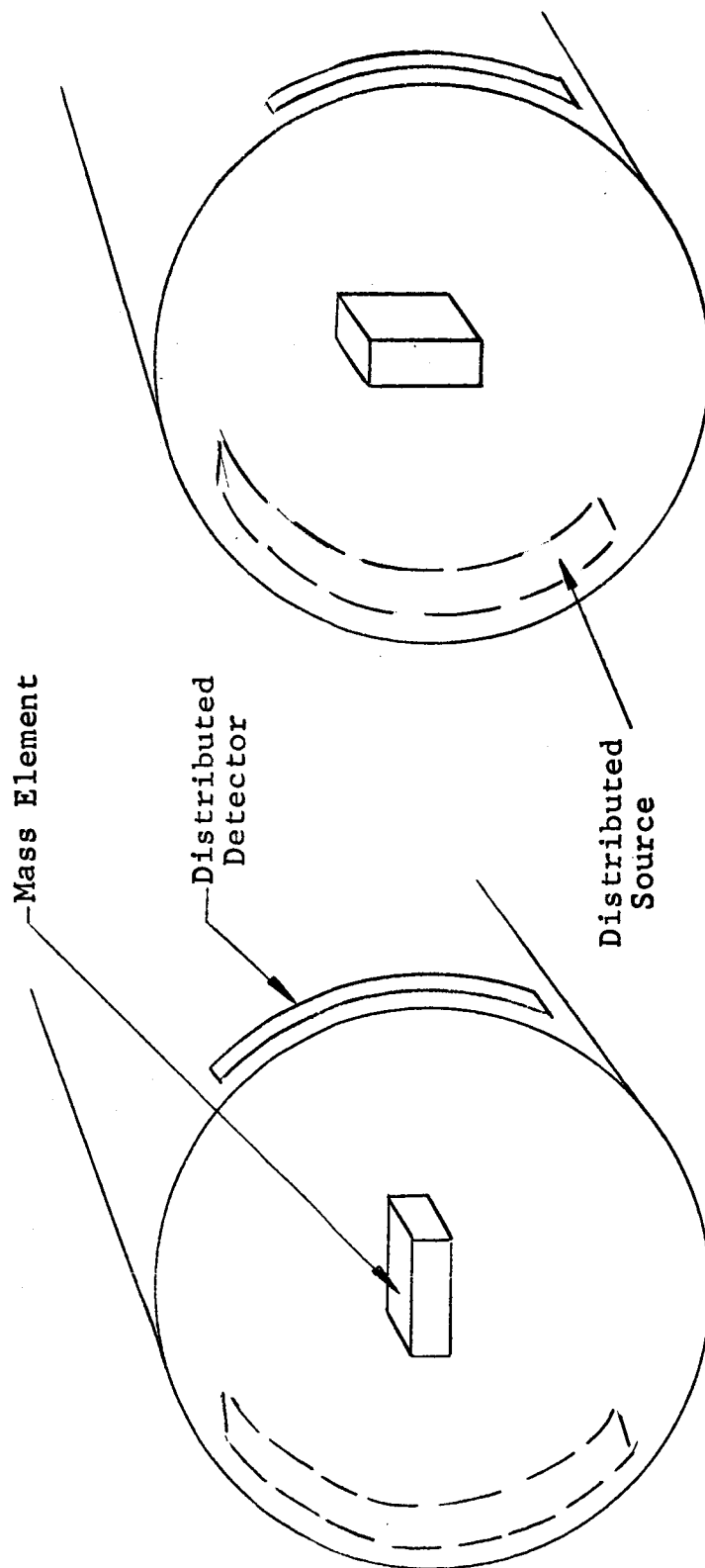
COUNT RATE VS DENSITY OF OXYGEN WITH AND WITHOUT DOSE BUILDUP
FACTOR FOR HARD AND SOFT X RAYS

FIGURE 3-5



PLACEMENT OF PULSE HEIGHT WINDOW DISCRIMINATOR
FOR "VIEWING" PHOTOPEAK ENERGIES ONLY

FIG. 3-6



POSSIBLE ORIENTATIONS OF ELEMENTAL MASS VOLUME
ILLUSTRATING NEED FOR A LINEAR RELATIONSHIP BETWEEN COUNT RATE AND DENSITY

FIG. 3-7

compromise between the convex solid and concave dashed curves of Figure 3-5. Proper placement of this window discriminator gives a linear relationship of count rate and density (Figure 3-8). This is shown experimentally in Figure 3-9 where C_d^{109} gamma radiation was absorbed linearly with changes in density simulating an oxygen filled vent pipe.

The soft 80 kev gamma-photon source will be considered since less shielding is required and a greater percentage change in count rate occurs from zero quality to 50% quality than for hard gamma-photons.

For hydrogen (see Figure 3-4), the greatest normalized count rate (for the no liquid case) is approximately 1.08×10^{-3} . A 5% of full scale density change corresponds to a 1.38% change in count rate. The allowable statistical error should not exceed $1.38\%/2 = .69\%$. To maintain this 2 sigma error, the required count rate (I) can be determined as explained in Section 2.0:

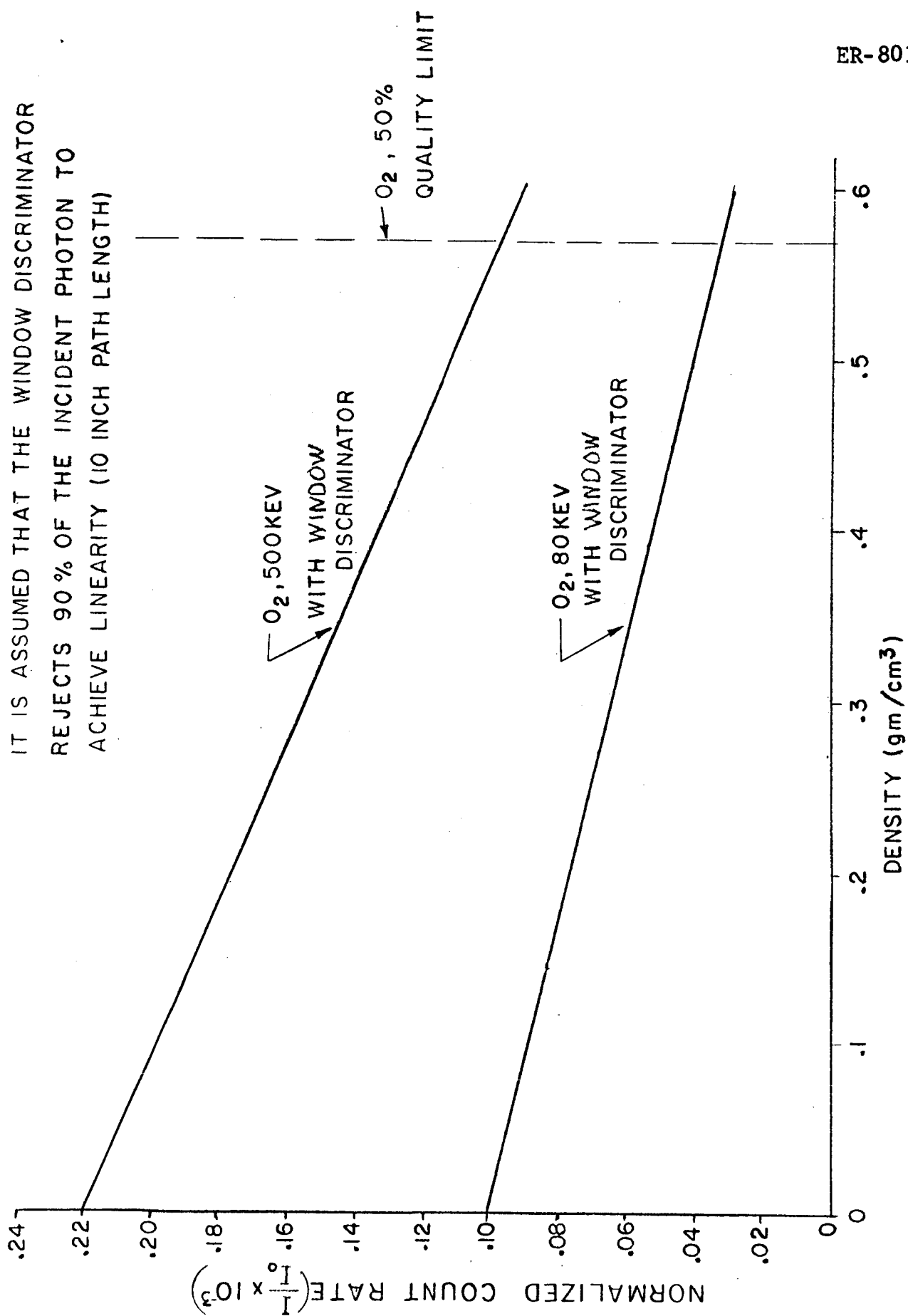
$$\frac{1}{\sqrt{2\pi}} = 6.9 \times 10^{-3}$$

Where τ is the resolving time = .1 sec. The required count rate is then 1.05×10^5 .

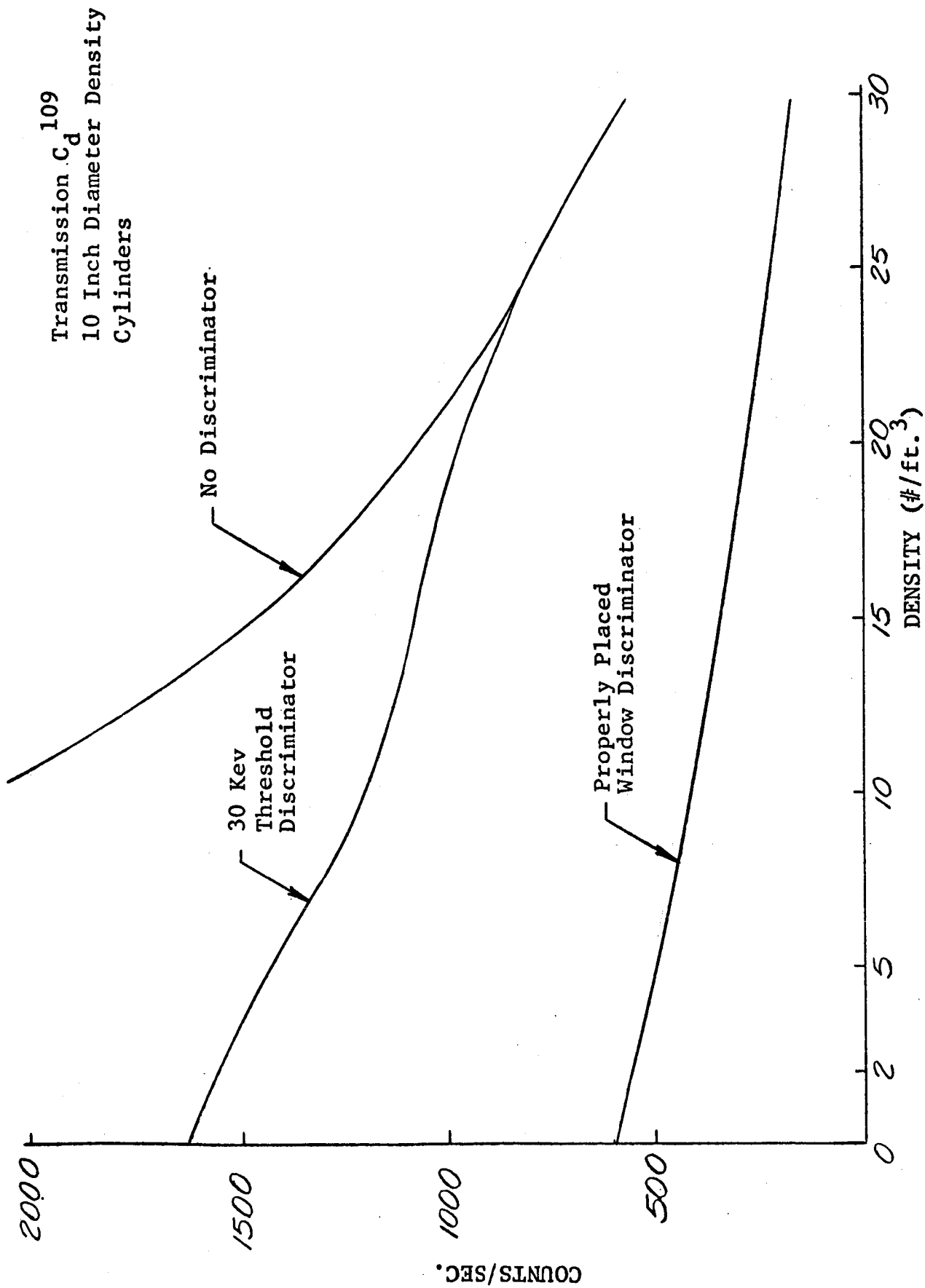
The source strength (I_o) needed to maintain the required statistical error is related to the worst case count rate (50% quality) shown in Figure 3-5. Therefore,

$$\begin{aligned} I_o &= \frac{I}{.82 \times 10^{-3}} = \frac{1.05 \times 10^5}{.82 \times 10^{-3}} \\ &= 1.28 \times 10^8 \text{ photons out} \\ &\quad \text{second} \end{aligned}$$

IT IS ASSUMED THAT THE WINDOW DISCRIMINATOR
REJECTS 90% OF THE INCIDENT PHOTON TO
ACHIEVE LINEARITY (10 INCH PATH LENGTH)



ANTICIPATED COUNT RATE VS DENSITY OF OXYGEN WITH WINDOW
DISCRIMINATOR PROPERLY PLACED
FIGURE 3-8



EXPERIMENTAL γ -PHOTON COUNT RATE VERSUS
SIMULATED OXYGEN DENSITY FOR 10 INCH DIAMETER PIPE

FIGURE 3-9

If Cd^{109} is used:

$$1.28 \times 10^8 \frac{\text{photons}}{\text{sec.}} \times \frac{\text{millicuries}}{3.7 \times 10^7 \frac{\text{photons}}{\text{sec.}}} = 3.46 \text{ millicuries}$$

The feasibility of using soft gamma-radiation for an oxygen quality sensor will now be considered. From Figure 3.8, a 5% change in oxygen density corresponds to a 3.90% change in count rate. The statistical error should not exceed $3.90\%/2$ or 1.95%. To maintain this error, the required count rate can be determined from

$$\frac{1}{\sqrt{2I}} = 1.9 \times 10^{-2}$$

The required count rate is then 1.3×10^4 counts/second. The output flux required to maintain statistical accuracy is related to the worst case count rate (50% quality) shown in Figure 3-8. Therefore:

$$I_o = \frac{I}{.032 \times 10^{-3}} = \frac{1.3 \times 10^4}{.32 \times 10^{-4}} = 4.1 \times 10^8 \frac{\text{photons}}{\text{sec.}}$$

If Co^{57} is used

$$4.1 \times 10^8 \frac{\text{photons}}{\text{sec.}} \times \frac{\text{millicuries}}{3.7 \times 10^7 \frac{\text{photons}}{\text{sec.}}} = 1.1 \text{ millicurie}$$

are needed.

It is concluded that the gamma absorption method will meet all requirements. The source strengths will be reasonable, and shielding weight will be low.

4.0 DENSITY MEASUREMENT BY NEUTRONS

The neutron scattering and absorption cross sections for hydrogen are quite high. Therefore, there is some advantage in sensitivity if neutrons are employed in hydrogen density measurement. Unfortunately, the same is not true for oxygen.

4.1 Neutron Interactions with Matter

Neutron interactions are much more complex than those of gamma, beta, or alpha particles. Neutrons undergo elastic and inelastic scattering and diffraction, and are also captured by nuclei. The probabilities of scattering or capture depend upon the type of nuclei present, and the neutron energy. Since the cross sections vary with energy, the relative proportions of scattering and absorption vary as the neutrons lose energy by scattering. In addition, there are resonances in the capture process. Finally, when a neutron is captured, the capturing nucleus usually emits gamma rays. In view of these complexities, all analytical treatments of neutron absorption leave much to be desired. Fortunately, however, the behavior of neutrons of less than 10 mev in hydrogen is fairly well known.

4.2 Thermalization of Fast Neutrons by Hydrogen

λ , the mean free path for neutron scattering is given by:

$$\lambda = \frac{1}{N\sigma_s} \text{ cm} \quad (4-1)$$

where N is the number of nuclei per cc and σ_s the cross section for scattering. For hydrogen

$$\begin{aligned} N &= 6 \times 10^{23} \rho \\ \sigma_s &= 2 \times 10^{-24} \end{aligned} \quad (4-2)$$

Therefore,

$$\lambda = \frac{1}{1.2\rho} \approx 11 \text{ cm} \quad (4-3)$$

The number of collisions required to reduce the 5 mev neutrons to thermal levels (less than 25 ev) is given by:

$$n = \log_e \frac{W_0}{W} \quad (4-4)$$

where W_0 is the initial energy and W the final energy (25 ev in this case). Since W_0 is 5 mev and W is 25 ev

$$n = \log_e 2 \times 10^5 \approx 12 \quad (4-5)$$

Therefore, about 130 cm of path is required to thermalize all the neutrons. In a 10 inch pipe about 28% of the neutrons entering the pipe would be thermalized. The interior of the pipe then would appear to detectors arranged around the pipe as a source of thermal neutrons whose intensity is proportional to the number of hydrogen atoms in the pipe. The actual source strength would be:

$$I = 0.28I_0 \quad (4-6)$$

The thermal neutron flux from within the pipe will be omnidirectional. Suppose an effective detection area of 25 cm^2 is used. The equivalent source strength at the center of the 10 inch pipe must be

$$I_0 = \frac{4\pi (12.5)^2}{25} I \quad (4-7)$$

where I is the desired detector count rate. If ρ is to be determined to 5%, then I must be 1600 sec^{-1} . Therefore, I_0

will be $1.28 \times 10^5 \text{ sec}^{-1}$. Since only 28% of the incident neutrons are thermalized, the incident flux must be $4.6 \times 10^5 \text{ sec}^{-1}$.

To obtain this number of neutrons from an Am^{241} , Be source, the Am^{241} activity must be $7.7 \times 10^{11} \text{ sec}^{-1}$, or about 20 curies.

4.3 Shielding

The high source strength required imposes rather severe shielding requirements. The fast neutron flux must not exceed $39 \text{ cm}^{-2} \text{ sec}^{-1}$. This would require about 18 cm of water or other hydrogenous substance to surround the installation. Moreover, the alpha emitters useful for the source emit gammas. Am^{241} is about the least objectional in this regard. The gamma dose rate constant for Am^{241} is 0.12 roentgens per hour at 1 cm. To reduce the gamma dose rate at the surface of the source to 2 mr/hr, an attenuation of about 4000 is required. This can be obtained with about 0.2 inch of tungsten.

4.4 Conclusion

It is doubtful that this method will be useful, since the source cost will be quite high, and rather large amounts of shielding are required. In cases where cost and weight are no object, the method will provide very sensitive results with hydrogen.

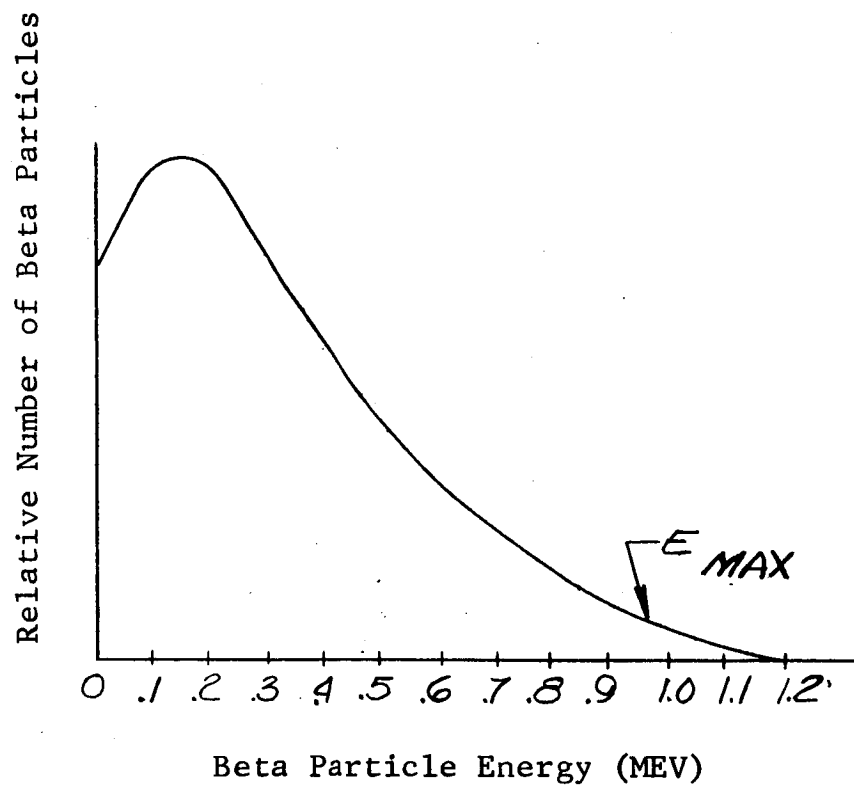
5.0 DENSITY MEASUREMENT WITH BETA PARTICLES

Beta particles are electrons which have been ejected from a nucleus. An unstable nucleus may attain a stable state by changing a neutron into a proton and ejecting a negative beta particle (electron) or by changing a proton into a neutron and ejecting a positive beta particle (positron).

Beta particles exhibit all the properties of fast electrons. A beta ray spectrum is continuous from zero energy to some given maximum depending on the particular radioisotope. An example of such a spectrum is shown in Figure 5-1.

Beta particles lose energy by a number of different processes when passing through matter. Energy is lost either by ionization of the matter or by production of x-rays (Bremsstrahlung).

5.1 Beta Absorption - Heavy charged particles undergo a large number of small energy losses as they pass through matter and the statistical variation in their total energy loss is small. This total range is therefore well defined. Beta particles on the other hand with their low mass have a much greater variation in energy loss with distance into a material. This results from the devious path taken by the beta particles even though the distance traveled by the individual particles is fairly well defined. This uncertainty in maximum range is termed "straggling". The percent transmission follows an exponential relationship very closely until



BETA PARTICLE SPECTRUM FOR RADIUM E

FIGURE 5-1

the maximum range of the beta particle is approached (until the attenuation factor is about 1/20).

The slope of this absorption curve and the maximum range are related to the density of the absorbing material and the energy range of the beta particles used. As an example, Table 5.1-1 gives the approximate mass absorption coefficients for various beta emitting radioisotopes.

For the geometry given in Figure 5-2, the detector count rate (I) is related to density (ρ) as with gamma-rays, as follows:

$$I = I_o \frac{A_d}{4\pi d^2} e^{-\mu \rho d}$$

Where: I_o = output flux
 d = pipe diameter

μ = beta-particle mass absorption coefficient

Differentiating the detector count rate with respect to density

$$dI = \frac{-I_o A_d \mu d}{4\pi d^2} e^{-\mu \rho d} d\rho$$

Dividing by I,

$$\frac{dI}{I} = -\mu d d\rho$$

5.1.1 Hydrogen Vent Pipe - Using $R_u^{106} - R_h^{106}$ source on a 10 inch hydrogen filled pipe, a $\pm 5\%$ change in (50% quality) density reflects a $\pm 15\%$ change in count rate.

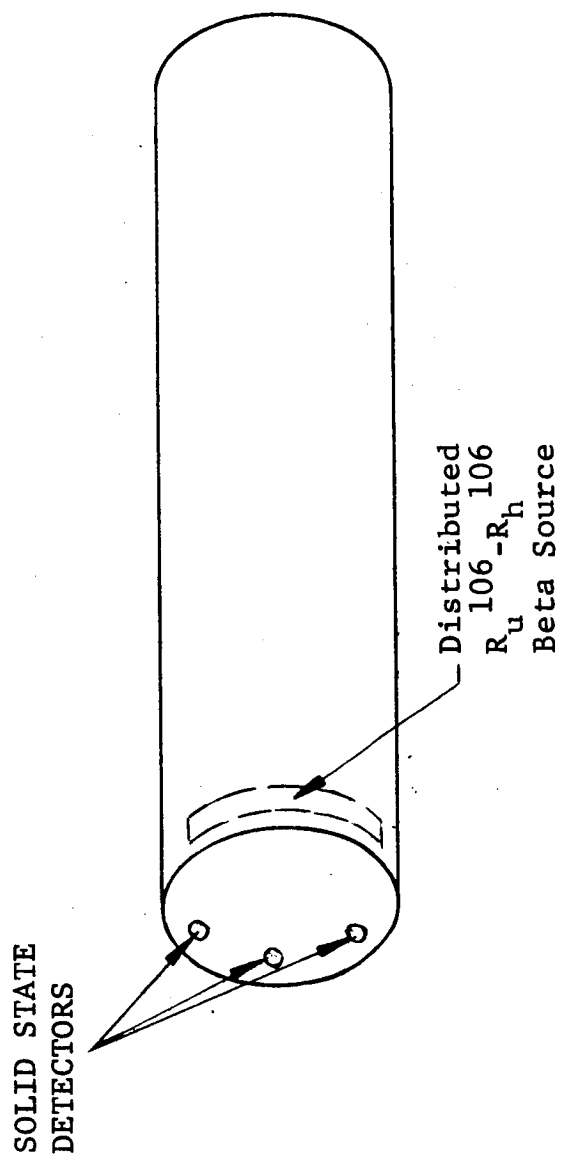
The 2 sigma statistical error is then related to count rate as follows:

$$\% \text{ error} = \frac{2 \times 100}{\sqrt{172}}$$

TABLE 5.1-1

Sources of Beta Radiation Used for Density Measurement

ISOTOPE	HALF-LIFE	MAXIMUM ENERGY (MEV)	APPROPRIATE MASS ABSORPTION COEFF (cm/gm ²)
Hydrogen 3	12 Yrs.	.018	
Nickel 63	85 Yrs.	.062	1000
Carbon 14	5,600 Yrs.	.155	250
Promethium 147	2.6 Yrs.	.223	140
Krypton 85	10.6 Yrs.	.67	30
Thallium 204	2.5 Yrs.	.77	20
Strontium 90 + Yttrium 90	28 Yrs. (64 Hrs.)	2.24	7
Cerium 144 + Praesodymium 144	285 Days (17.5 min)	3.12	4.6
Ruthenium 106 + Rhodium 106	1.0 Yrs. (30 sec.)	3.5	3.4



SOURCE-DETECTOR GEOMETRY CONSIDERED FOR
BETA ABSORPTION TECHNIQUE

FIG. 5-2

or:

$$I = 8.2 \times 10^2 \text{ counts/second}$$

At 50% quality the detector count rate is related to the beta particle disintegration rate (I_o) as follows for three 1 cm^2 solid state detectors mounted inside the 10 inch pipe:

$$\frac{I}{I_o} \text{ (at 50% quality)} = 1.81 \times 10^{-5}$$

Therefore, the disintegration rate required is 4.53×10^7 disintegrations/second. This corresponds to a 1.31 millicurie source strength.

5.1.2 Oxygen Vent Pipe - A $R_u^{106} - R_h^{106}$ source used to monitor a 10 inch diameter vent pipe containing liquid and gaseous oxygen will be considered next. A $\pm 5\%$ (50% quality) density change yields a $\pm 204\%$ change in count rate. The corresponding count rate required to maintain this 2 sigma statistical accuracy is approximately 20 counts/second. At 50% quality the disintegration rate of $R_u^{106} - R_h^{106}$ required would be 13.1×10^{25} disintegrations/second which corresponds to a prohibitive 3.54×10^{15} curies of $R_u^{106} - R_h^{106}$.

5.1.3 "Zero G" Requirement - The "Zero-G" requirement as outlined in Section 3.0 is another prohibitive limitation for the beta absorption technique since no foreseeable means of linearizing the absorption with density or mass orientation has been determined. Without linear absorption, changes in mass orientation can cause erroneous density indication changes.

5.1.4 Conclusions - Beta particle transmission techniques therefore cannot be used for two reasons. This type of sensor would be sensitive to mass orientation and therefore, would not satisfy the "Zero-G" requirements. Also, for large oxygen vent pipes even using extremely high energy beta particles the source strength is prohibitive.

5.2 Beta Scattering - Beta particles (electrons) moving through a material are scattered as a result of their interaction with electric fields of the nucleus and orbital electrons. Scattering of electrons of high energy through large angles is essentially nuclear.

The scattering of beta particles is best described by the classical Rutherford equation. This model uses the atom as a point charge at the center of a spherical shell of electrons. When the beta particle penetrates such an atom large angular deflections result when the particle passes close to the positively charged nucleus.

The source detector configuration considered for this application is shown in Figure 5-3.

The Rutherford law of single scattering is given as follows:

$$\frac{d(I\uparrow)}{d\Omega} = \frac{(I_0\uparrow) \eta z_1^2 z_2^2 e^4 dr}{64\pi^2 \epsilon_0^2 m_1^2 v_0^4 \sin^4 \frac{\theta}{2}}$$

Where: $\frac{d(I\uparrow)}{d\Omega}$ = number of incident particles scattered in scattered angle

$(I_0\uparrow)$ = number of incident particles per sampling period (\uparrow)

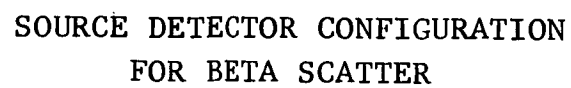


FIGURE 5-3

η = number of scattering centers per unit volume

Z_1 = atomic # of incident particle = 1 for beta particles

Z_2 = atomic # of scattering liquid

e = electric charge

dr = distance from pipe wall to scattering center

ϵ_0 = permittivity of liquid

m_1 = incident particle mass

v_0 = incident particle velocity

θ = angle of deflection

The number of scattering centers per unit volume is related to density as follows:

$$\eta = N\rho$$

Where N = number of atoms per gram

and ρ = density (gm/cm³)

Substituting gives:

$$\frac{d(I\gamma)}{d\Omega} = \frac{(I_0\gamma)N\rho Z_1^2 Z_2^2 e^4 dr}{64\pi^2 \epsilon_0^2 m_1^2 v_0^4 \sin^4 \theta/2}$$

or:

$$\frac{d(I\gamma)}{d\Omega} = K(I_0\gamma) \frac{dr}{\sin^4 \theta/2}$$

The ratio of particles scattered to those incident in a beam per unit solid angle Ω is:

$$\frac{d\gamma}{d\Omega} = \frac{d(I\gamma)}{d\Omega/I_0\gamma} = \frac{K\rho dr}{\sin^4 \theta/2}$$

From the geometry of Figure 5-3

$$d\Omega = \frac{A_d r}{(r^2 + x^2)^{3/2}}$$

and

$$\theta = \pi - \tan^{-1} \frac{x}{r}$$

Substituting and combining these equations,

$$\frac{d\sigma}{dr} = K \rho A_d \frac{r}{(x^2 + r^2)^{3/2}} \frac{1}{\sin^4 \frac{(\pi - \tan^{-1} \frac{x}{r})}{2}}$$

This reduces to:

$$\frac{d\sigma}{dr} = \frac{4K \rho A_d}{x^2} \left\{ \frac{r/x}{(\frac{r}{x})^2 + 1} \right\} \left\{ \frac{(\frac{r}{x})^2 + 1}{2(\frac{r}{x})^2 + 2 \frac{1}{x} [(\frac{r}{x})^2 + 1]^{1/2} + 1} \right\}$$

Integrating this expression from zero to d would yield the ratio of the particles scattered into the detector to those emitted in the beam. However, beta absorption has not yet been considered. Moving the detector towards the beta beam ($x = d/2$) to minimize beta absorption by the liquid oxygen the maximum signal is:

$$\frac{I}{I_0} = \frac{A_d \sigma}{4\pi(\frac{d}{2})^2} e^{-\mu \frac{d}{2} \rho}$$

5.2.1 Beta Source Requirement - For a 10 inch pipe, even using a high energy beta source such as $R_u^{106} - R_h^{106}$ to minimize beta absorption and considering perfect scattering into the detector ($\sigma = 1$) the maximum 50% quality normalized count rate possible would be:

$$\frac{I}{I_0} = 1.04 \times 10^{-14}$$

To detect only one count per sampling period, the output flux rate required would be 4.8×10^{14} beta particles second which corresponds to approximately 2×10^4 curies which is prohibitive.

5.2.2 Conclusion - Beta scatter like beta absorption is of limited usefulness for this application because the maximum B ranges, and all equipment must be inside the pipe.

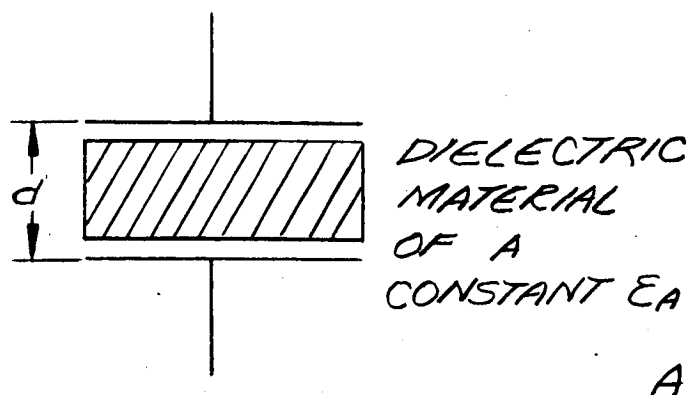
6.0 CAPACITANCE MEASUREMENT METHOD

The capacitance sensor for measuring quality of a cryogenic liquids relies on the very small change in capacitance caused by the difference in dielectric constant between vapor and liquid. Normally, capacitance gauges are highly accurate and reliable. Their desirable characteristics are continuous analogue readouts and lack of moving parts. The errors that are confronted in these systems are contributed by the non-homogenous property of the fluid.

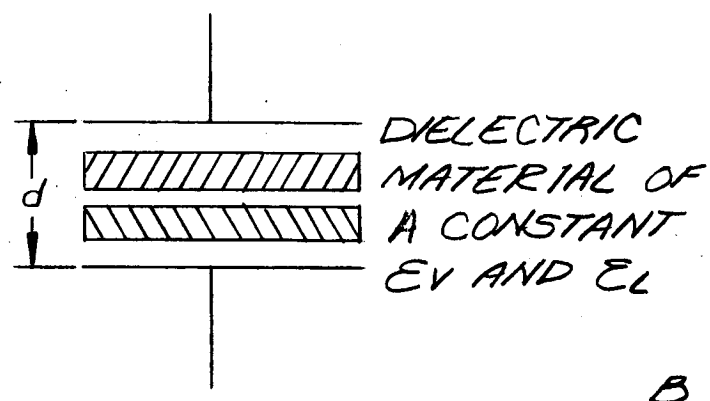
The influx of heat into the fluid decreases its density, and, therefore, convection currents arise which carry this warmer fluid to upper levels in the volume. Stratification occurs in density layers separated by sharp discontinuities. A primary requirement then of a capacitance quality meter would be one which would give a readout independent of the geometrical distribution of the fluid.

The non-homogeneity of the fluid precludes the use of a single parallel plate or coaxial capacitors, since the output of a capacitive sensor depends upon distribution of its dielectric material.

Three of many possible distributions of vapor and liquid are shown in the measured volume of a parallel plate capacitor. (See Figure 6-1). In these examples, the measured volume, plate area and spacing, and average density of the dielectric are shown to be equal. The only variable is the distribution of the liquid and vapor. In Figure 6-1A a homogenous fluid occupies the

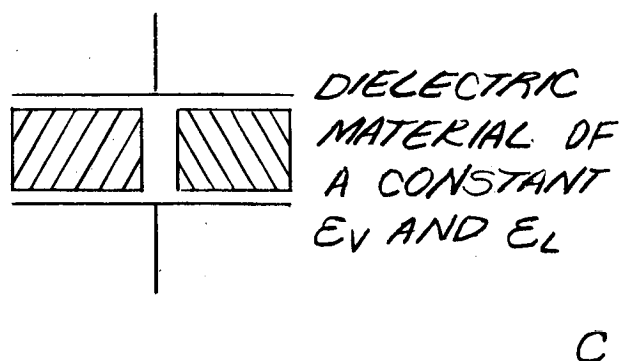


$$C_a = \frac{\epsilon_A A}{d}$$



$$C_b = \frac{C'_V C'_L}{C'_V + C'_L}$$

WHERE $C'_V = \frac{\epsilon_V A}{d/2}$
AND $\frac{\epsilon_L A}{d/2}$



$$C_c = C''_V + C''_L$$

$$C''_V = \frac{1}{2} \frac{\epsilon_V A}{d}$$

$$C''_L = \frac{1}{2} \frac{\epsilon_L A}{d}$$

Illustration Showing Effect Of Geometry On
Capacitance Measurements

FIG. 6-1

volume and its capacitive output is given by

$$C_a = \frac{\epsilon_a A}{d} \quad (1)$$

where ϵ_a = dielectric constant of two-phase fluid

A = area of plate

d = spacing between plates

In figures 6-1B and 6-1C the dielectric is distributed non-homogenously and in accordance with two possible geometries.

In Figure 6-1B the capacitive output would be equivalent to series connected and equal to

$$C_b = \frac{C_v C_L}{C_v + C_L} \quad (2)$$

where

$$C_v = \frac{E_v A}{d/2}$$

$$C_c = \frac{E_L A}{d/2}$$

and E_v and E_L are dielectric constants of the vapor and liquid respectively.

In Figure 6-1C the capacitive output would be equivalent to parallel connections and equal to

$$C_c = C'_v + C'_L$$

$$\text{where } C'_v = \frac{E_v A/2}{d} \quad (3)$$

$$\text{and } C'_L = \frac{E_L A/2}{d}$$

As shown by equations (1), (2), and (3), the output of each capacitor is not equal and depends on the particular distribution of the fluid chosen for the example. All three of these distributions are possible with single parallel plate or

coaxial capacitors; however, only that of example 1(a) is acceptable. In theory, this effect may be accomplished by homogenizing the fluid prior to entering the measured volume or dividing the measured volume into many small capacitive cubes so that a homogenous fluid will be measured in any one volume. The output of the sensor, arranged as such, would be the sum of the output of all the individual capacitive cubs.

6.1 Matrix Capacitors

One possible sensor configuration which meets the geometry requirements is the matrix capacitor. This sensor divides the total volume into a number of small parallel volumes for measurement of the dielectric constant. The capacitance of the complete matrix is the sum of these small capacitive cubes and it is, therefore, proportional to the dielectric constant, ϵ_A , of the fluid in the total volume.

6.1.1 Dielectric Constant of the Fluid: This relationship is given by

$$\epsilon_A = \frac{V}{V} \epsilon_v + \frac{V_v}{V} \epsilon_L \quad (4)$$

where V is the total measured volume of the fluid and v is the volume occupied by the vapor with V .

6.1.2 Dielectric Constant of Vapor: ϵ_v is a direct function of pressure,

$$\epsilon_v = K_1 p \quad (5)$$

where p is the pressure of the vapor and K_1 is a constant.

6.1.3 Dielectric Constant of Liquid: The dielectric constant of the liquid is temperature dependent. For liquid hydrogen, nitrogen, and oxygen, as well as many other fluids, the relationship between temperature t , and ϵ_L is

$$\epsilon_L = K_2 - At \quad (6)$$

where K_2 and A are constants for the liquid. ϵ_L , therefore, is determined by measuring the temperature.

6.1.4 System Equation: By combining equations (4), (5), and (6), the percent vapor in a measured volume is given by

$$\% \text{ vapor} = 100 \frac{(\epsilon_A - K_2 + At)}{K_1 p - K_2 + At} \quad (7)$$

To fully implement equation (7), the dielectric constant, ϵ_A , of the cryogenic must be measured with a simultaneous measurement of its liquid temperature and vapor pressure in the volume it occupies.

6.2 Description of Cryogenic Quality Meter

The instrument described in Reference 1 is designed to indicate the quality of the fluid in a measured volume of a cryogenic flow system. Equation (5) is implemented in the design of this instrument. The sensing element for the dielectric constant of the fluid ϵ_A is a precision-built matrix capacitor. A thermo-resistive element transduces the ϵ_L of the liquid while ϵ_v is set into the instrument manually.

The instrument consists of a test section and an electronic readout package. The test section contains a temperature transducer and the matrix capacitor and is vacuum-jacketed and

super-insulated to minimize heat leakage paths into the volume being measured. The cylindrical-shaped matrix capacitor occupies a volume of two to three cubic inches in a one-inch line. This sensor arrangement minimizes the geometrical effects normally associated with the capacitance measurement methods. Rugged construction of the matrix is required to reduce dimensional distortion due to thermal shock. The temperature of the fluid is measured with a thermo-resistive element prior to entering the matrix volume.

The readout package is a highly sensitive special-purpose analog computer with power supplies, meters, chart recorder, and test equipment. Automatic and continuous inputs to the computer are temperature and capacitance from the test section. The vapor dielectric constant input is set into the computer by a potentiometer on the readout package. This readout package occupies a space about 21 cubic feet, weighs 500 pounds, and consumes about 1,000 watts.

The operating range is 0 to 100% of quality with an accuracy of $\pm 1\%$ at a flow rate of 2 to 20 lbs/hr.

6.3 Advantages and Disadvantages of Matrix Capacitor

The reliability of the matrix capacitor principle is high, since no moving parts are involved. The accuracies attainable in a homogenous fluid of a complete system are better than 1%. Its accuracy is limited, however, by the nature of the liquid whose quality it measures. If the sensor can be introduced in the flow system without any side effects, it would be equally accurate in non-homogenous fluids.

The installation requirement complicates the design of the sensor and its associated installation hardware. The sensor must be rugged to withstand thermal shock, and its installation hardware must be designed to permit only negligible heat leakage into the measured volume. Both distortion of the sensor and temperature variations would introduce uncompensable system errors.

An analogue input to the computer from a temperature transducer corrects variations of the liquid temperature. This device can do no more than indicate the temperature it attains and at its best the temperature of the liquid or vapor in which it is immersed. Transducer response and installation effects will both degrade system accuracy. For optimum performance, the temperature should be measured in the same volume measured for quality. Its installation design should be considerate of the probability of being immersed in a vapor especially when the vapor to liquid ratio is high.

The matrix capacitor is sensitive to position in a 1 g environment and difficult to calibrate dynamically. These difficulties are believed to be caused by a disproportionate flow characteristic to a two-phase fluid. Dynamic calibration of the instrument described in Reference 1 was unsuccessful due to this effect.

It is concluded that capacitance methods will give adequate results in homogeneous flows at 1 g. Capacitance meters would have large errors under zero g conditions.

Reference 1 - Technical Documentary Report No. ARL-TDR-64-18

7.0 DENSITY MEASUREMENT BY SOUND VELOCITY

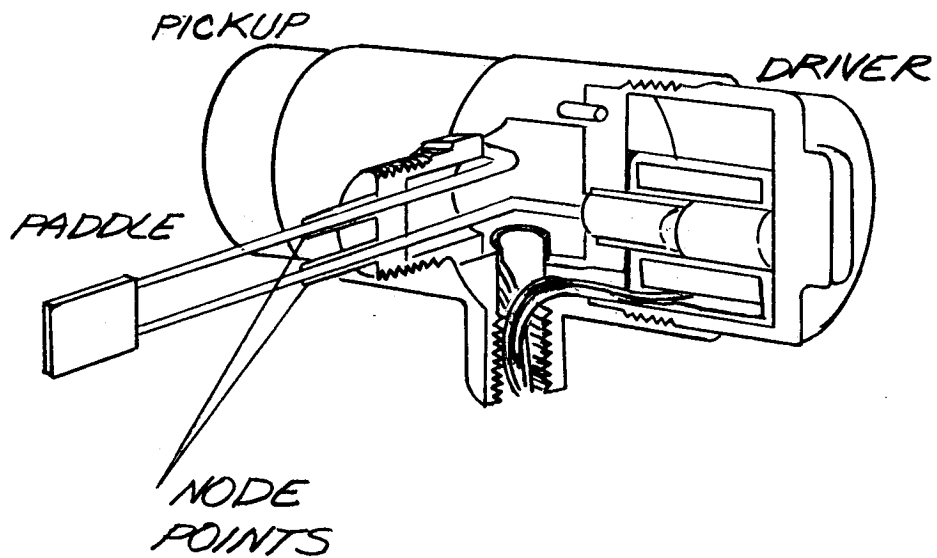
The velocity of sound in Cryogenic liquid is very high. As the amount of vapor in the liquid increases, the velocity of sound decreases because of the increased compressibility. A method of measuring the velocity of sound which also results in measurement of the fluid transport velocity was discovered. In view of NASA interest in mass flow meters, the subject method seemed to "kill two birds with one stone". Accordingly, the capabilities of the technique were fully investigated. The study was performed by the Powertron Division of Giannini Controls Corporation . The results of Powertron's investigation is included separately in Volume 3.

The results indicate that the method will not be useful to the purpose at hand, i.e., that of measuring density from 0 to 50%. However, the method combined with a nucleonic density measurement is applicable to a mass flow meter when the flow contains no more than 20% gas.

8.0 VIBRATING PADDLE SENSOR

Vibrating paddle detectors (see Figure 8-1) have been used with relatively good results as cryogenic point level sensors. A small shaft mounted paddle is set into vibration by an electrical source at 60 or 400 cps. A variable reluctance transducer measures the mechanical damping experienced by the paddle as it comes in contact with the fluid. It is feasible that this principle could be applied as a quality meter, depending upon its sensitivity to density changes. As sensor of quality in a transfer line, its use would be limited to sampling the small volume which would be impingent on its surface. This, of course, would not be the average density of the fluid unless the fluid was homogenized prior to measurement.

Another disadvantage of the sensor is its size, weight, and installation complexity. As a point level sensor, its main desirable feature is its ability to remove clinging droplets of liquid during level changes.



VIBRATING PADDLE

POINT LEVEL

SENSOR

FIG. 8-1

9.0 OPTICAL ABSORPTION

Both hydrogen and oxygen have strong absorption lines in the gas phase which are not present in the liquid phase. Therefore, the total absorption of radiation at these critical wavelengths is a direct measure of the quantity of material in the gas phase. The absorption lines alluded to are in the 4000A° to 4200A° band for oxygen and 4600A° to 4800A° band for hydrogen. There are solid state detectors and scintillation sources in these regions. The method may pose the design problem of providing an optical window in the pipe. On the other hand, a simple, reliable direct measure of the quantity of interest is offered, and the method should be noted.

9.1 Description of Method

The problem is to provide a diffuse illumination of the interior of the pipe at a wavelength which is strongly absorbed by the gas, but not by the liquid. Figure 9-1 illustrates a possible solution to the problem.

The source S illuminates the reflecting grating G. The light is refracted at G according to:

$$\sin \theta_1 + \sin \theta_2 = \frac{n\lambda}{d} \quad (9-1)$$

where θ_1 is the angle between the normal to the grating and the incident beam θ_2 , the angle between the normal and refracted beam λ , the wavelength, d the grate spacing, and n the order of refraction.

For discussion, assume that the incident light is normal to the grating. In this case, equation (9-1) reduces to:

$$\sin \theta = \frac{n\lambda}{d} \quad (9-2)$$

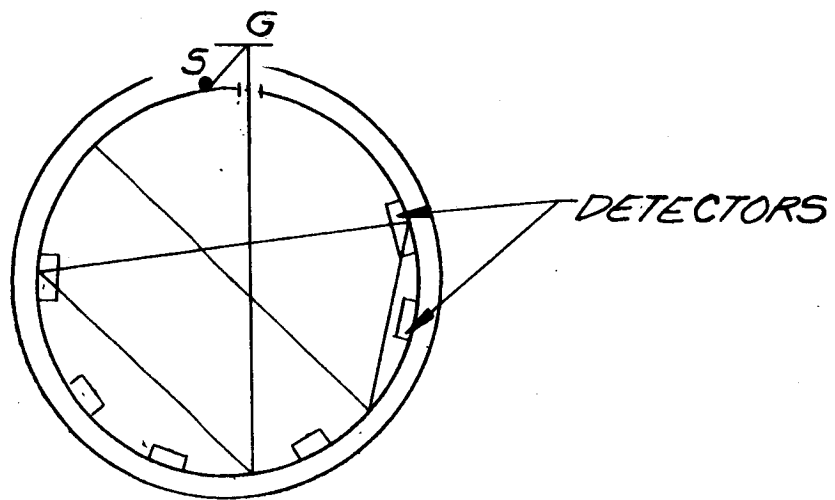
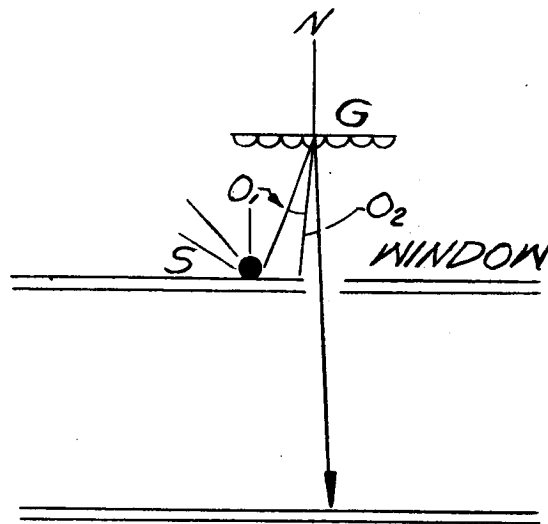
The angular dispersion of the spectrum is given by

$$\frac{d\theta}{d\lambda} = \frac{n}{d \cos \theta} \quad (9-3)$$

Gratings with d as low as 2.5×10^{-5} cm can be made easily.

Therefore, it is evident from equations (9-2) and (9-3) that a choice of d can be made which results in very high angular dispersion as a function of wavelength. The desired wavelength band can be selected accurately.

It is doubtful that this technique could be applied to the present problem, since an optical window is required. This would pose difficult design problems and the window may be obscured by frost or condensation.



OPTICAL GAS LINE ABSORPTION
METHOD

FIGURE 9-1

10.0 DENSITY MEASUREMENT USING MICROWAVE TECHNIQUES

A vent pipe made of aluminum could be used as a circular waveguide for microwave radiation. The radiation fields could be excited at one point and detected at another point down the vent pipe.

The presence of liquid in the vent pipe would cause changes in the amount of microwave energy monitored by the detector by two mechanisms. The first attenuation component results from energy dissipation in the liquid. The other attenuation results from scatter from the liquid vacuum interfaces.

The electric field distribution in a circular pipe depends upon the mode or modes in which the energy is propagated. The radial and longitudinal distribution of electric and magnetic fields in the waveguide depends upon the frequency used, the radius of the vent pipe, and the dielectric constant and distribution of the liquid. For the case of uniform liquid in the pipe, the propagation mode in the vent pipe would be transverse electric or transverse magnetic waves. These waves are distributed as n th order Bessel Functions. For the empty condition, the simplest (primary) mode would be used since for this condition the distribution is certain. However, as the effective dielectric constant of the liquid increases (more liquid is introduced) other modes would propagate. These other modes of propagation also occur when liquid discontinuities are present.

For zero-g conditions, uncertainty in size and location of

liquid mass causes uncertainty in microwave propagation for several reasons:

- 1) The electric field distribution is not uniform and thus the effect of a unit liquid volume in the center of the vent pipe has a different effect than a unit volume towards the size.
- 2) The discontinuities and their distribution in the vent pipe determine the modes of propagation and thus the amount of microwave dissipation and the degree of coupling to the receiver.
- 3) The number and distribution of liquid "globe" determine the amount of scattering from the gas/liquid interfaces.
- 4) The scatter from liquid in other parts of the vent pipe circuit provides an uncertainty in the amount of microwave power detected which also depends upon the amount and distribution of the liquid in the pipe.
- 5) Microwave absorption is exponentially related to path along the vent pipe.

Due to the many uncertainties, it is doubtful that this technique would be useful for determining fluid quality to an accuracy of $\pm 5\%$.

APPENDIX I

EXPERIMENTAL VERIFICATION OF BACKSCATTER CALCULATIONS

In Figure I-A , the configuration tested is shown. The source was placed on axis 3 pipe radii downstream of the detector. The detector was collimated conically to a half-angle of 45 degrees. In the spherical coordinates depicted in the figure, the contribution to the detector count rate of the element dv is:

$$dI = \phi \frac{NZ}{A} \rho [C(\theta)] A_D e^{-\mu PR} \sin \phi d\phi d\theta dr \quad (I)-(1)$$

Since the detector is 3 radii from the volume under consideration, the flux ϕ at the volume under consideration is essentially uniform and is given by:

$$\phi = \frac{I_0}{36\pi R_0^2} \quad (I)-(2)$$

where R_0 is the pipe radius. When the pipe is full at density ρ , (assumed to be uniform) the flux ϕ is given by:

$$\phi = \frac{I_0}{36\pi R_0^2} e^{-3\mu \rho R_0} \quad (I)-(3)$$

Substituting this value in equation (I)-(1) gives:

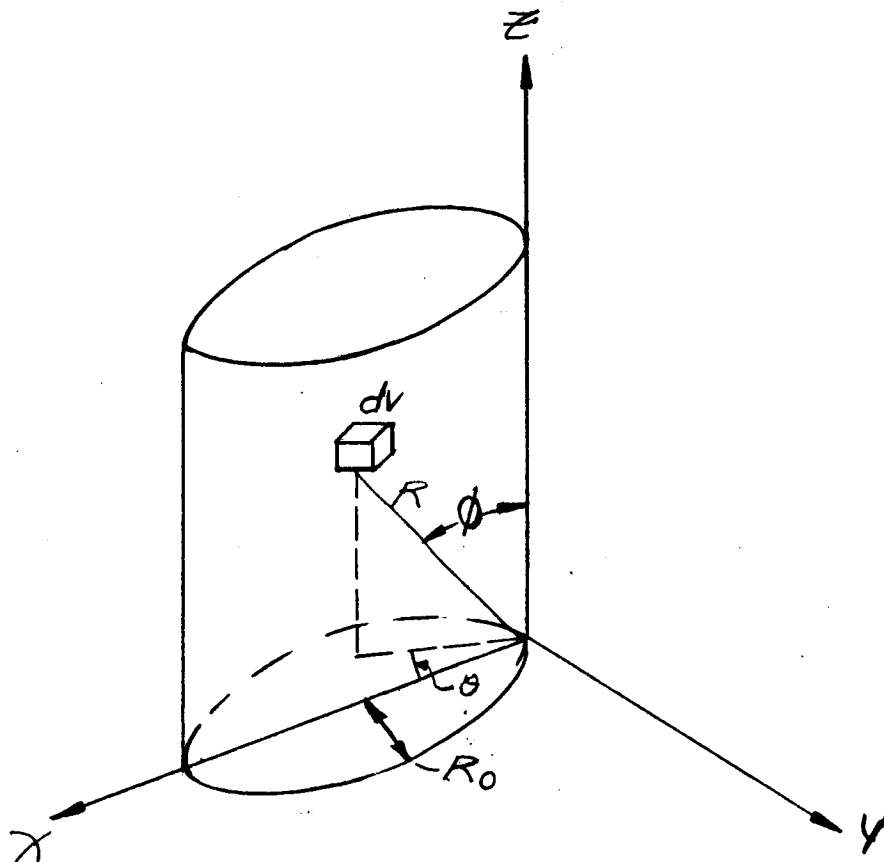
$$dI = \frac{I_0 e^{-3\mu \rho R_0}}{36\pi R_0^2} \frac{NZ}{A} \rho [C(\theta)] A_D e^{-\mu PR} \sin \phi d\phi d\theta dr \quad (I)-(4)$$

The limits of R can be seen from Figure I-A to be dependent upon ϕ and θ . The dependence is given by:

$$R = 2R_0 \cos \phi \cos \theta \quad (I)-(5)$$

The limits on θ and ϕ are $\pi/4$ by design.

Therefore:



GEOMETRICAL NOMENCLATURE
FOR EXPERIMENTAL SETUP

FIGURE I-A

$$I = \frac{I_0}{36\pi R_0^2} e^{-3\mu P R_0} \frac{N^2 \rho}{A} [C(\theta)] A_0 \int_{-\pi/4}^{\pi/4} \int_{-\pi/4}^{\pi/4} \int_0^{2R_0 \cos \phi \cos \theta} e^{-\mu P R} \sin \phi d\phi d\theta dR \quad (I)-(6)$$

The first integration can be carried out without difficulty:

$$I = \frac{I_0}{36\pi R_0^2} e^{-3\mu P R_0} \frac{N^2 \rho}{A} [C(\theta)] A_0 \int_{-\pi/4}^{\pi/4} \int_{-\pi/4}^{\pi/4} (1 - e^{-2\mu P R_0 \cos \phi \cos \theta}) \sin \phi d\phi d\theta \quad (I)-(7)$$

The transcendental function
expanded in the series:

$$e^{-2\mu P R_0 \cos \phi \cos \theta} = e^{-2\mu P R_0 \cos \phi} [1 - (\mu P R_0 \cos \phi) \theta^2 + \dots] \quad (I)-(8)$$

where the two terms shown represent the function of about 0.1% for the range of values in question. Substituting this series permits the second integration:

$$I = \frac{I_0}{36\pi R_0^2} e^{-3\mu P R_0} \frac{N^2 \rho}{A} [C(\theta)] A_0 R_0 \int_{-\pi/4}^{\pi/4} \int_{-\pi/4}^{\pi/4} -e^{-\mu P R_0 \cos \phi} \theta^2 \sin \phi d\phi d\theta \quad (I)-(9)$$

$$= -\frac{I_0}{36\pi R_0^2} e^{-3\mu P R_0} \frac{N^2 \rho}{A} [C(\theta)] \frac{A_0 R_0 \pi^3}{96} \int_{-\pi/4}^{\pi/4} e^{-2\mu P R_0 \cos \phi} d\phi \quad (I)-(10)$$

The integration, again, cannot be carried out in closed form.

However, the integrand of (10) can be placed in the form of the standard secant integral whose values are tabulated. The desired reduction comes about by letting:

$$\phi' = (90^\circ - \phi) \quad (\text{I})-(11)$$

Then

$$\begin{aligned} \csc \phi &= \sec \phi' \\ d\phi &= -d\phi' \end{aligned} \quad (\text{I})-(12)$$

The final expression for I then becomes

$$I = I_0 \frac{e^{-3\mu P R_0} e^{-\mu_w \rho_w t_w}}{1728 R_0^2} \frac{\pi^3 N Z}{A} [C(\theta)] A_D R_0 \rho \quad (\text{I})-(13)$$

The factor $e^{-\mu_w \rho_w t_w}$ accounts for the pipe wall absorption. The experimental setup was made according to Figure I-A with:

$$I_0 = 2.9 \times 10^8 \text{ at } 134 \text{ kev (Co}^{57}\text{)}$$

$$R_0 = 12.5 \text{ cm}$$

$$\frac{NZ}{A} C(\theta) = 10^{-2} \text{ (Computed from curves given in } \underline{\text{Radiation Shielding by Price, Horton and Spinney, McMillan 1957}} \text{)}$$

$$\mu = 0.028$$

$$\rho = 0 \text{ to } 0.5$$

$$A_D = 3.8 \text{ cm}^2$$

$$\rho_w = 8 \text{ gm cm}^{-3}$$

$$t_w = 0.203 \text{ cm}$$

$$\mu_w = 0.18 \text{ cm}^2 \text{ gm}^{-1}$$

Figure I-B shows the comparison of equation (I)-(13) with the experimental data. This result seems to justify the calculations in the body of the report.

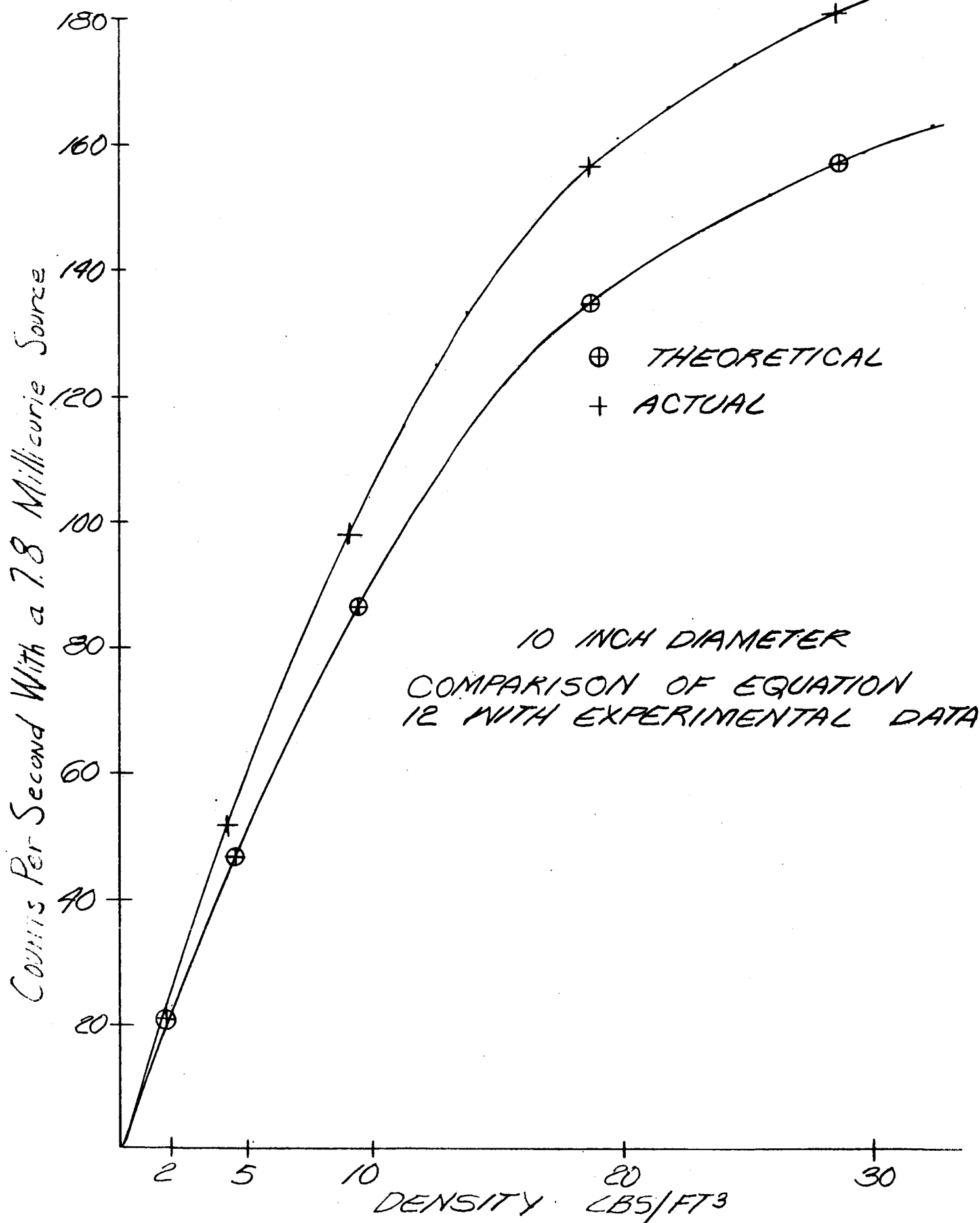


FIGURE I-B

APPENDIX IISTANDARD DEVIATION OF DC OUTPUT

In the body of the report, use was made of the fact that when a discrete signal of random frequency is smoothed by a R-C filter (i.e., integrated) the standard deviation of the filter output is the same as the standard deviation of samples of the input signal taken for time periods of 2τ where τ is the R-C time constant of the filter. A brief derivation of the relation between the input and output standard deviation is given in this Appendix.

It is supposed that a condenser is being charged through a very short time constant and discharged through the time constant $\tau = RC$. It is also assumed that the random pulses are constant in amplitude. Under these assumptions, each pulse contributes a small increment of charge Δq to the condenser.

If the input pulses follow a Poisson distribution (which they do) then the expected number of pulses between times t' and $t' + \Delta t$ is $n \Delta t$ where n is the average pulse rate. The increment of charge is Δq for each pulse. Therefore, the charge acquired by the condenser in Δt is $\Delta q n \Delta t$. At a later time t this charge has decayed to $\Delta q n e^{-\frac{(t-t')}{RC}} \Delta t$.

The expected total charge then is a result of all pulses prior to time t . In other words:

$$q = \int_{-\infty}^t n \Delta q e^{-\frac{(t-t')}{RC}} dt' \quad (\text{II-1})$$

That is, the average charge is

$$q = n \Delta q RC \quad (\text{II-2})$$

The standard deviation of the number of pulses occurring in Δt is $\sqrt{n \Delta t'}$ by definition of the Poisson distribution. Hence, the standard deviation of the charge accumulated in $\Delta t'$ is $\Delta q \sqrt{n \Delta t'}$. At time t this contribution to the output standard deviation is $\Delta q \sqrt{n \Delta t'} e^{-\frac{(t-t')}{RC}}$. The standard law of statistics states that the standard deviation of the sum of a number of contributions is equal to square root of the sum of the squares of the standard deviations of the contributions. Applying this law to the problem at hand gives:

$$\begin{aligned} \sigma^2 &= \int_{-\infty}^t n (\Delta q)^2 e^{-\frac{2(t-t')}{RC}} dt' \\ &= \frac{n (\Delta q)^2 RC}{2} \end{aligned} \quad (\text{II-3})$$

$$\sigma = \sqrt{n} \Delta q \sqrt{\frac{RC}{2}} = \Delta q \sqrt{\frac{n \tau}{2}} \quad (\text{II-4})$$

The standard deviation of the τ second samples of the charge transported by input pulses would be

$$\sigma_i = \Delta q \sqrt{n \tau} \quad (\text{II-5})$$

From equations (II-4) and (II-5) it can be seen that the standard deviation of the integrator output is the same as the standard deviation of the input counted over a period twice as long as the RC time constant of the integrator. Thus, if the integrator is to have a 0.1 second time constant, the standard

deviation of its output will be equivalent to the standard deviation of the input sampled on a 0.2 second basis.

APPENDIX IIICONVERSION OF AVERAGE DENSITY TO QUALITY

The system described in the body of the report determines the average density in a constant volume of the vent pipe. In this appendix, the relations between the average density and quality are discussed.

Let ρ_a denote the average density, and V , V_g , V_L respectively denote the total volume, gas volume, and liquid volume in the fluid under observation. Also, let ρ_g and ρ_L denote respectively the gas and liquid densities. Since the portion of V not occupied by liquid will be occupied by gas, the fluid in V satisfies the following relation:

$$\rho_g V_g + \rho_L V_L = \rho_a V \quad (\text{III})-(1)$$

Furthermore,

$$V_g + V_L = V \quad (\text{III})-(2)$$

Upon solving equations (III)-(1) and (III)-(2) for V_L and V_g , one obtains:

$$V_g = \frac{\rho_a - \rho_L}{\rho_g - \rho_L} V$$

$$V_L = \frac{\rho_g - \rho_a}{\rho_g - \rho_L} V \quad (\text{III})-(3)$$

Note that if $\rho_g \ll \rho_L$ the first of equations (III)-(3) reduces to:

$$V_g = \frac{\rho_a - \rho_L}{\rho_L} V \quad (\text{III})-(4)$$

Furthermore, since the range of pressure variation in the vent

meter section is small and since the compressibility of the liquid is small, ρ_L is nearly constant. Equation (III)-(4) is implemented directly by the density measurement. This was the assumption upon which the original proposal was based.

In other words, the system output measures the quality by volume directly as long as ρ_g is small compared with ρ_L .

If x_V denotes the true volumetric quality, then from equations (III)-(3)

$$x_V = \frac{\rho_a - \rho_L}{\rho_g - \rho_L} \quad (\text{III})-(5)$$

The percent error $\frac{x_e}{x}$ in assuming ρ_g is negligible is given by:

$$\left. \begin{aligned} \frac{x_e}{x} &= (\rho_a - \rho_L) \left(\frac{1}{\rho_g - \rho_L} + \right) \frac{1}{\rho_L} \frac{\rho_g - \rho_L}{\rho_a - \rho_L} \\ &= \frac{\rho_g}{\rho_L} \end{aligned} \right\} \quad (\text{III})-(6)$$

At 37°R, ρ_L is 4.4 PCF and ρ_g is about 0.1. This amounts to about 2.3%. It should also be noted that the error is systematic and therefore can be at least partially cancelled out by calibration. It is therefore concluded that the average density ρ_a measured by the system is a sufficiently accurate measure of the quality by volume.

Assuming that the vent pipe contains only liquid hydrogen in equilibrium with its vapor, then both ρ_L and ρ_g may be determined independently by means of a temperature measurement. This will permit the quality to be determined on a mass basis.

If x denotes the quality, then x can be expressed in terms of the average density ρ_a and the component densities ρ_L and ρ_g by means of equations (III)-(1)

$$x = \frac{\rho_a - \rho_L}{\rho_g - \rho_L} \frac{\rho_g}{\rho_a} \quad \text{(III)-(7)}$$

The block diagram of the system for implementing equation (III)-(7) is given in Figure (III)-(1)

It should be noted that many tradeoffs are possible in the computation of x from ρ_a , ρ_g , and ρ_L .

First, the volumetric quality may suffice for the requirement. In this case, the average density ρ_a will suffice. Secondly, the thermodynamic coordinates in the vent pipe may have sufficiently small ranges of variation to permit simplification through one or more of the following assumptions:

$$\rho_g \ll \rho_L$$

$$\rho_L = \text{const.}$$

$$\rho_g = \text{const.}$$

Another possibility is to measure ρ_a , and T on board and implement equation III-(7) on the ground. This would reduce the amount of airborne hardware.

Finally, one may decide to compute x on board as discussed. The proper approach should be determined by additional review of the over-all requirement.

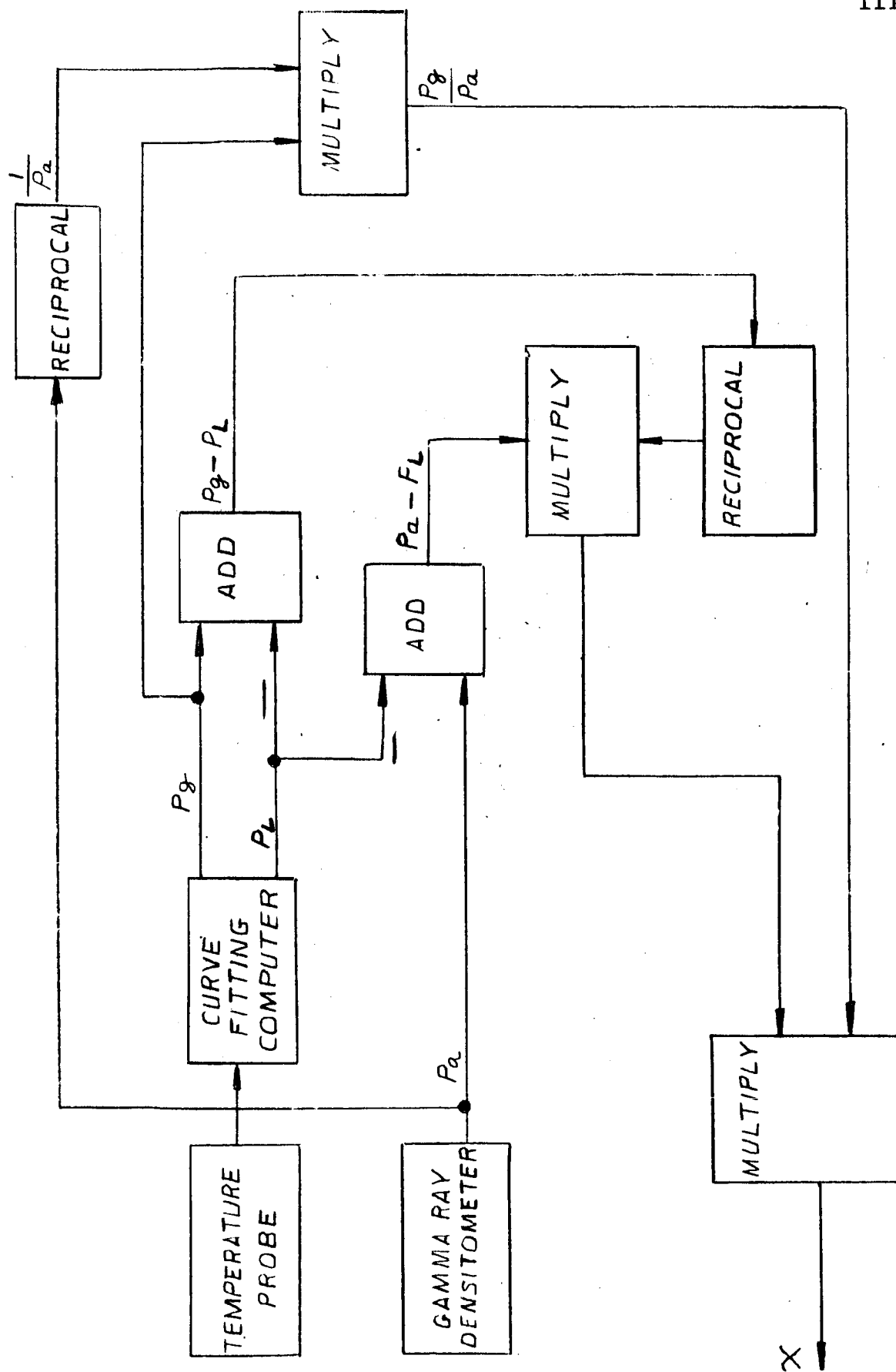


FIGURE (III-1)

APPENDIX IVPRELIMINARY CONSIDERATION OF WAIL WETTING PROBLEM

It has been pointed out that under very low g conditions at low flow rates liquid present in the vent pipe will adhere to the pipe walls in the meter section and result in erroneously low quality readings. In this appendix some preliminary considerations of possible solutions to the problem are given.

It should be noted that the phenomenon under consideration is a problem of vent cycle control as well as of quality measurement. It has been shown in References 1 and 2 that, because of the dependence of vapor pressure on the curvature of the liquid surface, the equilibrium condition would imply (among other things) that the vent pipe would fill with liquid. Therefore, the vent valve must be in the tank vapor space to prevent the vent pipe filling with liquid. This implies that there is no liquid in the vent pipe at the start of the vent cycle. An estimate of the thickness which may be attained by the coating of liquid is presented.

The gas is to be vented at a minimum rate of about 0.1 lb/sec. The gas density is of the order of 0.1 pound per cubic foot. Assuming high quality (which is desired), the flow velocity is about 29 feet per second. According to simple boundary layer theory, the boundary layer thickness would be of the order of 10^{-4} feet. Thus at 10^{-4} feet away from the wall, the gas flow velocity is about 29 feet per second. No liquid layer thicker than the 10^{-4} foot boundary layer would adhere to

the wall. Inasmuch as a liquid layer of 3×10^{-2} feet could be tolerated without exceeding 2% accuracy, it seems doubtful that a problem would exist.

Another consideration which bolsters this conjecture is as follows: It should be noted that the force of adhesion between the wall and liquid is of the order of 50 dynes cm^{-2} . Any liquid present in the pipe would have been entrained in the gas flow. Assuming that the liquid droplets so entrained will enter the pipe with 25 percent of the gas velocity, the droplets would be travelling 7 feet per second. The kinetic energy possessed by a droplet δ cm in radius would be $\frac{2}{3}\pi r^3 \rho \times (210)^2$ dyne-cm. In addition, the droplet will experience a drag force of at least $\frac{1}{2}\rho v^2 C_D \pi r^2$. C_D is greater than 1. The retarding force cannot exceed $200\pi r^2$. Thus, it is doubtful that the adhesion forces would dominate even under the conditions assumed.

Finally, one foolproof solution can be applied, regardless of the foregoing considerations. It may safely be assumed that no significant amount of liquid adhesion could build up in a short time. Therefore, one could close the vent valve upon receiving a low quality indication. This would probably be done anyhow. If a low reading persists after the valve is closed, it would indicate a large amount of fluid adhered to the wall. The line could be blown clear by the tank pressurizing system, and the cycle repeated if necessary. Inasmuch as control of the vent cycle is to be based on the quality meter reading, this provision would not increase the system complexity by a large amount.

REFERENCES:

1. Neu, J. T, and Good, Robert J.

Equilibrium Behavior of Fluids in Containers at Zero Gravity.

AIAA Vol. No. 4 April 1963

2. Benedikt, E. T.

Scale of Separation Phenomena in Liquids Under Conditions of Nearly Free Fall.

ARS February 1959

Giannini Controls Corporation

GIANNINI CONTROLS CORPORATION
Control/Nucleonics Division
Duarte, California

ER-80194

VENT QUALITY METER STUDY

FINAL REPORT

VOLUME II

In Support of

Contract No. NAS8-11814

Prepared for

NATIONAL AERONAUTICS AND SPACE ADMINISTRATION
Marshall Space Flight Center
Huntsville, Alabama

W. J. McKinney, Contracting Officer
C. D. Arnett, Contracting Officer's Representative
Fluids Mechanic Section
Fluids Mechanic and Thermodynamics Branch
Propulsion Division
Propulsion and Vehicle Engineering Laboratory
Research Operation

7 December 1964

Giannini Controls Corporation

Prepared by:

J. G. Kyser

J. G. Kyser
Project Engineer

Approved by:

J. B. Fishman for

D. E. Wright
Manager, Advance Systems
Control/Nucleonics Division

TABLE OF CONTENTS

	<u>Page</u>
1.0 COMPARISON OF VARIOUS METHODS	1
1.1 Summary of Advantages and Disadvantages of Various methods	1
2.0 RECOMMENDATIONS	3
3.0 DESIGN CONSIDERATIONS	4
3.1 Source Considerations	4
3.2 Detector Considerations	9
4.0 SYSTEM DESIGN PARAMETERS	11
4.1 System Block Diagram	11
4.2 Mechanical Considerations	13
5.0 Analysis of Source Strength Requirements	14
5.1 Small Pipe with Hydrogen	14
5.2 Shielding Required	19
5.3 Intermediate Pipe Diameters with Hydrogen	20
5.4 Large Pipes with Hydrogen	20
5.5 Source Strength for Small Oxygen Lines	20
5.6 Larger Oxygen Pipes	21
6.0 SHIELD DESIGN	21
7.0 ELECTRONIC CIRCUIT CONSIDERATIONS	24
8.0 SYSTEM SPECIFICATIONS	25
9.0 TEST AND CALIBRATION	26

TABLE OF CONTENTS
(Continued)

	<u>Page</u>
 <u>LIST OF FIGURES</u>	
Figure 3-1 Photon Energy	6
Figure 4-1 System Block Diagram	12
Figure 4-2 Configuration for 8 to 10 inch Diameters	15
Figure 4-3 Configuration for 1 to 3 inch Diameter	16
Figure 4-4 Configuration for 3 to 8 inch Diameter	17
Figure 6-1 Shield Arrangement for Small Pipes	22
Figure 6-2 Shield Arrangement for Large Pipes	23
 <u>LIST OF TABLES</u>	
Table 2-1	5
Table 3-1	7

1.0 COMPARISON OF VARIOUS METHODS

The descriptions and characteristics of several techniques for measuring average density in pipes from 1.0 inch to 10.0 inch diameters were given in Volume I. In this section, the various methods will be compared on the basis of the following parameters:

- (a) Sensitivity and accuracy
- (b) Ability to function at zero g
- (c) Cost
- (d) Size and Weight
- (e) Ease of Calibration and use

1.1 Summary of Advantages and Disadvantages of Various Methods

1.1.1 Gamma Ray Backscatter: This method appears to be very attractive. It can be implemented with simple hardware. The source strengths required are reasonable which will result in low cost and light weight. It has two disadvantages.

- (a) The source must be installed inside the pipe to avoid excessive scattering from the pipe walls.
- (b) The linearity is inadequate for large pipes at high density.

1.1.2 Gamma Ray Absorption: This method likewise appears feasible. It can be implemented with simple hardware and reasonable source strength. It can be designed to cover the full range of performance required. It has a single disadvantage

which is that a minimum absorption path length of 10 inches is required. All equipment can be mounted externally.

1.1.3 Neutron Absorption and Thermalization: This method can be designed to meet the full range of performance requirements. All equipment can be mounted externally. However, the source strength requirements are severe, and heavy shielding is required. The source would be prohibitively expensive.

1.1.4 Beta Ray Density Measurements: It is doubtful that beta ray techniques could be implemented at all. If they could, the source strengths are very high and the sources and detectors must be inside the pipe.

1.1.5 Capacitance Density Measurements: This method is very practical for measurement when the fluid is relatively homogenous. For the reasons discussed in Section 6.0, it seems extremely doubtful that the capacitance method can be successfully applied under zero g, low flow conditions over the range of densities required.

1.1.6 Sound Velocity: No foreseeable method permits measurement of sound velocity over the range of fluid density required. However, the ultra sonic velocity method seems very promising for flow meter application provided the gas content does not exceed 20%.

1.1.7: Density Measurement by Viscosity Effects: The use of vibrating reeds to distinguish between all liquid and all gas conditions has been successfully demonstrated. The change in total damping under these conditions is fairly large. It is

doubtful that the changes in damping which result from small density changes would be large enough to observe with a practical vibrating system. Moreover, the problem of locating the vibrating system to measure average changes in a zero g two-phase system is very complex. Finally, the reliability of vibrating systems is subject to question. Size and weight would be a problem.

1.1.8 Optical Absorption: This technique provides a direct measurement of the quantity of interest, i.e., the ratio of gas to liquid mass. The hardware required is obtainable. The only serious disadvantage, which is obvious, is the need for an optical window in the pipe. It is believed that in circumstances which permit such a window this technique would provide excellent results.

1.1.9 The microwave technique would probably not achieve the required accuracy under any conditions. Moreover, some severe design problems would be introduced in coupling the transmitter and receiver to the pipe.

2.0 RECOMMENDATIONS

The method which best meets the range of requirements is absorption of soft gammas. It appears that the gamma source quantum energy can be selected to be high enough to penetrate the pipe and still show strong enough absorption in the fluid to meet the accuracy needed for all fluids. The single disadvantage of this method is the need to maintain a minimum absorption path length. The description given in Section 3.0,

Volume I, analyzed the parameters of the system, assuming a 10-inch absorption path with H_2 . Actually, the minimum path usable is 8.0 inches. For pipes whose diameter is smaller than this, provision must be made to provide the required 8.0 inches in H_2 . If this cannot be done, then the backscatter method is applicable. In oxygen the minimum path needed is 2 inches which does not pose much problem.

To recapitulate, it is recommended that gamma ray absorption be used. If cases arise in which the minimum path requirement cannot be met, gamma backscatter should be used. The comparison of techniques is tabulated in Table 2-1.

3.0 DESIGN CONSIDERATIONS

The hardware for the two gamma ray techniques is virtually identical. Therefore, all remarks regarding source and detector selection may be considered to be the same for both techniques.

3.1 Source Considerations

It is desired to mount all system components outside the pipe. The total mass absorption coefficients for steel, aluminum, hydrogen and oxygen are given in Figure 3-1. Note that at slightly above 100 kev the coefficients for iron and hydrogen are about equal and are about $0.3 \text{ cm}^2 \text{ gm}^{-1}$. Below 100 kev the curve rises steeply for steel, but not much for hydrogen. There is no point in going below 100 kev to improve the absorption in hydrogen, but the pipe wall loss can be greatly reduced by going above 100 kev. In fact, the range from 100 to 200 kev is usable, the pipe wall loss decreasing steadily with the higher values.

Technique	Hardware Availability	Cost	Access to Pipe Interior Required	Shielding Requirements	Reliability	Covers full Range of Requirements	Remarks
Gamma Absorption	Excellent. Readily available.	Moderate	No	Moderate	High reliab. sys. available.	Yes, if minimum path can be provided	Method of choice where applicable
Gamma Backscatter	Excellent. Readily available.	Moderate	Probably yes	Moderate	High reliab. sys. available.	No	Supplements gamma absorption technique
Neutron	Readily available.	High	No	Severe	High reliab. sys. available.	No. Applicable only to hydrogen.	Not recommended.
Beta Ray	Readily available.	Moderate	Yes	Minimal	High Reliab. sys. available	Doubtful	Not recommended.
Capacitance	Available. Development required for this application.	Moderate	Yes	N/A	High Reliab. sys. can be designed.	Doubtful	
Ultra sonic	Available.	Moderate	Yes	N/A	High reliab. sys. can be designed	No. Does not function with high vapor content.	Recommended for flow meter application where vapor content does not exceed 20%.
Damping of Vibrating System	Unknown. Method has been used for point level sensing	Probably low	Yes	N/A	Doubtful	No	Not recommended
Optical Absorption	Comp. Avail. Sys. Develop. required for this application.	Low	Optical window required	N/A	High reliab. sys. can be developed.	Yes	Provides direct meas. of gas to liquid mass ratio. Should give excellent results if optical window requirement can be met.

TABLE 2-1

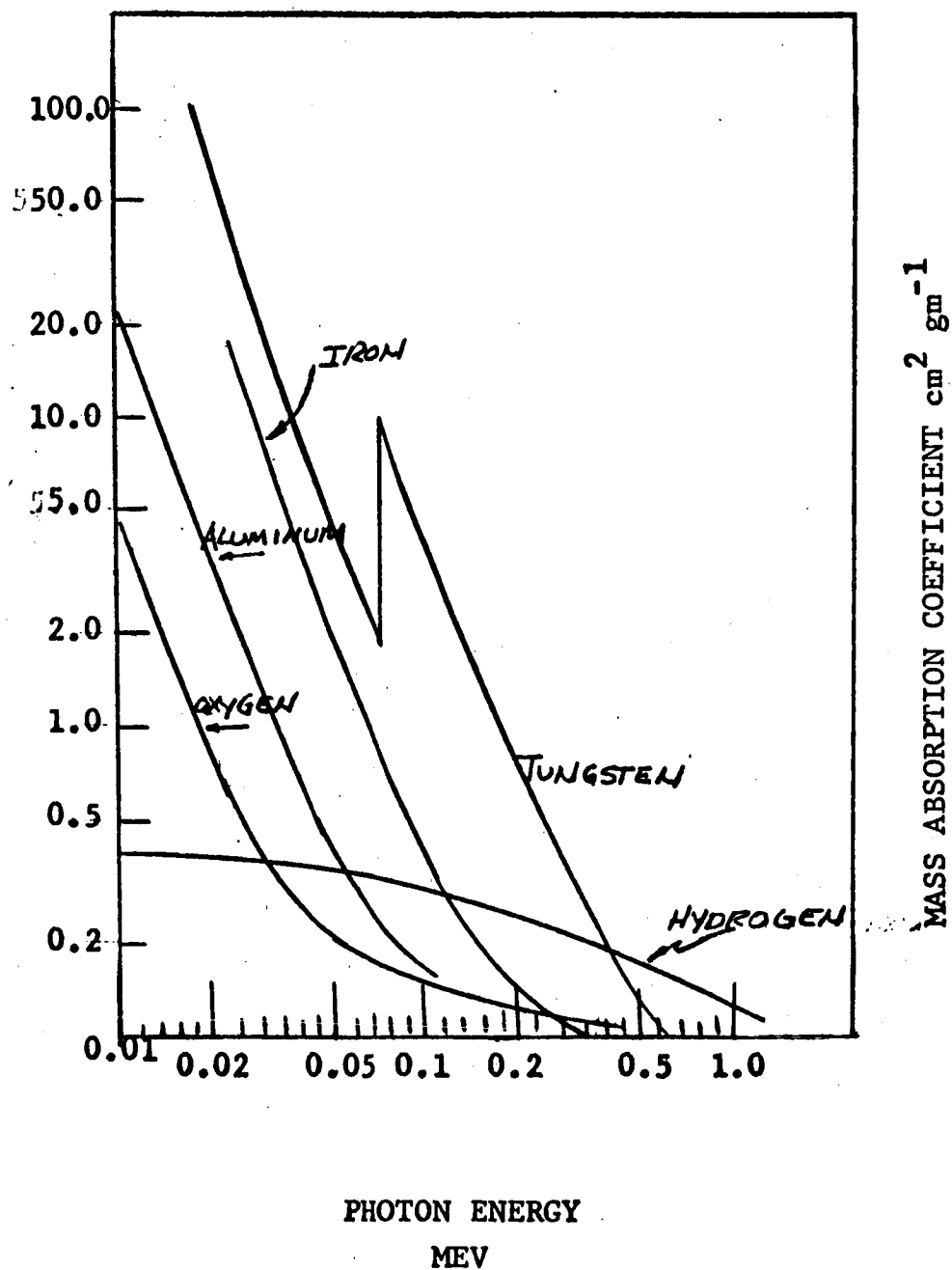


FIGURE 3-1

Isotope	Gamma Ray Photon Energy (mev)	Half Life (years)	Price
Americium 241	0.06	458	\$2.00/mc
Cadmium 109	0.087	1.3	50.00/mc
Cobalt 57	0.122	0.74	6.00/mc

TABLE 2-1

This is not the only consideration involved, however. Table III-1 lists then the isotopes available and gives their half lives and approximate prices. A number of other isotopes have gamma lines in the range of interest, but are not considered for one or more of the following reasons:

- (a) They have other high energy gammas, which would make shielding difficult.
- (b) They have impossibly short half lives.
- (c) They are prohibitively expensive.

From the three considered, Cd^{109} can be eliminated. This reasoning is as follows: Although the half life of Cd^{109} is considerably longer than that of Co^{57} , it is still too short to meet the usual storage life requirements. Therefore, one would either have to schedule source procurement according to operational plans or purchase excessive source strength in the beginning to assure adequate source strength at the time of use. Co^{57} is cheaper even considered on a half life basis. Therefore, use of Cd^{109} would result in extra cost without additional real advantage.

The choice then is between Americium and Cobalt. Americium has no half life problem and is cheap, but the gamma photon energy is a little below the optimum. It will be heavily absorbed in the pipe wall, so that additional source strength is needed to make up for the pipe wall absorption. The absorption of 60 kev is about 14 times more than that at 122 kev. The shield requirement for Americium will be greater than for Cobalt, both because of the additional source strength and because the Americium gamma is below the K-edge of the useful shielding material. Again, on a half life basis, Americium is cheaper. Therefore, the trade

is between price, operational simplicity, and weight.

The shield weights for both sources will be given in Section 6.0.

3.2 Detector Considerations

The standard types of gamma ray detectors are

- (a) ion chambers
- (b) geiger tubes
- (c) solid state detectors
- (d) scintillators.

Of these, the first two are automatically eliminated by the environment. The gases involved would freeze well above the low temperature limit involved.

The choice is therefore between solid state detectors and scintillators. This choice in turn resolves to a consideration of the relative efficiencies.

The absorption efficiency of solid state detectors is considered first.

At 60 kev (assuming Americium is used), the mass energy absorption coefficient for silicon is $0.12 \text{ cm}^2 \text{ gm}^{-1}$. Detectors with depletion thickness of 2 to 3 mm are commonly available. Therefore, the absorption efficiency is:

$$\left. \begin{aligned} \eta_a &= 1 - e^{-0.12 \times 0.3 \times 2.4} \\ &= 1 - e^{-.086} \\ &= 1 - 9.25 \\ &= 7.5\% \end{aligned} \right\} \quad (3-1)$$

The area of these junctions is about 0.5 cm^2 commonly. The price of a detector of the above description is about

\$300.00. The pulse height at the detector can be estimated from the following considerations. Three electron volts are required to produce an ion pair in silicon. Thus, a fully absorbed 60 kev particle would produce 20,000 pairs. Assuming all the ions could be collected in 10^{-8} seconds, the average value of the current pulse would be 2×10^{11} electrons per second. This is in turn 3.2×10^{-7} amperes. The assumption of a pulse width of 10^{-8} seconds precludes a load resistance of more than 100 ohms, and also implies rather high bias voltages (500 to 1000 volts). Thus, the voltage pulse height at the detector output could not exceed 3×10^{-5} volts. It should be noted that back current pulses at room temperature would be of the same order of magnitude. One would have to employ a high gain pre-amplifier, and the detector junction would have to be maintained well below room temperature in order to utilize a silicon device at all. It is therefore concluded that the only practical detector capable of fulfilling the requirement at hand is the scintillator.

By way of comparison, it is noted that the absorption efficiency of sodium iodide scintillator is virtually 100% at the energy under consideration. A crystal with an active area of 5 cm^2 can be obtained for about \$100.00. As for pulse height, about 15 ev are required for release of a visible photon in NaI. Therefore, full absorption of 60 kev would produce 4,000 visible photons. About half these photons become incident on the cathode of a photomultiplier tube under good coupling conditions. About one in forty of the photon incident on

the cathode will eject a photo electron. Thus, about 50 photo electrons correspond to a 60 kev photon absorption. Typical PMT current gains are around 10^7 . Therefore, the PMT anode current (assuming the same circuit parameters as postulated for the solid state detector) is about 6×10^{16} electrons sec^{-1} , or about 9.6×10^{-3} amperes. The voltage output at the photomultiplier anode is then nearly one volt which can be handled without further amplification. The room temperature dark current pulses from a good photo tube are of the order of 1000 ev. Thus, the noise pulses can be easily sorted from the signal on an amplitude basis.

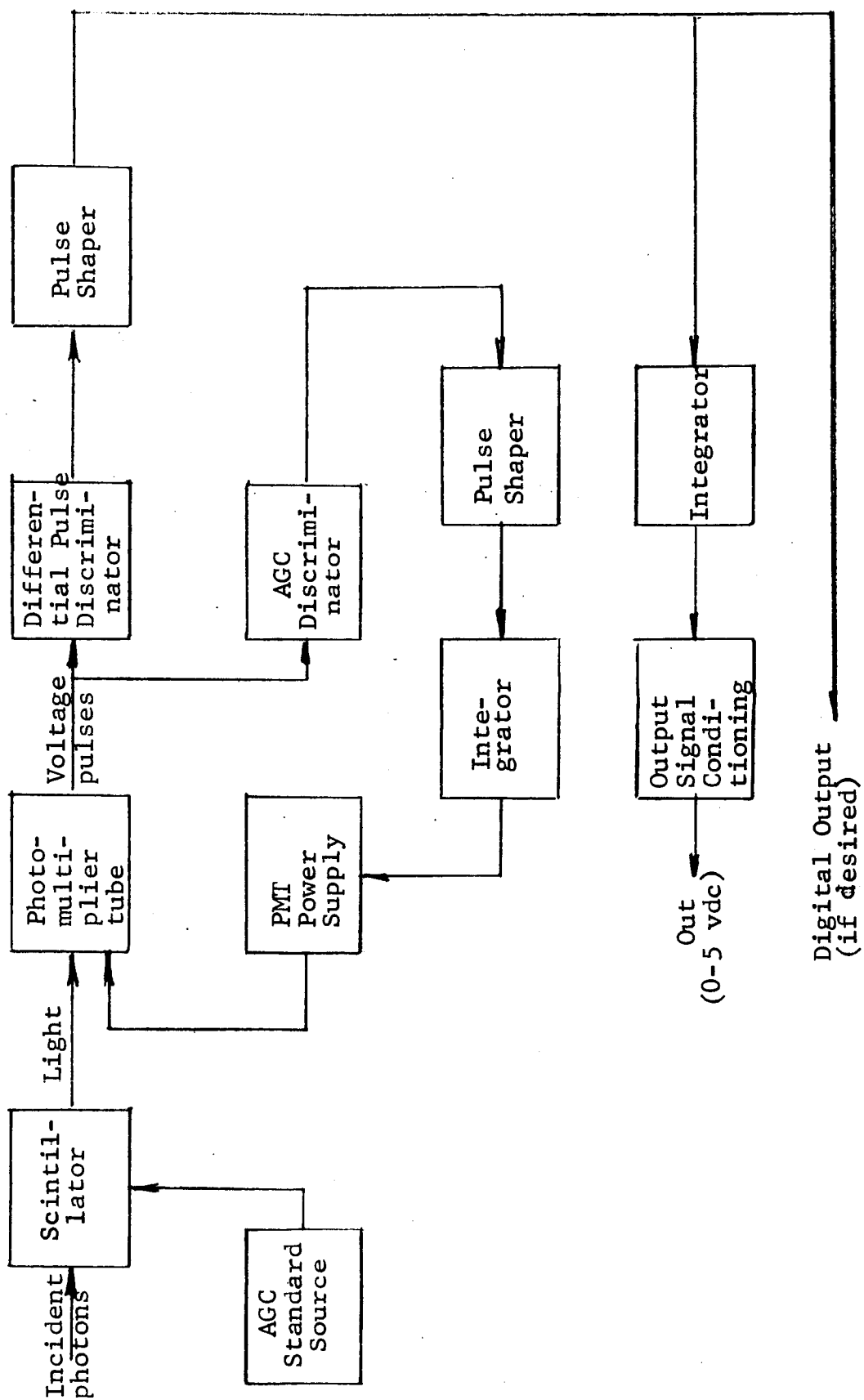
The choice of detectors seems to be the scintillator in light of the foregoing considerations.

4.0 SYSTEM DESIGN PARAMETERS

4.1 System Block Diagram

Figure (4-1) is a block diagram for either a gamma ray absorption system or a gamma ray backscatter system.

The system operation is as follows. The incident photons which have either been transmitted through or back-scattered from the fluid in the pipe impinge on the scintillator. Each photon results in a light pulse whose amplitude is proportional to the energy absorbed from the photon. Each photon may leave any part or all of its energy in the detector. The light pulses are transmitted to the photomultiplier tube which converts each light pulse to an electrical pulse. The photomultiplier tube introduces some distortion in amplitude since each incident photon does not always produce the same number

SYSTEM BLOCK DIAGRAM
FIGURE 4-1

of photo electrons. The scintillator itself introduces some amplitude distortion since the light loss in the scintillator depends to an extent upon the particular element of volume of the scintillator in which the light pulse originates. Suffice it to say that in the energy range of interest about 85% of the incident photons can be found under the total absorption peak.

The differential pulse height analyzer is used to select only the desired portion of those pulses which are caused by photons which have not interacted in any way with the fluid, and those which have partially interacted. This operation is needed to achieve the necessary linearity as discussed in Sections 2.0 and 3.0 of Volume I.

The selected pulses are passed to a pulse shape which transmits a pulse of uniform height and duration for each input pulse regardless of the input pulse shape. These pulses are passed to the integrator and output signal conditioning circuits to generate the desired 0-5 volt dc output.

4.2 Mechanical Considerations

Figures 4-2 to 4-4 illustrate methods of fitting the vent quality meter hardware to the pipes.

4.2.1 For pipes of diameter 8 inches and over: (It should be noted that pipes up to 18 inches diameter could be suitably instrumented by this method.) No modification of the pipe is required for pipes of this size. The source and detectors are merely clamped around the pipe as shown in Figure 4-2. The source is a distributed line source shaped to give a uniform

flux throughout the cross section of interest. On the larger pipes, several detectors are used to give uniform coverage. It is believed that four detectors will give adequate coverage for the 10-inch pipe with 14-inch outer jacket.

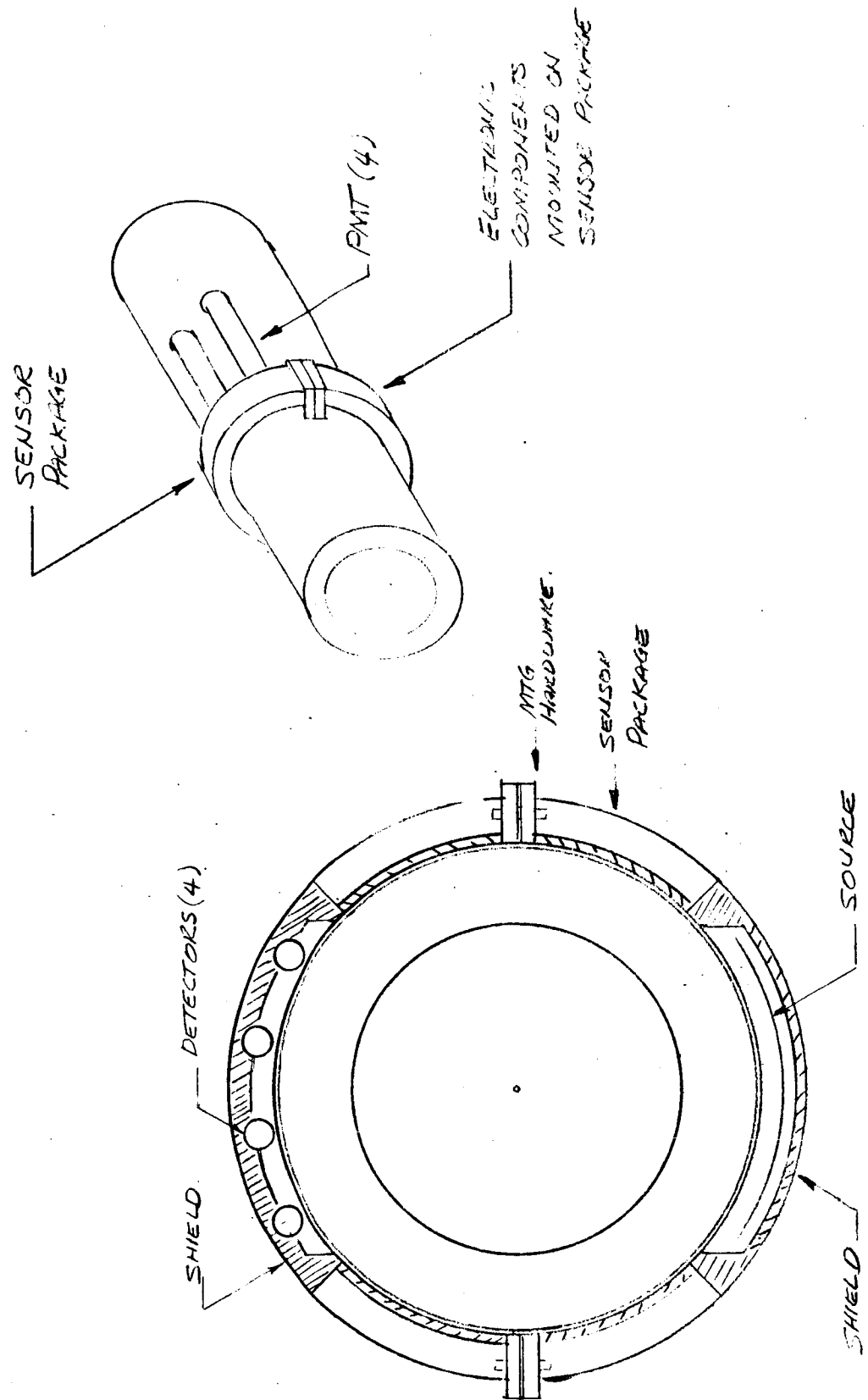
4.2.2 Figures 4-3 and 4-4 show methods of obtaining the required 8 inch minimum absorption path. A single detector is used for the 1-inch to 3-inch range, two for the 3- to 5-inch range, and three for the 5- to 7-inch range.

5.0 Analysis of Source Strength Requirements

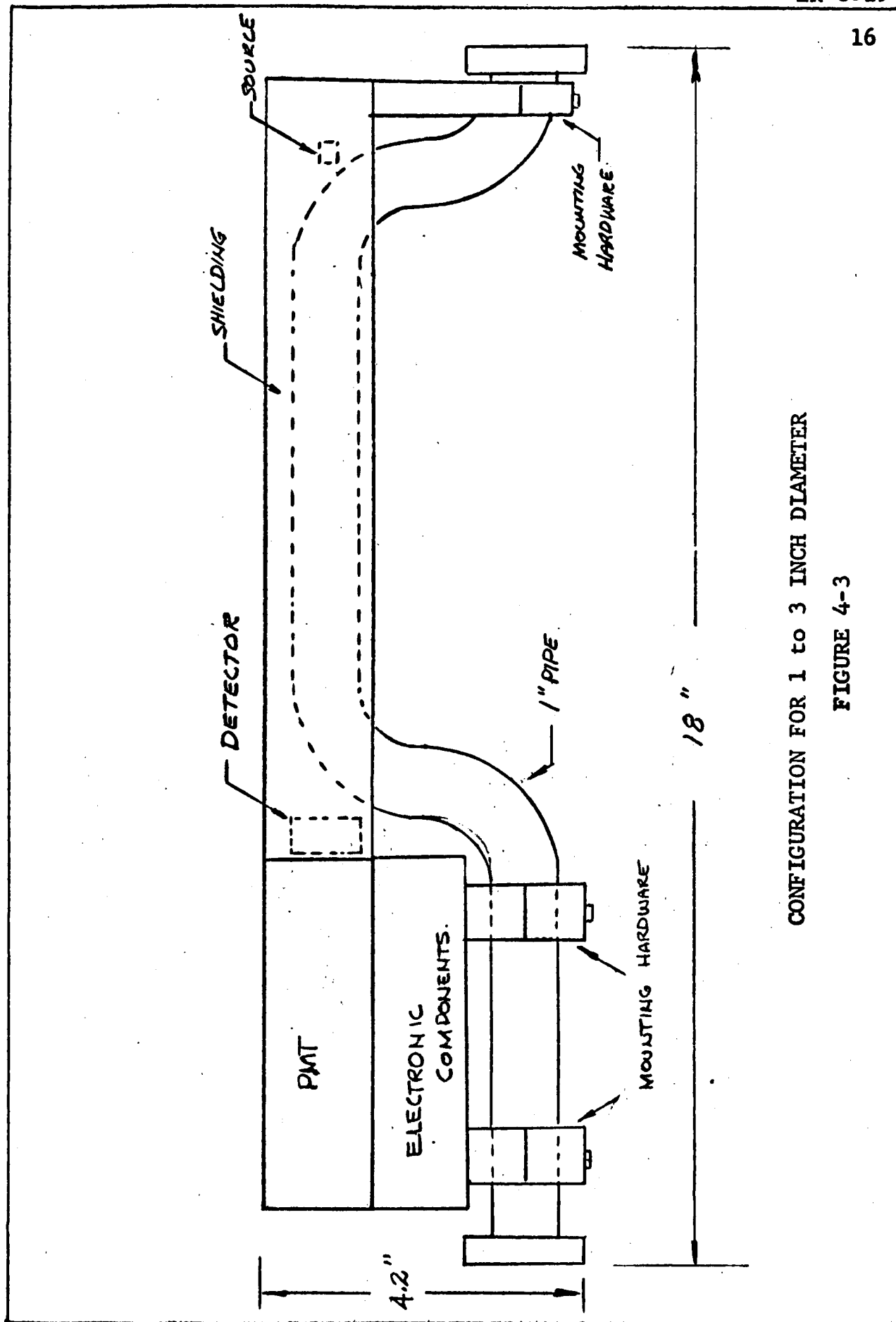
The source strength analyses given in Sections 2.0 and 3.0 of Volume I were primarily derived to illustrate the explanation of the various techniques. In this section a more detailed discussion is given for each design case.

5.1 Small Pipe with Hydrogen: The worst case is an 8-inch absorption path. On a 1-inch pipe, with the detector installed as in Figure 4-3, the detector area available is 5 cm². If the detector is 1 cm thick it absorbs all the incident radiation. It is assumed that the pipe is vacuum jacketed so that four wall thicknesses must be penetrated. It is further assumed that the wall thickness is 0.035" or 0.089 cm and is made of steel. From Figure 3-1 it is noted that the mass absorption coefficient for steel is about 1.2 cm² gm⁻¹. The density is about 8 gm cm⁻³. Therefore, the loss in traversing four walls is given by:

$$\left. \begin{aligned} \frac{I}{I_0} &= e^{-1.2 \times 8 \times 0.356} \\ &= 0.033 \end{aligned} \right\} \quad (5-1)$$

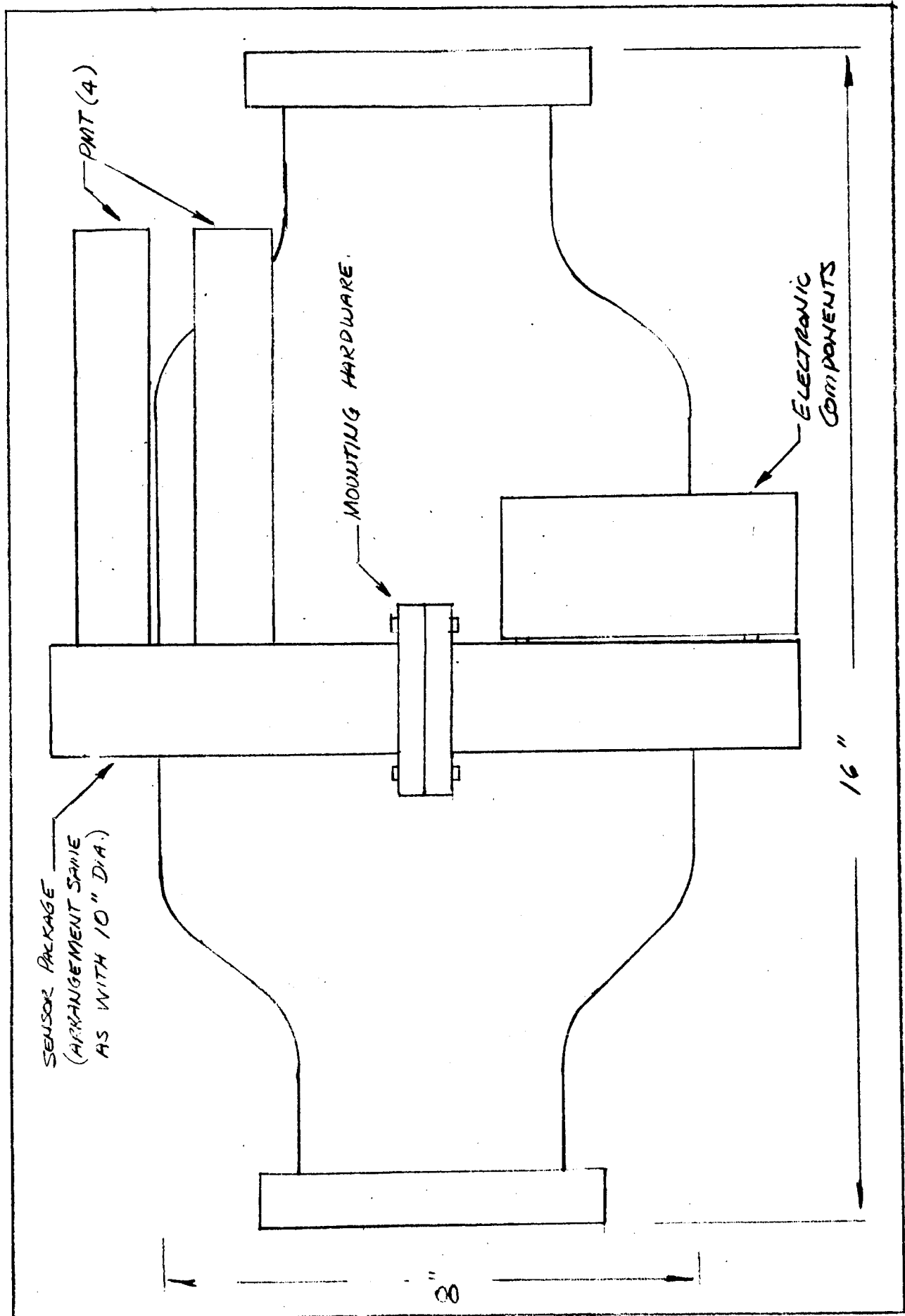


CONFIGURATION FOR 8 TO 10 INCH DIAMETERS
FIGURE 4-2



CONFIGURATION FOR 1 to 3 INCH DIAMETER

FIGURE 4-3



CONFIGURATION FOR 3 TO 8 INCH DIAMETER
FIGURE 4-4

Thus, a loss of about thirty times occurs if Americium 241 is used. If Cobalt 57 is used, this loss will be reduced to about 1.8 times since the mass absorption coefficient of steel at 120 kev is only $0.2 \text{ cm}^2 \text{ gm}^{-1}$.

The detector count rate is given by:

$$I = \frac{I_0 A_D}{4\pi x_0^2} W e^{-\mu x_0 \rho} \quad (5-2)$$

where I_0 is the source strength, A_D the detector area, x_0 the distance from source to detector, W the wall loss, μ the mass absorption coefficient for hydrogen, and ρ the density of the fluid in the pipe.

For hydrogen, the maximum value of $\mu x_0 \rho$ will be about 0.24 in the range of interest. Therefore, the first two terms of the series expansion for equation (5-2) can be used with the less than 1% error. Equation (5-2) then becomes:

$$I = \frac{I_0 A_D}{4\pi x_0^2} W (1 - \mu x_0 \rho) \quad (5-3)$$

The derivative of equation (5-3) is:

$$\frac{dI}{d\rho} = -\frac{I_0 A_D W}{4 x_0^2} \mu x_0 \quad (5-4)$$

Combining equations (5-3) and (5-4) gives:

$$\frac{dI}{I} = \frac{-\mu x_0}{1 - \mu x_0 \rho} d\rho \quad (5-5)$$

By specification $d\rho$ is to be $\pm 5\%$ of the full scale density. Full scale is assumed to be when the gas content is 50%, since only sensing is required when the gas content is less than 50%. The maximum value for $d\rho$ then is $.05 \times .036$ or 1.8×10^{-3} .

In equation (5-5) μ is 0.34, x_0 is 20.3, and ρ as mentioned is 0.036. The relative change in count rate is then:

$$\left| \frac{dI}{I} \right| = \frac{0.34 \times 20.3 \times 1.8 \times 10^{-3}}{1 - .248} \quad (5-6)$$

$$= 1.6\%$$

If the count rate is determined to $\pm 0.8\%$, then the determination of ρ will be $\pm 5\%$ with 95% confidence. If equal error contributions are allowed for random photon emission and the electronic system, then each error source must be kept to 0.56%. This implies that the detector count rate must be given by:

$$\frac{1}{\sqrt{2I}} = 5.6 \times 10^{-3} \quad (5-7)$$

or:

$$I = 1.6 \times 10^5 \text{ sec}^{-1} \quad (5-8)$$

The source strength needed to produce this count rate is found by substituting the value of I given by equation (5-8) together with the assumed values of A_D , x_0 , ρ , μ , and W into equation (5-2), and solving for I_0 :

$$I_0 \approx \frac{4 \pi x_0^2 I}{A_D W} \quad (5-9)$$

$$= \frac{12.56 \times 400 \times 1.6 \times 10^5}{5 \times .033}$$

$$\approx 5 \times 10^9 \text{ (if Am}^{241} \text{ is used)} \quad (5-10)$$

$$\approx 2.9 \times 10^8 \text{ (if Co}^{57} \text{ is used)}$$

5.2 Shielding Required

5.2.1 For Americium 241 Source: From equation (5-10)

it is seen that the Am²⁴¹ source strength would be

135 millicuries. The dose rate constant for Americium is $0.12 \text{ R cm}^2 \text{ mc}^{-1} \text{ hr}^{-1}$. The dose rate is to be kept to 2 mr hr^{-1} .

If the 135 millicurie source is completely unshielded, the dose rate is within the 2 mr hr^{-1} limit at a distance of 2.8 feet or 85 cm. The mass absorption coefficient of tungsten is about $2.5 \text{ cm}^2 \text{ gm}^{-1}$ at 60 kev. The density of suitable tungsten alloy is about 16 gm cm^{-3} . Therefore, y, the tenth value layer of tungsten for the source is given by

$$y = \frac{2.3}{2.5 \times 16} \\ = 0.0575 \text{ cm}$$

5.3 Intermediate Pipe Diameters with Hydrogen

The path length is still 8.0 inches. The detector area is increased, so smaller sources can be used.

5.4 Large Pipes with Hydrogen

The path length increases by a factor of 1.25. Assuming that the same count rate requirement is maintained (a reduced one is permissible) the source strength requirements are still lower than determined for the small pipe since larger detector area can be used.

5.5 Source Strength for Small Oxygen Lines

A one inch oxygen line can be treated by the method used for the 8.0 inch hydrogen line.

$$I = \frac{I_0 A_D (1 - \mu x_0 \rho)}{4\pi x_0^2} \quad (5-11)$$

This leads to:

$$\frac{dI}{I} = -\frac{\mu x_0}{1 - \mu x_0 \rho} d\rho$$

For oxygen, the allowable value of dP is 2.5×10^{-2} . μ is 0.18, x_0 is 2.5. Therefore:

$$\frac{dI}{I} = \frac{0.18 \times 2.5 \times 2.5 \times 10^{-2}}{1 - 56}$$

$$= 2.6\%$$

This in turn requires a count rate of $16 \times 10^4 \text{ sec}^{-1}$. This in turn will be produced by a source strength of

$$I_0 = \frac{4 \pi x_0^2 I}{A_D W} = 3 \times 10^7 \text{ sec}^{-1}$$

This is equivalent to about one millicurie.

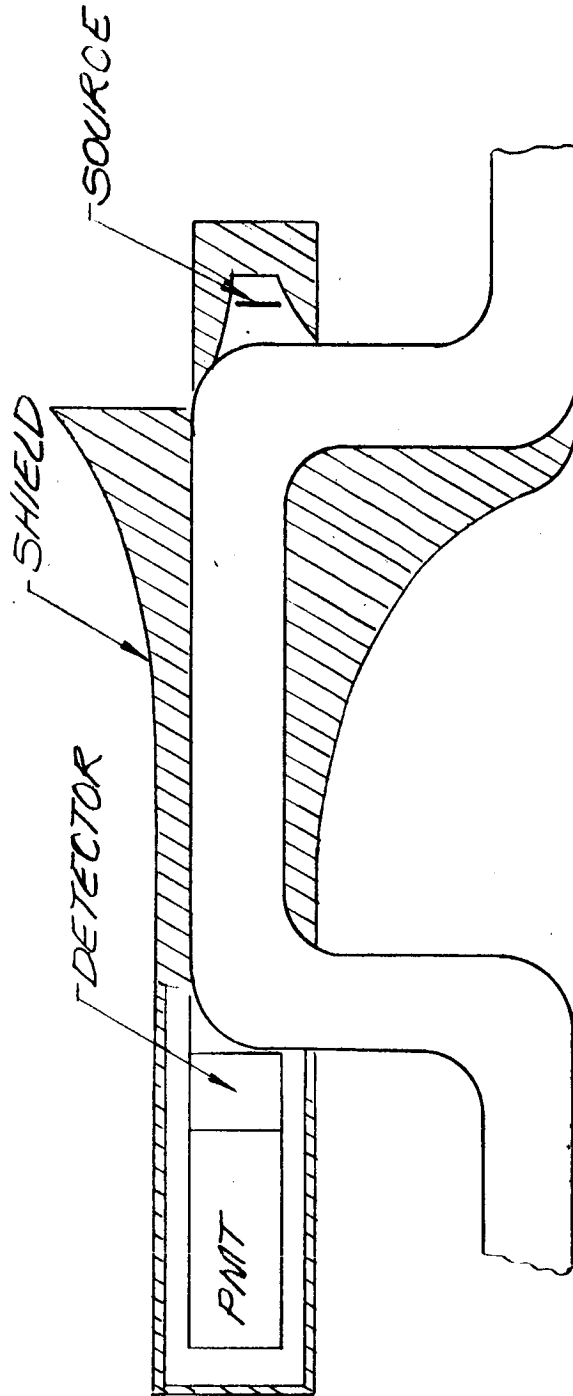
5.6 Larger Oxygen Pipes

The simplification of equation (5-11) does not apply in larger pipes. For the 10-inch pipe, the slope of the curve will be only about one-half that given by equation (5-11). To maintain the same accuracy, the detector count rate must be increased by a factor of 4. Considering that the source detector distance is increased by a factor of 10, and that the detector area is increased by four times, the source strength must be increased 100 times. In other words, 100 millicuries are needed for 10-inch oxygen pipes.

6.0 SHIELD DESIGN

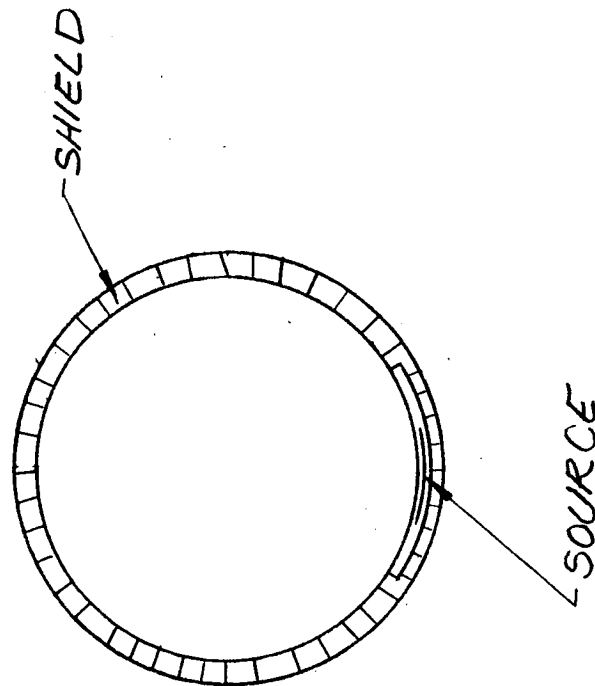
It has been shown that a maximum of 135 millicuries is required if Am^{241} is used. If Co^{57} is used, about 10 millicuries would be required. In either case, shielding is needed to reduce external radiation levels to acceptable values.

As noted previously, the dose rate due to the unshielded source is below the permissible level at 85 cm. The source



SHIELD ARRANGEMENT FOR SMALL PIPES

FIGURE 6-1



SHIELD ARRANGEMENT FOR LARGE PIPES

cannot be approached closer than 2.5 cm. when it is installed. Therefore, an attenuation of about 1200 times is needed at 2.5 cm from the source. At 30 cm only eight times attenuation is needed. The shield may then taper from about 0.25 cm to about 0.06 cm as shown in Figure 6-1. The maximum shield weight for this case would be about 4.0 pounds.

For the larger pipes, the situation for shielding is given in Figure 6-2. The worst case for this type installation is the 4-inch pipe. The source can be approached in the unshielded direction no closer than 10 cm. The shield attenuation needed then is about 70 times. This is obtained with 0.1 cm of tungsten. The total shield weight for this case would be about 2 pounds.

The shielding of Co^{57} may be estimated from the fact that the Co^{57} dose rate constant is five times that of Am^{241} . The mass absorption coefficient is about the same, and the source strength is about 14 times less. Thus, about one-third as much shielding is needed. Since this would amount to only a 3 pound saving at most, it seems that the cheaper price and greater convenience of Americium justify its selection as the source.

7.0 ELECTRONIC CIRCUIT CONSIDERATIONS

The system block diagram was given in Figure 4-1. The accuracy required of the electronic counting and signal processing circuits is as high as 0.56%. This accuracy can be attained but the following steps must be taken to assure it:

- (1) The photomultiplier gain must be controlled. This is accomplished by "salting" the scintillator with a small amount of Sr 90. Sr 90 emits a 0.5 mev beta particle. The pulse height from the beta particle is much higher than from the 60 kev gammas which form the signal. The beta pulses can be separated from the signal and used as a reference to control the photomultiplier tube gain as indicated in Figure 4-1.
- (2) The pulse height discriminator pulse shaper, and integrator must be kept at reasonably constant temperature. This may require that these components be installed in an oven.

It is estimated that the electronic system can be packaged in about 30 in³. The PMT power supply is concentric with the PMT. The power requirement is about 2 watts for each PMT and about 7 watts for the signal processing circuitry.

8.0 SYSTEM SPECIFICATIONS

The considerations of the previous sections are summarized in the form of detailed specifications for the vent quality system.

The source will be Am²⁴¹. The maximum source strength required is 135 millicuries. The detectors will be sodium iodide thallium activated crystals coupled to photomultiplier tubes. All system components are mounted externally. The system accuracy is $\pm 5\%$ of full scale with 95% confidence. The

The weight and power requirements are as follows:

	<u>Weight</u>	<u>Power</u>
Detector (including power supply)	0.31#	1.8 watts
Shielding (approximately)	4.0#	
Electronic Package	1.0#	7.0 watts

The total weight for a pipe of 7 - 10 inch diameter should be about 6.8 pounds and would require 11 watts. The size of the installation can be seen in Figure 4-1.

9.0 TEST AND CALIBRATION

The systems can be calibrated on a test fixture which simulates the actual installation. Poly urethane foam inserts can be molded in any desired density from 1.5 pounds per cubic foot to 40 pounds per cubic foot. These inserts can be used for calibration. Once made, the calibration will not shift since the system is equipped with an automatic gain control referenced to a nuclear standard.

Giannini Controls Corporation

GIANNINI CONTROLS CORPORATION
Control/Nucleonics Division
Duarte, California

ER-80194

VENT QUALITY METER STUDY

FINAL REPORT

VOLUME III

In Support of

Contract No. NAS8-11814

Prepared for

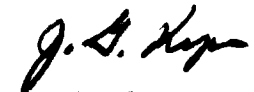
NATIONAL AERONAUTICS AND SPACE ADMINISTRATION
Marshall Space Flight Center
Huntsville, Alabama

W. J. McKinney, Contracting Officer
C. D. Arnett, Contracting Officer's Representative
Fluids Mechanic Section
Fluids Mechanic and Thermodynamics Branch
Propulsion Division
Propulsion and Vehicle Engineering Laboratory
Research Operation

7 December 1964

Giannini Controls Corporation

Prepared by:

J. G. Kyser
Project Engineer

Approved by:

D. E. Wright
Manager, Advance Systems
Control/Nucleonics Division

TABLE OF CONTENTS

	Page
1.0 INTRODUCTION	1
2.0 SYSTEM DESCRIPTION	8
2.1 Geometric Considerations	8
2.2 Stability Considerations	14
2.3 Circuit and Component Description-- Measuring Oscillator	22
2.3.1 Transducers	23
2.3.2 Signal Amplifier	23
2.3.3 Demodulator	23
2.3.4 Gain Characteristics	23
2.3.5 Buffer Amplifier	24
2.3.6 Limiter	24
2.3.7 Modulator and Accessory Circuits	25
2.3.8 Summary	26
2.4 Overall Circuit Description	26
2.4.1 Filter	26
2.4.2 Reversing Circuit	26
2.4.3 Time Generator	28
2.4.4 Updown Counter	29
2.4.5 Readout-Volume Flow Rate	29
2.4.6 Readout, Total Volume	30
2.4.7 Summary	30

TABLE OF CONTENTS
(Continued)

	Page
3.0 ERROR ANALYSIS	31
3.1 Phase Shift	31
3.2 Counting Error	34
3.3 Error in Basic Path Length	34
3.4 Time Generator	35
3.5 Error From Bubbles	35
3.6 Flow Profile	35
3.7 Miscellaneous Errors	37
3.8 Total Error	37
4.0 LABORATORY RESULTS	38
5.0 RELIABILITY	43
6.0 CONCLUSION	43

LIST OF FIGURES

Figure 1	Path of Ultrasound	3
Figure 2	Simplified Block Diagram	4
Figure 3	Phase Shift Versus Frequency for Fixed Time Delays	5
Figure 4.1	Ultrasonic Waves in Fluid	8
Figure 4.2	Primary and Other Waves	12
Figure 4.3	Beam Reflections	13
Figure 5	Bode Plots	16
Figure 6	Phase Shift and Amplitude Versus Frequency in a Phase Shift Oscillator	17
Figure 7	Amplitude Limiting Non-Linearity	21

LIST OF FIGURES
(Continued)

	Page
Figure 8 Detailed Block Diagram of Measuring Oscillator	22
Figure 9 Complete Flow Rate and Volume Measuring System	27
Figure 10 Typical Sound Transmission Path	36
Figure 11 Basic Delay Oscillator	39
Figure 12 Carrier Type Delay Oscillator	39
Figure 13 Rectifier Modulator	41
 APPENDIX A Barkhausen Conditions for Sinusoidal Oscillation at Constant Amplitude	
APPENDIX B Velocity Relationship with Transmission Across the Tube	
APPENDIX C Error from Non-Uniform Velocity Distribution	
APPENDIX D Buildup of Carrier-Type Delay-Line Oscillator	
APPENDIX E Transducer and Pipe Section	

ABSTRACT

The transport velocity of two-phase cryogenic fluids is measured by utilizing a longitudinal section of the flowing fluid as the frequency determining element of a measuring oscillator. By utilizing a pair of identical ultrasonic transducers the transport velocity is measured simply and accurately, independent of the effective speed of sound in the liquid, bubbles, changes in density, or variations in electronic parameters.

TRANSPORT VELOCITY MEASUREMENT
FOR TWO-PHASE CRYOGENIC FLUIDS

This report describes in detail a new method of measuring the average velocity of liquid or liquid-gas flow through tubes.

1.0 INTRODUCTION

This report describes a new technique for measuring transport velocity of fluids, cryogenic or otherwise. It is estimated that accurate measurements can be made with up to 5% gas and useful measurements up to 10% gas, when present in liquid hydrogen.

The fundamental principle of operation is similar to one used previously to measure the transport velocity of liquids. Certain inherent difficulties in the early technique are minimized here. Pulse techniques which measure the increase or decrease of the effective velocity of sound within the liquid because of transport have been developed and tested. There are some problems with these. First, the techniques are designed around single-phase liquid flow. Bubbles, if present, give ambiguous results in the form of jitter on the pulses whose position in time must be determined. The average arrival time of the pulses does not in general contain the desired information. What is required is a measurement of the earliest arrival. For any path except direct from the transmitting to the receiving element, the time delay is longer. If a bubble is present between the transmitter and the receiver, it appears as a reflector of the incident ultrasonic energy. The energy

at the receiver, when there is a bubble directly in the path, is delayed as a result of having taken an indirect path. If there are many small bubbles, the roundabout path, although not much longer than the direct, varies in length as a function of the instantaneous location and size of the bubbles. With this method, the best measurement of transport velocity that can be obtained in the presence of bubbles is the shortest time of transmission from the ultrasonic driver to the receiver. If a long time period is utilized so that many pulses are available, it is in theory possible to search out those pulses having the minimum delay. This minimum delay then represents the transport velocity.

The difficulty with making the measurement described is a result of the need to measure a small time deviation (less than 1%, say) from a relatively large time delay. This problem can be overcome by using one transmitting transducer and two receiving transducers located equidistant upstream and down from the transmitter. The difference of arrival time at the two receivers is then a measure of the flow velocity. The problem remaining is the accurate determination of the average time difference in arrival of the pulses. The reason why the average time difference now represents the flow velocity is that the difference in arrival times is measured. Either or both paths may involve bubbles, thus either or both pulses may be delayed.

The system of velocity measurement described herein is a derivative of the standard pulsed technique. It automatically

searches out the equivalent of the average time delay. It has hardware and basic accuracy advantages over the pulsed technique.

The technique now described utilizes continuous waves rather than pulses. The time delay between the transmission and reception of the ultrasound through the transport medium is utilized as the frequency controlling element of an oscillator. Figure 1 shows the transmitter T and the receiver R in the tubing that carries the fluid. Figure 2 shows a simplified block diagram of the equipment used in the velocity measurement.

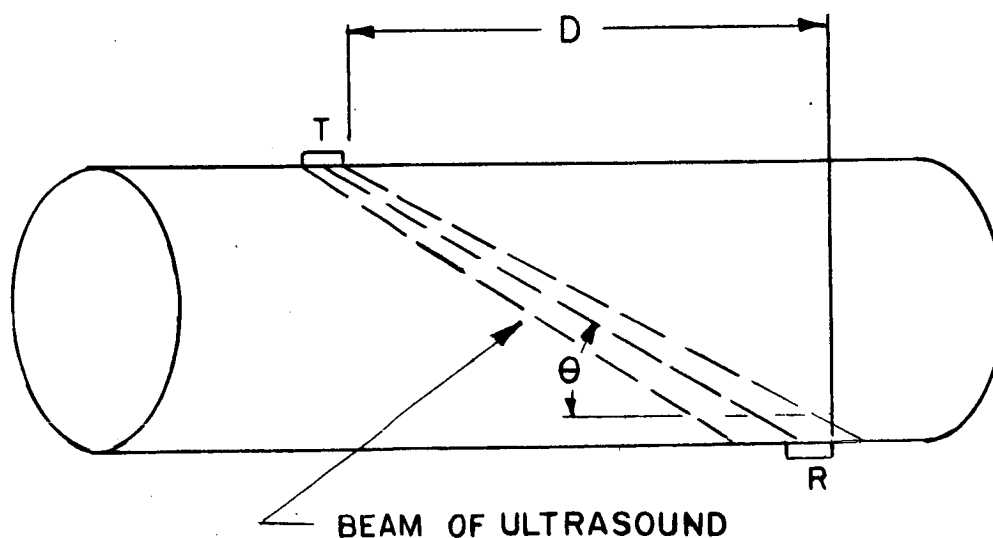


Figure 1
Path of Ultrasound

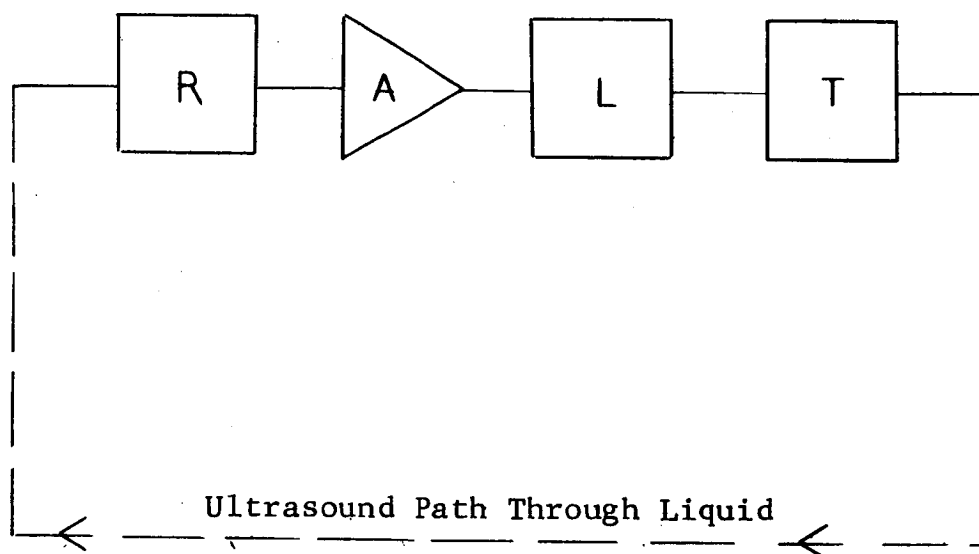


Figure 2

Simplified Block Diagram

The receiving transducer accepts all the ultrasound impinging upon it. This signal is then amplified in amplifier A. Following this is the limiter L. The output of the limiter, after suitable amplification, drives the ultrasonic transducer which created the original ultrasound which has been processed.

Consider now the block diagram of Figure 2 as a possible oscillator. In an oscillator the Barkhausen condition for oscillation can be stated simply. The loop gain must equal exactly one and the loop phase shift must equal exactly zero (or integral multiple of 360°). See Appendix A.

Consider now Figure 3.

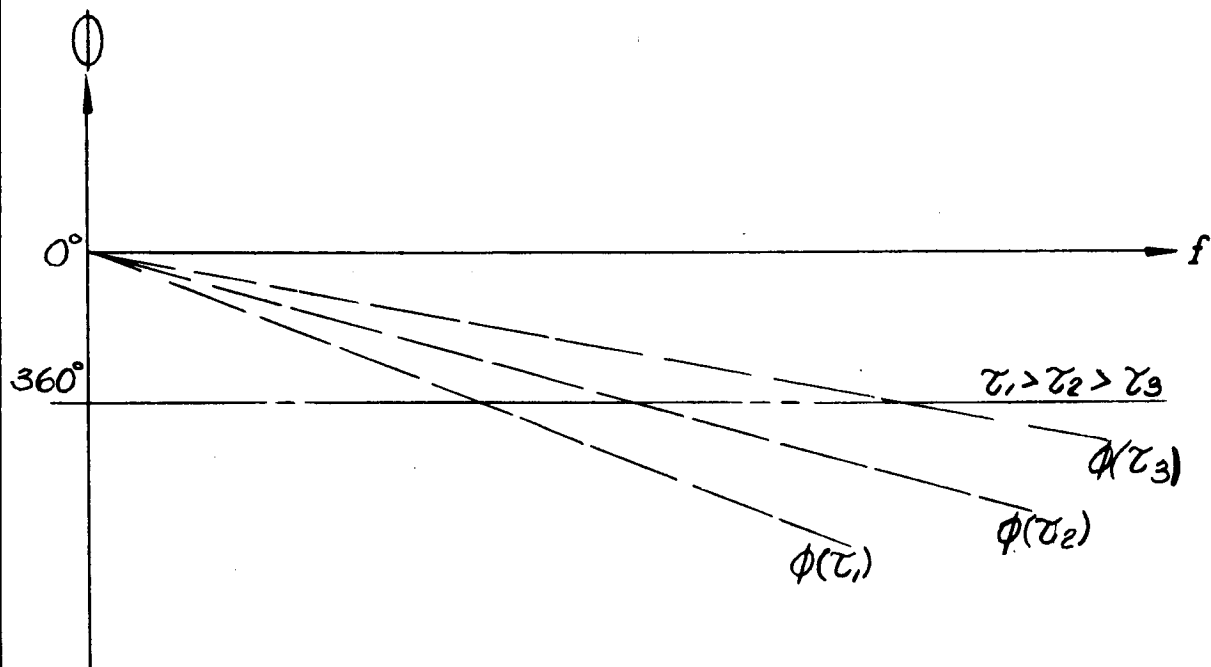


Figure 3

Phase Shift Versus Frequency
for
Fixed Time Delays

It shows the phase shift as a function of frequency for an assortment of fixed delays. For given geometry, both of the transducers in the tube and also of the path between the two transducers, the delay is determined strictly by the transport velocity of the fluid and the velocity of sound within the fluid. For a given maximum delay, the phase curve $\phi(\tau_1)$ would hold. Likewise for decreasing delays the curves $\phi(\tau_2)$ and $\phi(\tau_3)$ hold. Note that the frequencies at which 360° phase shift occurs vary inversely with the delay. Going back to Figure 2, it is seen that there is the equivalent of 0° phase shift in

the first amplifier. If there is no other phase shift in the system then oscillation occurs at a frequency corresponding to the delay which yields 360° phase shift in the liquid. As is pointed out in Appendix A, the total phase shift of 360° satisfies the condition for oscillation at that frequency. The amplitude builds up until the limiter reduces the net loop gain to exactly one. At this amplitude the oscillation is stable in amplitude and in frequency. If the gain is not correct for stable oscillation, the amplitude adjusts itself. If the phase is not correct, the frequency changes.

The frequency is a direct measure of the sum of the speed of sound and the transport velocity of the liquid. For most cases the transport velocity is much less than the speed of sound. It is necessary in essence to make two measurements and to remove the speed of sound. This is done by interchanging the receiving and transmitting transducers; one is used as a transmitter and the second as a receiver for a period of time. The transducers are then reversed and the second used as a transmitter and the first as a receiver. By this means, two independent measurements are made and the velocity of sound, even though variable, can be removed from the measurement or separated out and recorded. Several incidental benefits accrue from this type of measurement. Variations or uncertainties in the geometry and changes in phase shift throughout the electronics as a function of time all cancel out.

The transport velocity, with the assumptions made above, is directly proportional to the difference in the two frequencies of oscillation, that upstream and that downstream and inversely proportional to the distance between them. See Section 2.1.

The preceding paragraphs discuss the mechanics of the measurement. Why is this measurement superior to those made previously using the pulse techniques, when they both depend basically on the effective change in the velocity of propagation of sound from the one transducer to the other? The reason is that the oscillator, which uses the delay of the ultrasound between transmitter and receiver, has pseudo intelligence. It searches out the frequency of oscillation which is the highest possible and suppresses all the lower frequencies of oscillation. As bubbles pass by there is an instantaneous change in frequency as the oscillator adjusts itself to the momentary delay. This change in frequency appears as a distortion in the wave form of the oscillator, which is not purely sinusoidal. On the average, however, the oscillator searches out the shortest transmission time which in turn represents the velocity of the liquid. This technique is equivalent to that using pulse techniques if an infinitely high pulse rate or an infinitely long time of measurement were made during which one could decide which pulses represented the shortest path. The continuous oscillator method automatically oscillates at that frequency which has a phase shift of exactly 360° in the liquid. This frequency is directly convertible into a measurement of the transport velocity, or sound velocity.

2.0 SYSTEM DESCRIPTION

The preceding section considered the general principles of transport velocity measurement. It ignored a number of practical details. In this section a more complete discussion of the velocity measurement is given.

2.1 Geometric Considerations. In a practical measuring system it is probably necessary for the sending and receiving transducers to be separated by at least two pipe diameters in order that the transport velocity remain a prime parameter, capable of measurement. In Figure 1 the transducers are shown on the opposite sides of the tube conducting the liquid. Since the measurement made by this technique is basically that of the average transport velocity along the path of the ultrasound, it is desirable to choose this path to be as representative of the average flow velocity as possible.

For the sake of discussion, it is assumed that the delay within the fluid is an integral number times 360° and there is no phase shift in the electronics.

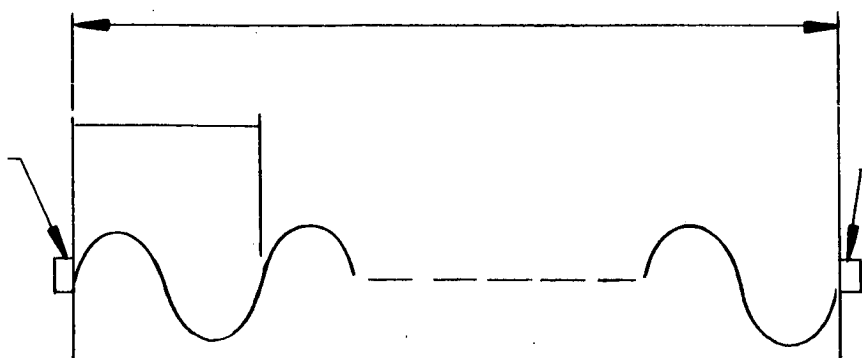


Figure 4.1
Ultrasonic Waves in Fluid

Referring to Figure 4, the conditions for oscillation can be expressed as follows:

$$\tau = \frac{T}{n} \quad (1)$$

where, T = time delay between transducers,

n = integer

The frequency is given by Equation 2:

$$f = \frac{1}{\tau} = \frac{n}{T} \quad (2)$$

The time delay is related to the distance that the sound travels and its effective velocity.

Equation 3:

$$T = \frac{D}{a + v} \quad (3)$$

where, D = distance sound travels between transducers

a = velocity of sound

v = velocity of transport

Substituting Equation 3 into Equation 2 yields Equation 4:

$$f_d = \frac{n(a + v)}{D} \quad (4)$$

Equation 4 gives the downstream velocity. For the upstream measurement, the same equation is valid except that the sign on the transport velocity v is changed:

$$f_u = \frac{n(a - v)}{D} \quad (5)$$

The subscripts d and u stand for downstream and upstream respectively. Solving Equations 4 and 5 for the velocity yields Equations 6:

$$v = \frac{D}{2n} (f_d - f_u), \text{ or:} \quad (6)$$

$$a = \frac{D}{2n} (f_d + f_u)$$

Note that in actual measurement the relations of Equations 6 are not exact because the relationship given in Equation 3 is not valid as the path goes across the tube. Appendix B derives the actual relationship, which is similar in form. It involves the other dimensions required to describe the transmission path.

At this point, it is necessary to define the problem under consideration. A specific problem is to measure the flow of LH_2 over a velocity range of 1 to 40 feet per second, in a 10-inch pipe. These numbers are small compared to the 3500 feet per second velocity of sound in LH_2 and it is desirable to increase them. A measuring section diameter of five inches will be used with resultant flow rates of four to 160 feet per second. Appropriate reducing sections between the 10" and 5" sections are required to maintain laminar flow.

Spacing between transducers is determined by examination of Appendix B. It is seen that the velocity term is modified by a $\cos \theta$ term, thus it is desirable to keep $\cos \theta$ as high as possible. A spacing of one foot gives an angle of 22.5° and a value of 0.92 for $\cos \theta$. In subsequent calculations $\cos \theta$ is assumed equal to one. "n" is chosen as equal to five so that the system resolution is high. Referring to Equation 6:

$$\frac{\Delta f}{v} = \frac{2n}{D} = 10 \text{ cps/fps}$$

The center frequency is determined from Equation 4 to be 17,500 cps, where it is assumed that $a = 3,500$ fps.

A redundant condition will occur when there are four or six wave lengths between the transducers. These occur at frequencies of 14,000 and 21,000 cps. The maximum desired downstream frequency will be 19,100 cps. Therefore a band pass filter is required that will allow passage of a range of frequencies around 17,500 cps. This subject is discussed further in Section 2.2.

Waves in Pipe Section. There are basically four types of ultrasonic waves which can impinge on the receiving transducer causing an electrical output. Refer to Figure 4.2.

I. Primary wave--This is the information wave which is sent from the transmitter to the receiver.

II. Transducer reflected wave--This is the wave which bounces between the receiver and transmitter.

III. Reflected waves--These are waves which strike some object in the piping system and then return through a devious path to the receiver.

IV. Direct coupled waves--These are waves which travel through the metallic pipe section from transmitter to receiver.

Wave I is the one we are interested in; all the others represent interference and noise. The pipe geometry problem is to reduce or eliminate these waves so that the receiver sees only the primary wave.

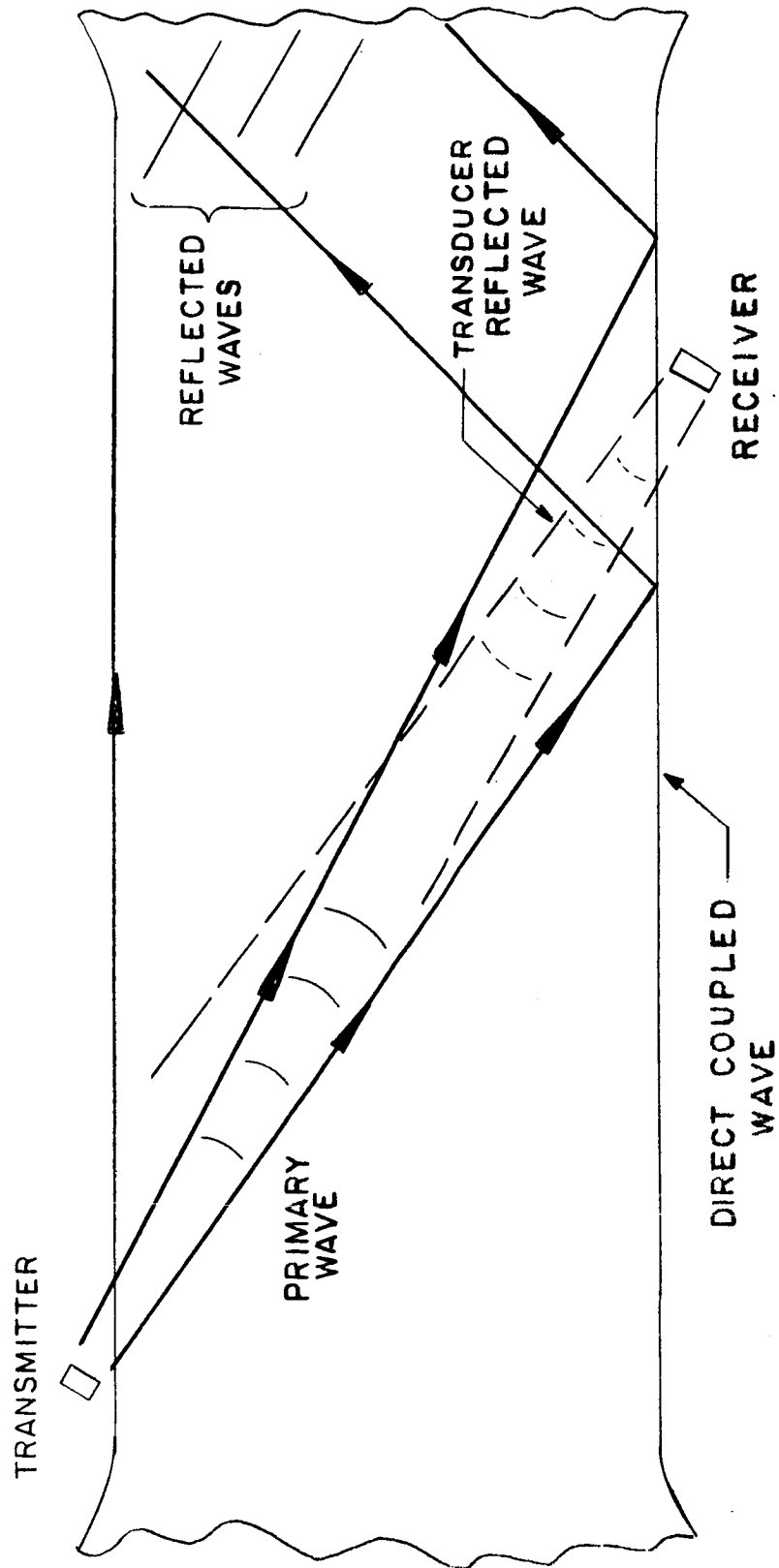


FIGURE 4.2
PRIMARY AND OTHER WAVES

1. Attenuation. Attenuation of sound in LH_2 is indicated to vary as the square of frequency.⁽¹⁾ Based on measurements at 44 mc, an attenuation constant α in $P_x = P_o e^{-\alpha x}$ would equal 0.001 cm^{-1} at a frequency of 3.5 mc. Thus for every 30 feet, the sound pressure would decrease by a factor of three.

2. Beam Versus Crystal Area. The primary beam will be directed at the receiving crystal and will be three times the diameter of the crystal. The crystal will be positioned near the outer edge of the beam where the pressure is lower than at the center. The energy reflected from the receiver toward the transmitter will be approximately 10% of the beam energy. The reflection is reduced by a factor of ten at the transmitter and again by a factor of ten at the receiver so that the transducer reflected wave is attenuated by 40 db due to proper choice of beam and crystal areas. Figure 4.3 illustrates this.

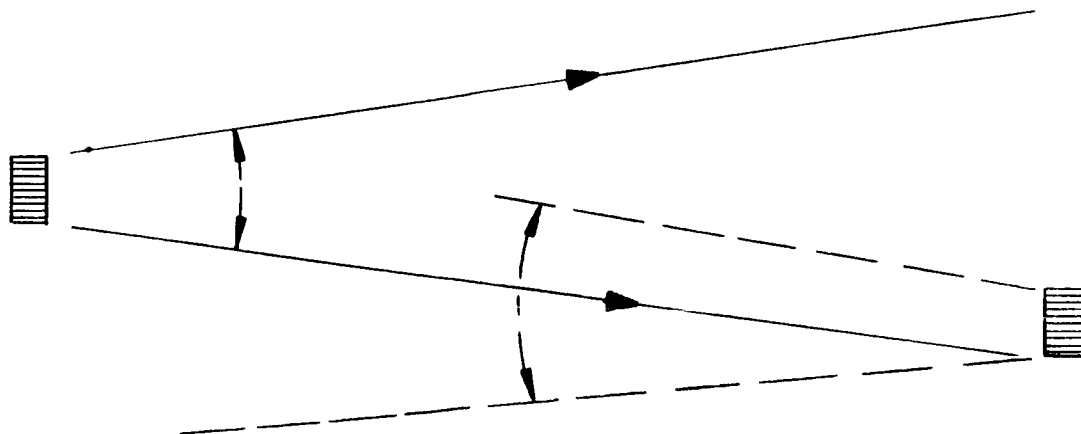


Figure 4.3

Beam Reflections

(1) Sound absorption and velocity in liquified Argon, Oxygen, Nitrogen, and Hydrogen, J.K. Galt, J. Chem. Physics 16(1948)

3. The pipe section will be designed such that the energy from the primary wave not striking the receiver will be reflected down the pipe away from the measuring section. This energy will be attenuated as it travels through the pipe and tank system. That portion of it that is somehow reflected back toward the measuring section are the reflected waves.

It is not known what portion of the energy will return to the measuring section although it is felt the percentage will be small. There are two things that will further reduce the effect of reflected waves which get back to the measuring section:

a) Path length--There will be some attenuation due to path length. The wave will leave the measuring section, travel down the pipe, (while traveling down the pipe it will bounce from wall to wall because it was injected at an angle). That part of the original wave which returns will again traverse the pipe bouncing from wall to wall. Resultant attenuation will be based on total path length including all bounce paths.

b) Area--The energy will leave the measuring pipe in a narrow beam (0.5 in^2) and any that returns will be spread over the pipe section area (20 in^2).

4. Frequency modulation of the carrier wave will further reduce the effect of any reflected waves which hit the receiving transducer.

5. Direct coupling must be eliminated at the source--the transmitter through design.

2.2 Stability Considerations. Consider first the simple case when $n = 1$. The rudimentary oscillator shown as Figure 2

could have its Bode plots as shown in Figure 5. For a given delay between transmitting and receiving transducer, the phase shift is linear with frequency as is shown in Figure 5a. The typical amplitude characteristics of Figure 5b must be considered as relative to the frequency oscillation. In other words, the ordinate 1.00 is shown for f_1 , the lower frequency limit. Actually this is just a relative gain. At the frequency of oscillation, for instance f_2 , the transmission of the total loop is 1.00 and the gain at less than f_2 is less than unity. At the same time, however, the gain at frequencies higher than f_2 is greater than unity. There are no components higher than f_2 consistently available, or the oscillation would occur at that higher frequency.

With a multiwavelength delay, the problem is somewhat more complicated. Figure 6 shows the phase and amplitude response for the delay line and the same for a mode-selecting filter to be described below. Consider first the saw-tooth phase response in the upper plot. If the gain is constant within the oscillator loop, then oscillation could occur at any one of an infinite number of frequencies; these are given by Equation 2:

$$f = \frac{n}{T} \quad (2)$$

To prevent oscillation at the undesired frequencies, it is necessary to predetermine which multiple of -360° phase shift is to be used, i.e., $n = 5$. The mode-selecting filter, a second order filter having a Q of 2.5 is assumed. Its phase shift, as well as the combined phase shift of the delay line and the filter are shown. The composite gain is the same as that of the filter,

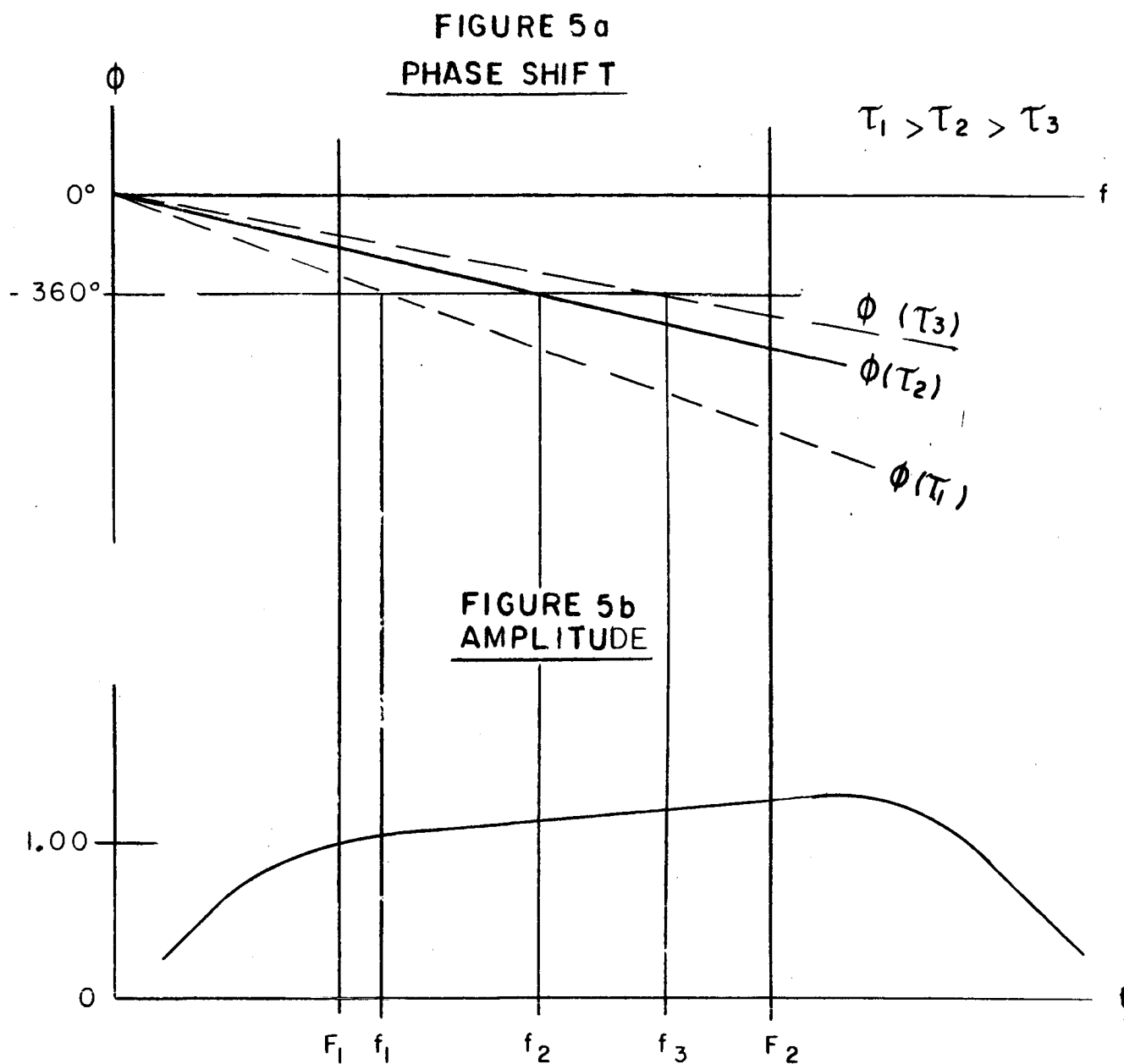


FIGURE 5
BODE PLOTS

PHASE SHIFT AND AMPLITUDE VERSES FREQUENCY
IN A PHASE SHIFT OSCILLATOR

($n=1$)

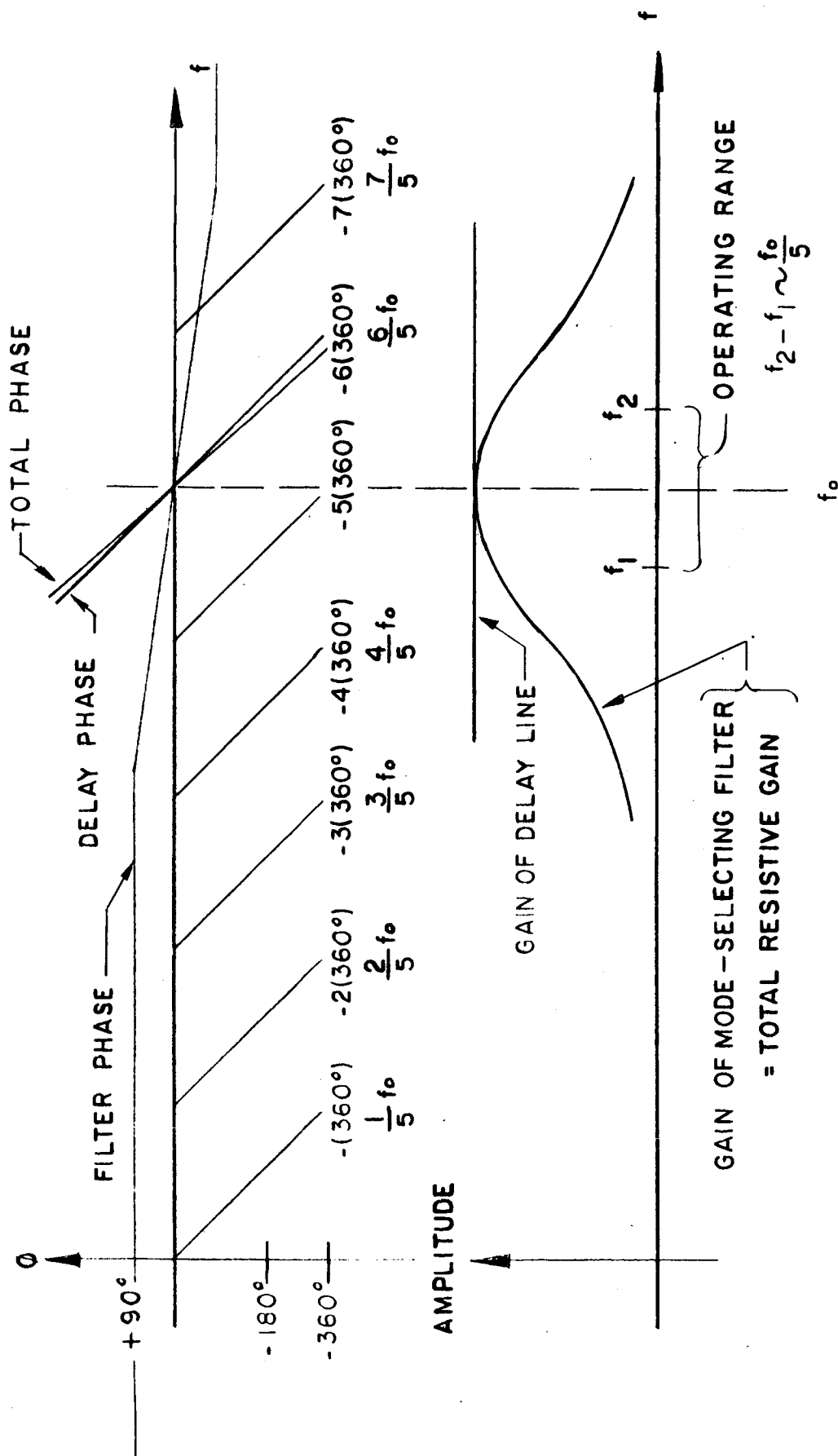


FIGURE 6
 PHASE SHIFT AND AMPLITUDE VERSUS FREQUENCY
 IN A PHASE SHIFT OSCILLATOR ($n=5$)

since the delay line is assumed to have a flat amplitude response to frequency.

Oscillation is still possible at the frequencies given by Equation 2 after the mode-selection filter is inserted. The requirement remains unchanged. The loop gain must be greater than unity at a frequency where the phase shift is an integral multiple of 360° for oscillation to start. If the loop gain were 2.00 at f_0 , theoretically oscillation is possible at $4/5 f_0$, f_0 and $6/5 f_0$ with the filter described. With such a small differential in gain, it is probable that stable oscillation would usually start at f_0 . It would be possible, however, to start oscillation at either of the other two frequencies.

Let us digress for a moment to consider the simple oscillator. It is normal to discuss purely sinusoidal oscillators. The analysis commonly is done on the basis of sinusoidal oscillation. Sometimes overlooked is the fact that there is no such thing, except in theory, as a constant-amplitude, sinusoidal oscillator. Oscillations in general either decrease or increase with time. A usable oscillator has a possible loop gain exceeding one plus some sort of a limiting device to reduce the gain as the amplitude increases. When the amplitude is at exactly the right value, the loop gain of the amplifier is exactly unity and stable oscillations result. It is in general impossible to have this situation without some distortion of the sine wave. The oscillator here is no exception. Wave form however is not particularly critical as the parameter of interest is the frequency, as it does not have to be measured over a cycle,

but rather over a number of cycles.

For a non-homogenous liquid the wave shape is non-sinusoidal for another reason: that of the varying transmission delay as a function of time. Minor variations in the delay effectively cause minute changes in frequency (as the result of phase changes). It is assumed that for the most part a direct path exists from the transmitting to the receiving transducer. If a direct path does not exist, there is one which deviates in length from the direct path by a small amount. The variation appears as noise on the output signal. In other words, instead of having only a sinusoid with slight harmonic distortion, as the result of the amplitude limiting required to give stable oscillation, there is superimposed a signal that is very nearly the equivalent of random noise. This noise riding on top of the basic near-sinusoid is the result of the oscillator's continuously searching out the frequency to give the proper phase delay between the transmitting and receiving transducers.

This oscillator can be compared to an organ pipe. Instead of having sonic feedback from the open end of the pipe back to the source, the organ pipe instead would have to be terminated in its characteristic impedance. Then, with no energy fed back by reflection, an electrical signal would be taken off from one end and fed back to the driving end, where it would effect the generation of sound. From this analogy, it is also apparent that the Q is basically quite high.

It is perhaps constructive to consider the phase-shift or delay-time oscillator as a frequency-selective amplifier that

accepts noise as its input. Because reinforcement occurs only at certain discrete frequencies, the apparent Q is high. Variations in the flow rate or in the effective path, if occurring in a random fashion, change the frequencies at which reinforcement can come. Because of this change, which is not constant, the rate of build-up and the magnitude are both decreased. This in effect represents a lowering of the Q . Reflected in oscillator performance it degrades the frequency stability and decreases the rate of build-up of oscillations.

The first of these, degradation of frequency stability has these consequences. The circuits must be well isolated to prevent their being influenced in frequency by any other signals (a sort of synchronizing effect). The oscillator output signal probably requires some filtering before feeding the readout of the flow system.

The second of these is of interest as it is related to the problem of using the oscillator. An automatic gain control is required which attenuates the loop gain as a function of amplitude. Appendix D derives the build-up of a delay-line oscillator. If the gain is low, the build-up is essentially exponential, though actually it increases in steps every n cycles. If the loop gain is high, say greater than three, then the steps in the build-up are more abrupt, and the analysis is better carried out by arithmetic iteration.

The practical consequence of the analysis of Appendix D can be stated as follows: For loop gains above two, the build-up time is little affected by gain, but as the loop gain approaches

unity, the build-up slows to infinity. In this oscillator, it is probable that a potential loop gain of 10 or 20 is necessary to insure starting under all conditions. This gain must be reduced to unity rapidly as the oscillation builds up. Figure 7 shows possible non-linearities that can be used for amplitude limiting.

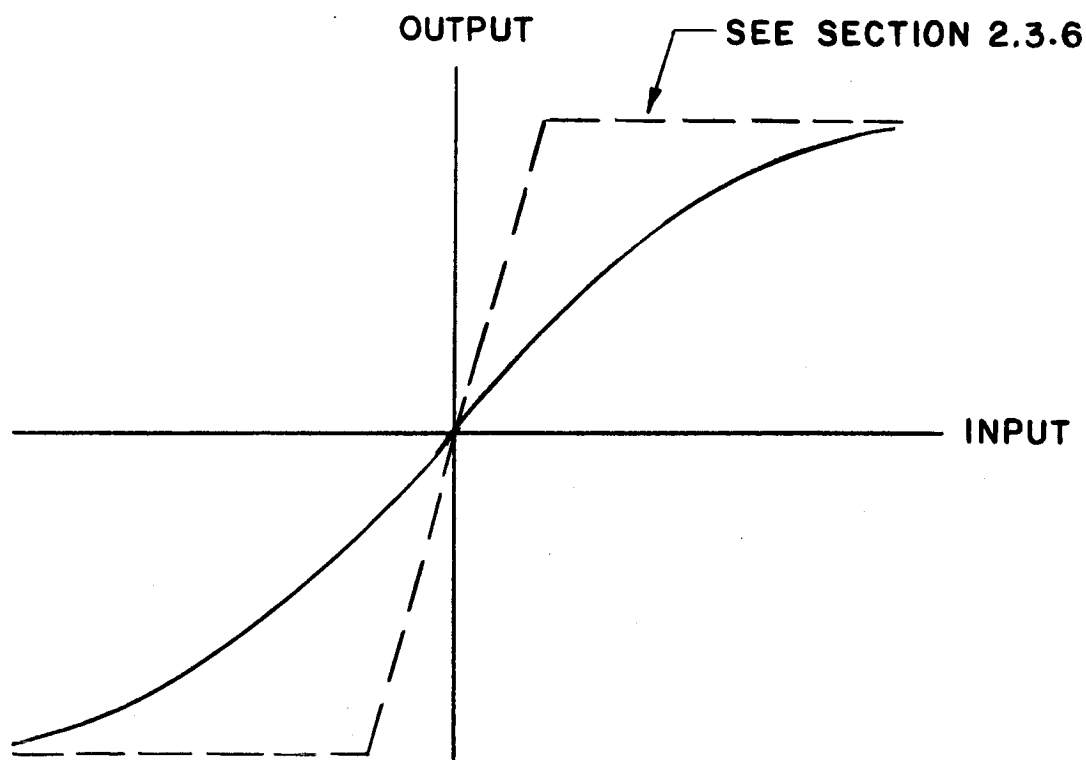


Figure 7
Amplitude Limiting Non-Linearity

Once stability of oscillation has been reached, the slope of the gain characteristic is a factor in the rejection of the various frequencies or the sharpness of tuning. It may be necessary to use a more formal automatic gain control in order to achieve steady-state oscillation smoothly and rapidly. This is a well-known art and the available techniques appear to be sufficient.

2.3 Circuit and Component Description--Measuring Oscillator

The preliminary block diagram as shown in Figure 2 is somewhat sketchy when it comes to describing the actual hardware to be used. In this section the components of a more complete block diagram (Figure 8) are discussed. This figure presents the measuring-oscillator part of the velocity measuring equipment. To this point in this report, discussion has been of nothing else than this measuring oscillator. In Section 2.4, a description of the entire system is given.

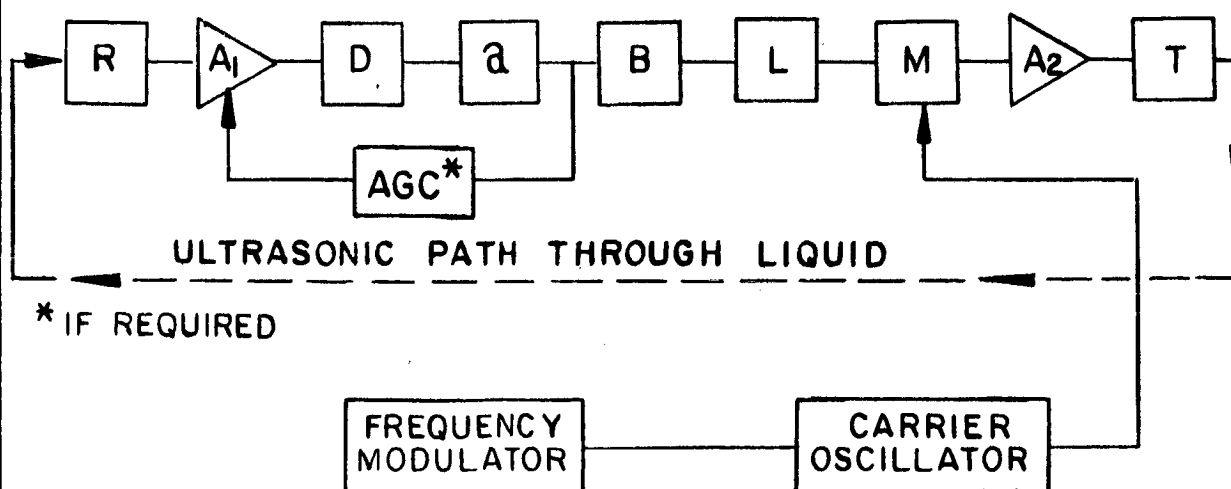


Figure 8
Detailed Block Diagram of Measuring Oscillator
(Path Reversal Circuit Omitted)

2.3.1 Transducers. Receiving and transmitting transducers will be lead zirconate piezoelectric crystals.

2.3.2 Signal Amplifier. In Figure 8 amplifier A_1 receives the 100 millivolt, 3.5 megacycle carrier frequency signal bearing 500 kc sweep frequency modulation and also signal frequency information represented by modulation at about 17,500 cps. This amplifier raises the 100 millivolt output from the receiving transducer to the volt level to drive the demodulator.. The requirements on this amplifier are mild, merely that it has reasonably stable gain and that it be matched to the impedances of the transducer and the demodulator..

2.3.3 The Demodulator. In Figure 8 the demodulator D is a standard carrier plus two-side band rectifier type demodulator as is commonly found in AM radio receivers. The carrier frequency received is varying because of the frequency modulation. The only implication of this is that the detector not be carrier-frequency sensitive.

2.3.4 The block which determines the gain characteristic with frequency of the oscillator has its amplitude response shown in Figure 6. With this type of amplitude characteristics, there is also a variable phase characteristic over the range of interest. With the parameters chosen, a zero-velocity oscillation occurs at 17,500 cps. With 10 cps/fps sensitivity and a maximum flow rate of 160 fps, the maximum frequency deviation is ± 1600 cps. The range of oscillation is thus 15,900 cps \leq to \leq 19,100 cps. With $n = 5$ (five cycles of delay) the two nearest frequencies of possible oscillation are 14,000 cps and 21,000 cps.

The frequency swing is about one-half the maximum possible.

The filter is chosen with a Q of 2.5. This yields 45° phase shift at both 14,000 and 21,000 cps and 25° phase shift at the two maximum operating limits of 15,900 cps and 19,100 cps.

If the oscillator is operating exactly at its design frequency, then the changes in frequency on the upstream and downstream paths are the same. Their signs are such that cancellation occurs and no error is introduced. If the speed of sound in the liquid changes because of temperature or gaseous content, the average frequency of oscillation changes and an error is introduced. See Section 3.1. If this error should turn out in practice to be consequential, it can be avoided by inserting an auxiliary phase shift into the loop and adjusting it for the proper average frequency of oscillation. Since both frequencies are available sequentially, the average is available every measuring cycle by in essence averaging the number of cycles in each half of the measuring cycle.

A network for the gain characteristic is not defined at the present because of the optimum slope of amplitude change with frequency awaits experimental determination. As this is basically a rather low performance bandpass filter, there is no particular difficulty in synthesizing the desired response in the low ultrasonic frequency operating range.

2.3.5 Buffer Amplifier. In Figure 8 the buffer amplifier B serves to match the filter a to the limiter network following.

2.3.6 Limiter. In Figure 8 the limiter L must generate the function shown in Figure 7. The optimum slope of output

versus input must be determined experimentally. There is no particular difficulty in generating slopes of the type required. A few words can be said as to the general choice of the compression. If the slope of output versus input does not change rapidly, then the oscillator is not particularly selective of its operating frequency. If, however, the amplitude limitation is more like that shown by the dashed line of Figure 7 then other undesirable characteristics may arise. The typical behavior of forced oscillations, such as jump phenomena, in a very non-linear system may result.

No difficulty in generating a suitable output-input response for the amplitude limiting non-linearity is envisioned as there is no particularly tight requirement on its conformity.

2.3.7 Modulator and Accessory Circuits. In Figure 8 the modulator M along with the frequency modulator and carrier oscillator are required to generate the 3.5 megacycle center frequency carrier swept at 500 kc with the signal information amplitude modulated upon it. The frequency modulator consists merely of a 500 kc sinusoidal (or perhaps trapezoidal) oscillator varying a reactance in the 3.5 megacycle carrier oscillator's frequency controlling element. There is no particular requirement for accuracy on either the 500 kc or the 3.5 megacycle frequencies or upon their amplitudes.

The standard carrier-plus-sidebands type of amplitude modulator is used. It is probable that the modulator and the amplifier A_2 are actually combined together with the carrier oscillator providing the energy required to operate the

ultrasonic transducer. If this method is utilized, then strictly standard circuits of a sort used in low power AM radio transmitters are applicable and no new circuit development is required. The power required by the transducer poses no particular requirement except perhaps on careful shielding of the oscillator, modulator, transducer, and associated wiring to prevent RFI.

2.3.8 Summary. The electronics required in the measuring oscillator are conventional to the point of calling upon the AM radio art. The approximate weight of the measuring oscillator exclusive of transducers, connectors and cabling but including power supply can be kept to one pound if desired. The size, depending on the packaging density, can be kept to a few cubic inches. There are no uncertainties in design. Rather the requirement is that conventional circuits be carefully applied to the specific problem at hand.

2.4 Overall Circuit Description. Figure 9 shows a block diagram for the complete flow rate and volume measuring system. In the upper left-hand corner is a measurement oscillator, described in Section 2.3.

2.4.1 Filter. A broadly tuned filter is used to purify the waveform of the oscillator so that no counting error is introduced.

2.4.2 Reversing Circuit. Not mentioned in the preceding discussion, except in a general way, is a reversing circuit; it accepts the control signal S_1 from the time generator and at regular periods interchanges the two transducers connected to the measuring oscillator. In this fashion, the transmission

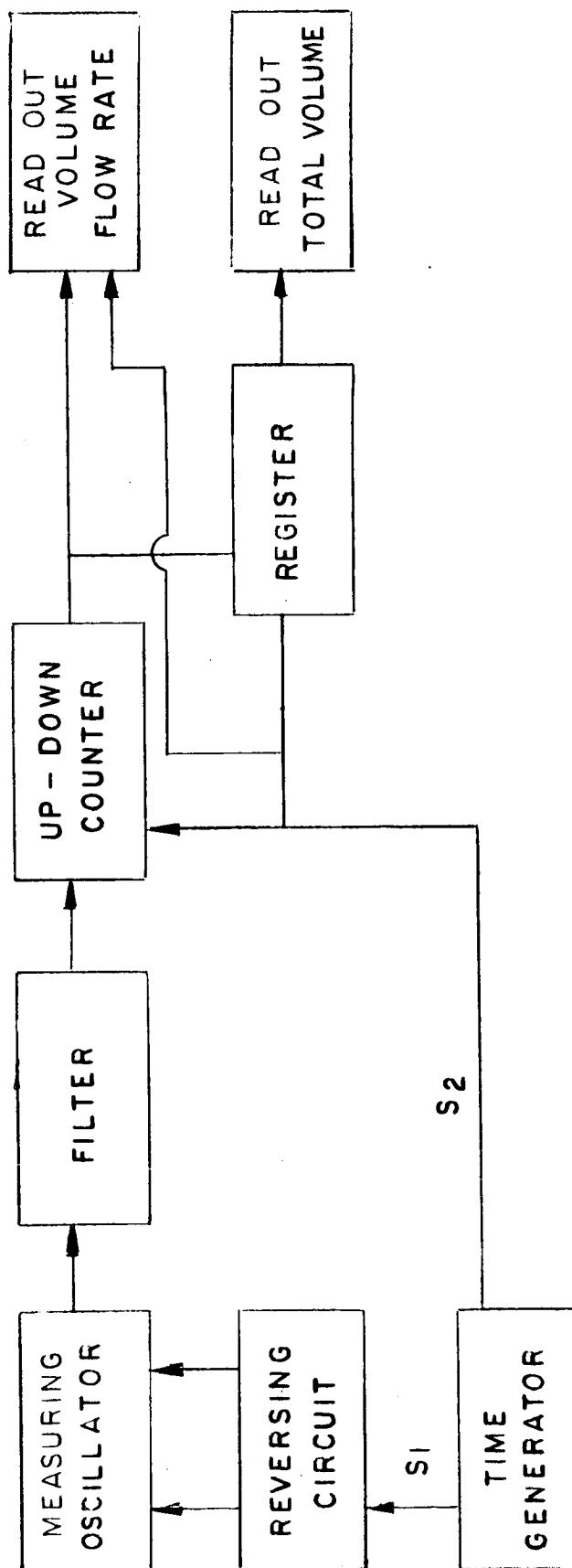


FIGURE 9
COMPLETE FLOW RATE AND VOLUME
MEASURING SYSTEM

path is alternately upstream and downstream. The measurement is made for one second upstream. Then there is a 0.1 second period during which switching takes place and oscillation again builds up. Then there is another 1 second measuring period followed by a second 0.1 second reversing and oscillation build-up period. The reversing circuit consists merely of two electronic switches appropriately connected to the two transducers and to the electronics of Figure 8.

The technical problems of the switching here are suitable isolation of the input circuits. In order to obtain the high degree of isolation required it is probably necessary to utilize dual series switches and to pay heed to the normal mechanical and electronic coupling problems. This represents keen electronic design but nothing that could be regarded as beyond the state-of-the-art.

2.4.3 Time Generator. In Figure 9, the time generator puts out control signals for the reversing circuit, the updown counter and register as shown. In essence the time generator is an oscillator, having frequency stability of 0.1 percent. Suitable dividing circuits are connected to the oscillator so that appropriate control pulses are generated at 1.0, 1.1, 2.1, and 2.2 seconds after the beginning of each cycle. It requires 2.2 seconds to make complete measurement of the upstream and downstream velocities and to perform the necessary switching.*

* The assumption of 1 second and 0.1 second periods is not binding. Depending upon the physical dimensions of the tube, the rate of change of flow, and other parameters, it may be desirable to choose other time intervals. The periods chosen are typical of those reasonable for application to the measurement over one foot of fluid.

2.4.4 Updown Counter. The updown counter is as its name implies. It receives essentially sine waves from the measuring oscillator as they are produced. Over the one-second downstream measuring period, the upstream counter measures the number of cycles received in a 1.000 second period. At the end of this time the counter is disabled for 0.1 second and then is reconnected to count in the opposite direction for another 1.000 second period. At the end of this time there is another 0.1 second interval during which the counter is read out and reset to zero.

The difference between the downstream count and the upstream count for the two one-second periods is a direct measure of frequency. Referring to Equation 6, it is seen that this difference in frequencies is directly proportional to the velocity of flow of the liquid.

The design of the updown counter and its inhibiting circuits represents standard digital logical design and there is no technical problem other than that providing the desired results using minimum circuitry.

2.4.5 Readout-Volume Flow Rate. In Figure 9 in the upper right-hand corner the block title readout-volume flow rate is merely a register which accepts the content of the updown counter at the end of every second one-second counting period. The reading of this register represents the average velocity of flow over two seconds of the preceding 2.2 second period. Every 2.2 seconds this readout, or register, changes its value to represent the average volume flow rate for the preceding period. The

contents of this register can be read in many ways for any desired application. The design problem here is merely that of a digital transfer register.

2.4.6 Readout, Total Volume. In Figure 9 the two boxes titled register and readout, total volume represent digital circuitry which continuously adds the output of the updown counter. Since the content of the updown counter at the end of every readout period (2.2 seconds) represents the volumetric flow during that period, the sum of all of these readings represents the total volumetric flow since signals from the time generator, can give total volume of flow if it is desired.

2.4.7 Summary. The circuit elements described in Section 2.4 in no case press the state-of-the-art. The reversing circuit requires particular care to provide the necessary isolation between input and output circuits. The digital circuitry requires the standard precautions to see that it is impervious to stray pulses picked up from either within or without the flow measuring system. The time generator can be made as accurate as is desired for any particular application. It is possible that it is a purely solid-state oscillator. For higher accuracy requirements, particularly those involving mild vibration environments, it may utilize a tuning fork for frequency control. For difficult environments it is probable that a crystal oscillator is used in the frequency determining circuit.

Depending upon the application and the sophistication of the output circuits the equipment described in Section 2.4 can have as little as three or four cubic inches volume and weight

of one or two pounds.

3.0 ERROR ANALYSIS

Various components of error are discussed in the following paragraphs and their total presented in Section 3.8.

3.1 Phase Shift. At first glance it appears as though uncontrolled phase shift any place within the measuring oscillator circuit gives error. This is not true. Phase shift of the carrier has no effect because of the carrier-plus-two-side-band modulation. Frequency independent phase shift of the elements within the oscillating loop of Figure 8 also has no effect upon the accuracy of the velocity measurement. This is demonstrated in the following paragraph.

Consider now an analysis of the velocity measurement corresponding to that performed in Section 2.1, Equations 1 through 6. If there is phase shift $\Delta\theta$ other than 360° , then Equation 7 is valid:

$$WT + \Delta\theta = 2\pi n \quad (7)$$

The notation is the same as in Section 2. The variation in phase shift is represented by $\Delta\theta$. The frequency of oscillation, in radians per second is given by Equation 8:

$$f = \frac{2\pi n - \Delta\theta}{T} \quad (8)$$

Equivalent to Equation 2 the frequency of oscillation is given by Equation 9:

$$f = \frac{W}{2\pi} = \frac{2\pi n - \Delta\theta}{2\pi T} = \frac{n}{T} - \frac{\Delta\theta}{2\pi T} \quad (9)$$

Substituting in for the time delay Equation 3 yields Equation 10, which corresponds to Equation 4 of Section 2:

$$f_d = \frac{n(a+v)}{D} - \frac{\Delta\phi}{2\pi T} \quad (10)$$

Note that Equation 10 shows that phase shift does cause a change in the frequency of oscillation. As long as this variation in phase shift $\Delta\phi$ is not a function of the frequency of oscillation, subtracting the upstream frequency from the downstream frequency yields:

$$f_u - f_d = \frac{2nv}{D} \text{ and is not } f(\Delta\phi) \quad (11)$$

Solving Equation 11 for the velocity of transport yields:

$$v = \frac{(f_u - f_d) D}{2n} \quad (12)$$

which is identical to Equation 6.

As stated earlier, frequency independent phase shift within the electronics has no effect upon the accuracy of measurement of transport velocity. The effect on frequency of an arbitrary phase shift is exactly the same on both the up and downstream measurements, and the frequency difference is unchanged.

Frequency-dependent phase shift in general causes error. Referring to Equation 10, we can write:

$$f_d = \frac{n(a+v)}{D} - \frac{\Delta\phi_d}{2\pi T} \quad (13)$$

$$\text{and: } f_u = \frac{n(a-v)}{D} - \frac{\Delta\phi_u}{2\pi T} \quad (14)$$

$$\text{or: } f_u - f_d = \frac{2nv}{D} - \frac{1}{2\pi T} (\Delta\phi_u - \Delta\phi_d) \quad (15)$$

and the equivalent of Equations 2 and 12 is:

$$v = \frac{f_u - f_d + 1/2 \pi T (\Delta\phi_u - \Delta\phi_d)}{2n/D}$$

or:

$$v = \frac{D}{2n} (f_u - f_d) + \frac{D}{4\pi nT} (\Delta\phi_u - \Delta\phi_d) \quad (16)$$

The second term in Equation 6 represents error. What is its magnitude per degree of total phase error ($\Delta\phi_u - \Delta\phi_d = 1$ degree = $\pi/180$ radians)?

Using the numbers postulated above as operating values:

$$D = 1 \text{ foot}$$

$$n = 5 \text{ cycles}$$

$$T = \text{delay time} = n/f \quad (17)$$

then:

$$\begin{aligned} \Delta v &= \frac{D}{4\pi nT} \frac{\pi}{180} = \frac{\Delta f}{4n^2} \frac{1}{180} \text{ fps/degree phase shift} \\ &= \frac{1 \text{ foot } 17,500 \text{ cps}}{4(5)^2 180} = 1 \text{ fps/degree} \quad (18) \end{aligned}$$

If this error, about 1 fps/degree of phase shift in the five-inch pipe is allowed (0.25 fps in the ten-inch pipe), from the 25° phase shift caused by the mode-selecting filter, its magnitude is 12 fps in the ten-inch pipe, since the phase leads for low frequencies and lags for high. If the velocity of sound within the liquid were relatively constant, then the phase shift error would be systematic, and could be calibrated out. More likely is the case where the velocity of sound within the liquid varies because of temperature or quality (percent gas).

One method of minimizing error from this source is to control the frequency of the oscillation so that the average of the upstream and downstream frequencies is held essentially at the design center of the filter. This could be done by controlling the phase shift of an all pass filter by means of a signal proportional to the deviation from the design frequency.

Another approach would be to start oscillations using the filter and then to reduce the effect of the filter as the oscillations build up.

Another approach, which would not use a filter, would be to count the number of cycles in the pipe. Oscillation would only be allowed to continue if there were five cycles in the pipe.

The uncorrected error predicted above can be reduced by an order of magnitude using one of the above approaches. The error analysis assumes 2.0 fps error from this source.

3.2 Counting Error. If only integral cycles of the output of the oscillator are counted over the 1.000 second measuring period, an error results from the fraction of a cycle which is omitted. This error is less than one cycle.

With the parameters previously considered in this report, the scale factor is 10 cps/fps. The ± 1 cps possible error yields ± 0.1 fps error in the five-inch pipe.

3.3 Error in Basic Path Length. The mechanical error in path length should be held to 0.05 inches with little difficulty. This represents an error of less than 0.5% of reading or less than 0.8 fps in the five-inch pipe.

3.4 Time Generator. Time generator accuracy can be held to any value desired. In this analysis it is assumed to be 0.1%. It yields an error of 0.1% reading or 0.2 fps in the five-inch pipe.

3.5 Error From Bubbles. A pessimistic error from bubbles is derived on the following basis. Assume that on the average there are two bubbles directly in the path of ultrasonic transmission from the transmitting transducer to the receiving transducer. These bubbles are assumed to have a diameter of 0.2 inches each and to be perfect obstacles to transmission. The bubbles are assumed to be located in such a fashion that the ultrasound must deviate 0.1 inch out of its path for every three inches along the path. This in effect could be caused by two bubbles placed so that the effective path is that shown in Figure 10. With the dimensions chosen, there is an increase in path length of 0.028 inches in the 12 inches of travel considered, and this corresponds to 0.23%.

The 0.23% is the error that would result if there were bubbles in the path from transmission upstream, for instance, when there were none in the downstream. Actually the average path should be extended by the same amount both upstream and downstream. Nearly perfect cancellation results on the average. For the purposes of error analysis, the bubble error is assumed to be less than 0.1% of full scale or 0.2 fps in the five-inch pipe.

3.6 Flow Profile. It is probable that the velocity flow profile of the liquid is non-homogeneous. If we assume that

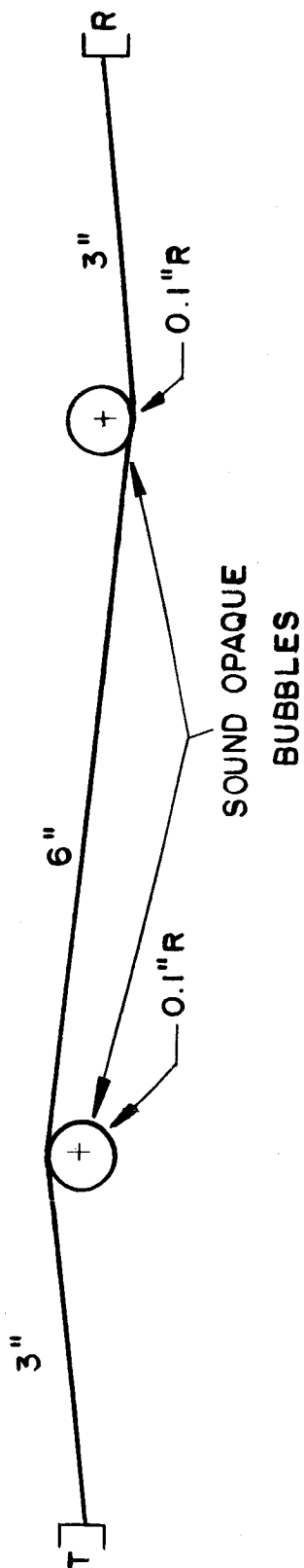


FIGURE 10
TYPICAL SOUND TRANSMISSION PATH

the variation of velocity over the path deviates no more than 2% from the average velocity, for given flow conditions it should be possible to calibrate this deviation to cause an error of no more than 0.25% of reading, the error is less than 0.4 fps in the five-inch pipe. Appendix C considers the problem in more detail..

3.7 Miscellaneous Errors. These are assumed to be no more than 0.2% or 0.3 fps in the five-inch pipe.

3.8 Total Error. If all of the errors of the seven preceding paragraphs are combined one gets:

$$\sqrt{2.0^2 + 0.1^2 + 0.8^2 + 0.2^2 + 1.2^2 + 0.4^2 + 0.3^2} \quad (19)$$

$$= 4.98 = 2.23 \text{ fps rss error}$$

in the five-inch pipe.

Since in Equation 19 one term overwhelms the other, it is perhaps safer to utilize the following error combination:

$$2.0 + \sqrt{0.1^2 + 0.8^2 + 0.2^2 + 0.2^2 + 0.4^2 + 0.3^2}$$

$$= 2.0 + 1.0 = 3.0 \text{ fps error in the five-inch}$$

pipe or 0.8 fps error in the ten-inch pipe.

4.0 LABORATORY RESULTS

Two experimental set-ups were utilized to demonstrate the basic feasibility of the system described and to give an idea as to some of the practical considerations involved. The first experiment used relatively low frequency oscillation and no carrier. The second experiment utilized a carrier. Both systems operated with air as the delay medium.

Basic Delay Oscillator. Figure 11 shows the electrical components used. Personal observation of the performance of public address systems in auditoriums left us with no question as to whether oscillations could be obtained. The only difficulty encountered was in initially not allowing for the rough frequency response of the loudspeaker used. The spacing D and the treble and bass controls were adjusted until the loop had its maximum gain in the 400-500 cps range. Then the loop was opened at a and an audio signal inserted. The gain of the preamplifier (nominally not a frequency response affecting adjustment) and the frequency of the oscillator were adjusted until the signal returned by the loop was identical in amplitude and phase to the signal put in. The oscillator dial read approximately 500 cps, which corresponds to one wavelength's delay in the path D which was 26".

When the loop was closed oscillation built up instantaneously, to the observer, to about twice the amplitude at which it was initially set up. The limit was apparently provided by the output capability of the power amplifier as the waveform

Figure 11

Basic Delay Oscillator

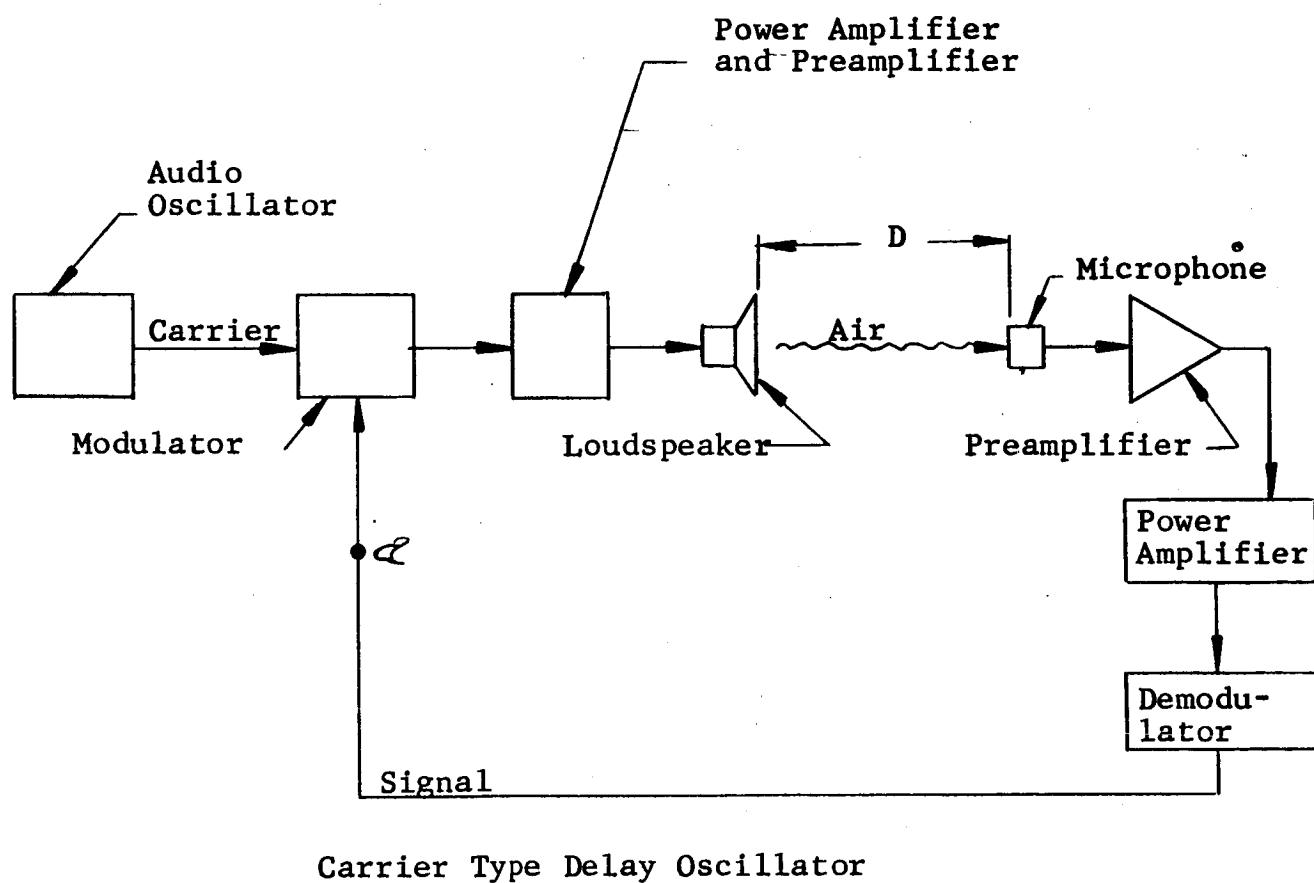
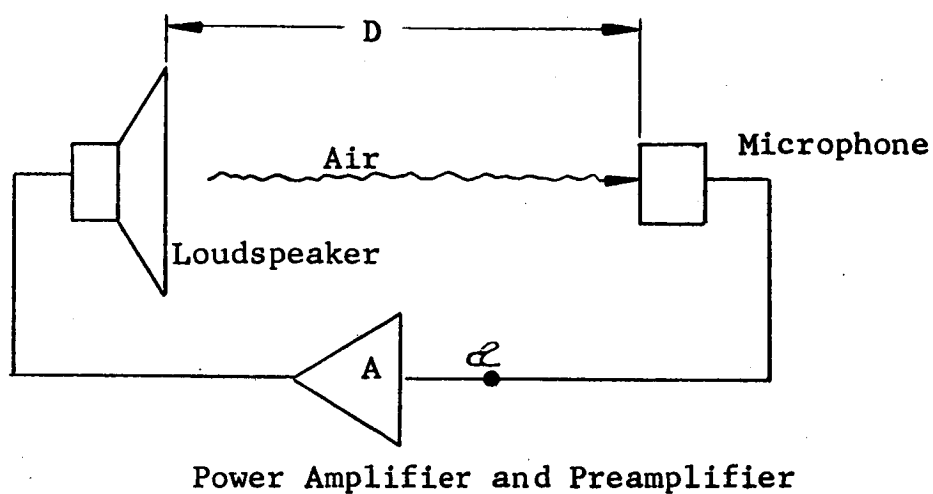


FIG. 12

was observed to be distorted there. The frequency of oscillation was unchanged (judged by oscilloscope) from that originally set up to satisfy Barkhausen's criterion for oscillation.

A fan was then used to blow air between its loudspeaker and the microphone. It could not be held close to the microphone without inserting so much noise that the oscillations became unstable. The following data were taken:

Air stationary:	483 cps	} 12 cps }	} 7 cps }
Fan near speaker:	495 cps		
Fan near microphone:	476 cps		

The computed air velocity component between the microphone and loudspeaker was then, from Equation 6:

$$v = \frac{D(f_d - f_u)}{2n} = \frac{2.2 (12)}{2 (1)} = 13 \text{ fps}$$

and: 8 fps, respectively

No measurement of actual air velocity was possible.

The experiment contributed little new, but was a useful step toward the next experiment.

Carrier-Type Delay Oscillator. Figure 12 shows the oscillator used. Experiments were conducted using both 5 kc and 10 kc for the carrier. With the two transducers used it was difficult to get sufficient signal level to overcome the ambient noise when using 10 kc. At 5 kc, the modulation frequency was limited to about 250 cps because of difficulties in filtering sufficiently to eliminate the modulation from direct transmission through the loop. The rectifier-modulator shown in Figure 13 functioned satisfactorily. The problem is basically that of having the

modulation and carrier insufficiently separated in frequency. The two hundred to one ratio of carrier to modulation (signal) frequencies used in the design eliminates this trouble.

The same general process as described for the first experiment was used. First, however, the carrier was adjusted to give a usable signal. Then, with the loop opened at a, an audio signal at about 250 cps was inserted. The gain was adjusted until the return signal equalled the input. The return wave form was distorted, showing high frequency components (from insufficient filtering) and also delay in following the descending crossover (from too much filter). However, when the loop was closed, oscillation at essentially the same frequency, slightly more amplitude, and considerably more distortion resulted.

Rudimentary tests with the fan showed that the modulating frequency changed with a change in the air velocity. The change was not smooth, but in steps. Changing the frequency by varying the path length D showed a similar effect, but over a much wider frequency range. As the distance increased evenly, the frequency increased in about one-quarter tone steps. The cause was the synchronizing by the carrier. Again using a 200/1 ratio of frequencies instead of 20/1 will eliminate the effect.

Summing up the experiment, it verified the principle of carrier type phase shift oscillation, it pointed out the type of problems one will encounter and the detailed design of the modulator, and it effectively demonstrated the powerful synchronization effect that is possibly useful in establishing the proper operating frequency.

5.0 RELIABILITY

There is nothing within the system described which has an inherent reliability limitation. The transducers, which are exposed to the cryogenic temperatures, will be piezoelectric crystals. The electronics are conventional requiring no state-of-the-art development. All standard reliability techniques apply and there are no particularly stringent requirements upon the performance of any of the circuits. The reliability from these can be essentially anything that is desired. Any unusual reliability requirements will be reflected in the cost.

6.0 CONCLUSION

The system described for the measurement of transport in two-phase cryogenic fluid is believed to represent a step forward in the state-of-the-art of fluid measurement. It is unique in several items. There are no critical time measurements to be made. No exotic component or circuit design is required; rather conventional circuits and components are applied to this particular application. It is a direct application of the Barkhausen requirements for oscillation in a most basic form. Basic independence from variations in the phase and amplitude within the electronics and transducers exists.

We believe that this velocity measuring system represents an important advance in the art.

APPENDIX A

BARKHAUSEN CONDITIONS FOR SINUSOIDAL OSCILLATION
AT CONSTANT AMPLITUDE

BARKHAUSEN CONDITIONS FOR SINUSOIDAL OSCILLATION AT CONSTANT AMPLITUDE

If a circuit or assemblage of circuits has its output exactly equal to its input, then one can make it into a constant amplitude oscillator by removing the input signal and connecting the input to the output. Standard texts discuss this requirement (Barkhausen's) in some detail.*

The Barkhausen condition, that the output exactly equals the input before the loop is closed, for constant frequency and amplitude oscillation, can be understood by study of simple examples. Figure A-1 shows an amplifier A and feedback network N driven by a sinusoidal signal generator S. With the switch Sw_1 in the "a" position, the signal from the generator is passed through the feedback network. Oscilloscopes (not shown) are connected to show the input and output voltages e_{in} and e_{out} .

Figure A-2 shows the inputs and outputs for variety of feedback networks.

Figure A-2a shows the situation where the input e_{in} and the output e_{out} are identical. It is apparent that operating switch Sw_1 to the "b" position does not affect the signal passing through A or N. The circuit is either an amplifier or a self-excited oscillator, depending upon the position of Sw_1 .

Suppose that A and N have gain less than unity, but still with zero phase shift, as shown in Figure A-2b. As an amplifier, there is little change from the preceding case when Sw_1 is in the "a" position. When Sw_1 is placed in the "b" position, however, there is not sufficient input to the amplifier to give the

* Vacuum-Tube Circuits and Transistors, Arguimbau 1956, Wiley and Co.

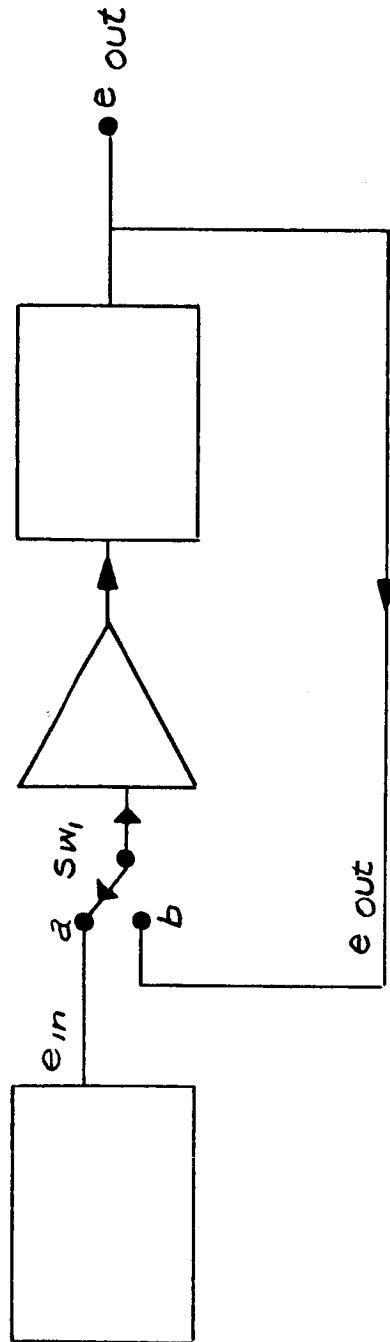


FIG. A-1

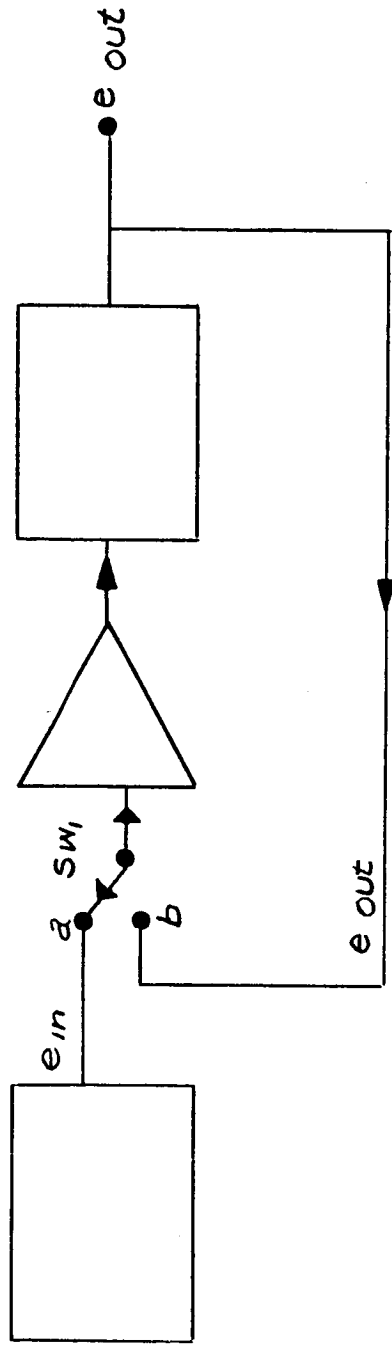


FIG. A-1

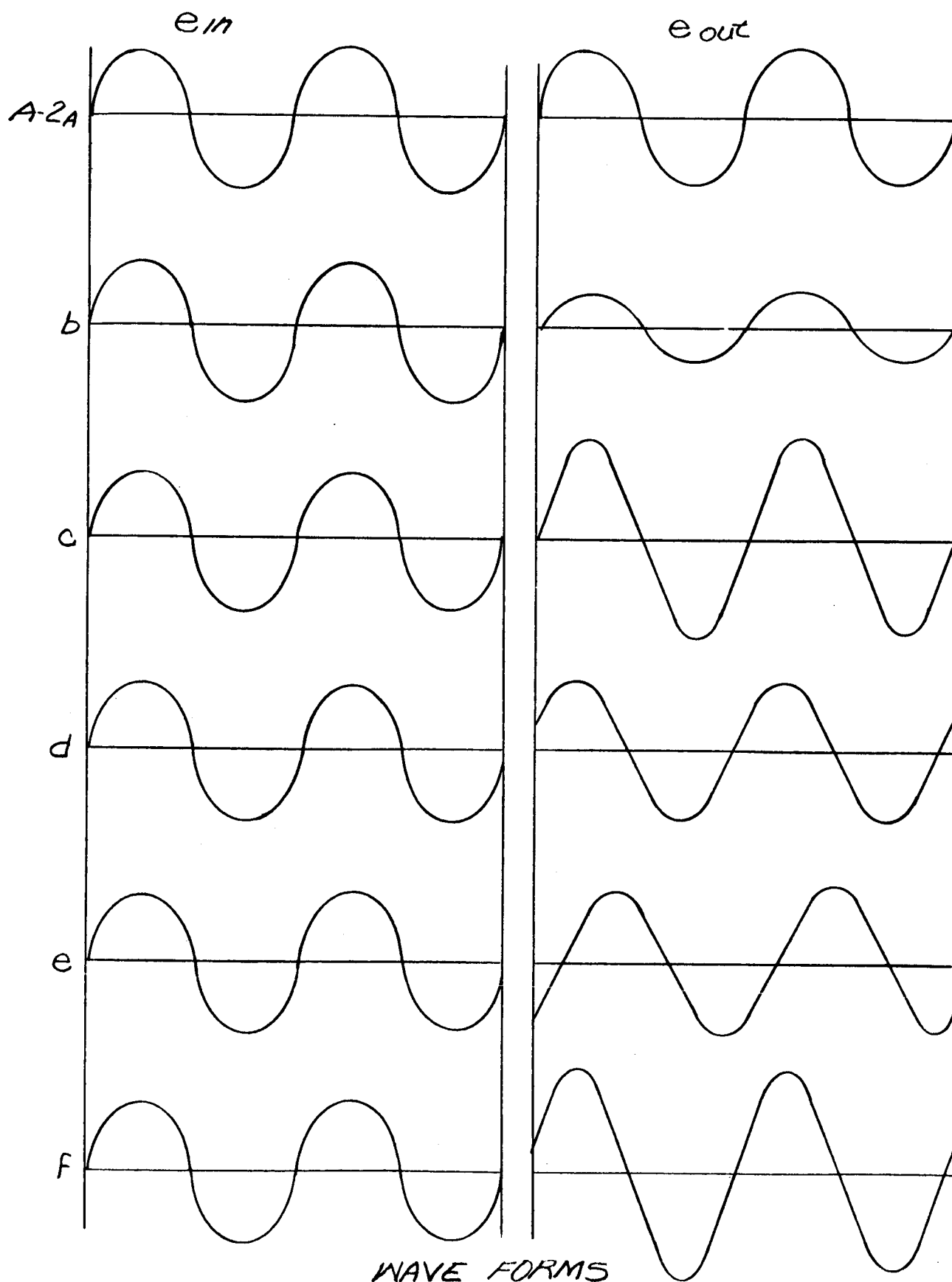


FIG. A-2

required output for constant amplitude oscillation. The amplitude drops off at about 50% per cycle, and soon is stopped completely.

If A and N have gain greater than unity, with zero phase shift, as shown in Figure A-2c, a different situation exists. When Sw_1 is placed in the "b" position, the input is then greater than was supplied by S. The output of N must then increase proportionally. The amplitude of oscillation builds up at about 50% per cycle. This process continues until something saturates and our assumptions become invalid.

Phase shift, rather than amplitude change, can also result from N. Figure A-2d shows the input and outputs at a particular frequency. Operating Sw_1 to the "b" position as shown gives the amplifier a positive input when it should be zero, for unchanged output. This input, after passing through A and N, is again in effect early. It leads the input. Intuitively, it is seen that the frequency of oscillation must increase. Were there no frequency dependence of the phase shift of N (or A), the frequency would increase continuously. In practice, realizable networks like N normally have an increase in phase delay with an increase in frequency. As soon as the phase shift in N is 180 degrees, the frequency stabilizes, and continuous oscillations occur. (For simplicity these examples ignore change in amplitude with frequency.)

Figure A-2e is similar to Figure A-2d except that there is phase lag (over the initial 180 degrees) in N. In a fashion similar to that described in the preceding paragraph, the frequency lowers.

Figure A-2f illustrates a more realistic example. The input frequency yields too much phase lead for oscillation and the gain is too high. When Sw_1 is placed in the "b" position, the frequency and amplitude both start to increase. At some higher frequency and larger amplitude, the oscillation becomes stable, i.e., each cycle is like the preceding cycle. In practice, two things affect the ultimate amplitude and frequency. This attenuation plus limiting in the amplifier adjust the amplitude so that the over-all gain is unity. The frequency determination goes on simultaneously, yielding a net 0° phase shift.

APPENDIX B

VELOCITY RELATIONSHIP WITH
TRANSMISSION ACROSS THE TUBE

VELOCITY RELATIONSHIP WITH TRANSMISSION ACROSS THE TUBE

Figure 1 shows the actual configuration of the tube carrying the liquid.

The component of transmission velocity from one transducer to the next $V = 2 + v \cos \theta$. The time for sound to travel from one transducer to the other is

$$t = \frac{D}{a + v \cos \theta}$$

and the downstream frequency of oscillation is

$$f_d = \frac{(a + v \cos \theta) n}{D}$$

Likewise $f_u = \frac{(a - v \cos \theta) n}{D}$

The frequency difference is given by

$$f_d - f_u = \frac{2 v n \cos \theta}{D}$$

The transport velocity is given by

$$v = \frac{D (f_d - f_u)}{2 n \cos \theta} = \frac{(\lambda^2 + d^2) (f_d - f_u)}{2 n \lambda}$$

This is seen to be the same as Equation (1) of Section 2A.

Giannini Controls Corporation

APPENDIX C

ERROR FROM NON-UNIFORM VELOCITY DISTRIBUTION

ERROR FROM NON-UNIFORM VELOCITY DISTRIBUTION

If the flow through the tube is non-uniform, then the average velocity of flow does not equal the average velocity along the measuring path.

At high Reynold's numbers, the flow is assumed to have cylindrical symmetry of the type described by*

$$v(r) = V_0 (1 - r/R)^{1/7} \quad (C-1)$$

Where $v(r)$ = velocity

V_0 = maximum velocity

r = distance from center

R = radius of tube

then the average velocity \bar{v} along the measuring path is given by

$$\bar{v} = \int_0^R (1 - r/R)^{1/7} dr \quad (C-2)$$

$$= 7/8 V_0 = .877 V_0 \quad (C-3)$$

The average velocity v over the whole cross section is given by

$$v = \int_0^R (1 - r/R)^{1/2} a r dr \quad (C-4)$$

$$= \frac{98}{120} V_0 = .818 V_0 \quad (C-5)$$

If no correction for the flow were made, an error of 7% would result from this cause. Because of the low viscosity of liquid hydrogen, the velocity profile will be similar to that assumed for higher flow velocities. If a constant correction is made to cancel out the 7% systematic offset, then an error is

* Fluid Mechanics, 3rd Edition, R.C.Binder, Prentiss-Hall, p.122

introduced at low flow rates. Fortunately, the error is reduced in magnitude as the velocity decreases. This occurs because the velocity distribution error is of the percent-of-reading type.

Since this error is systematic, it can be calibrated out almost completely if necessary.

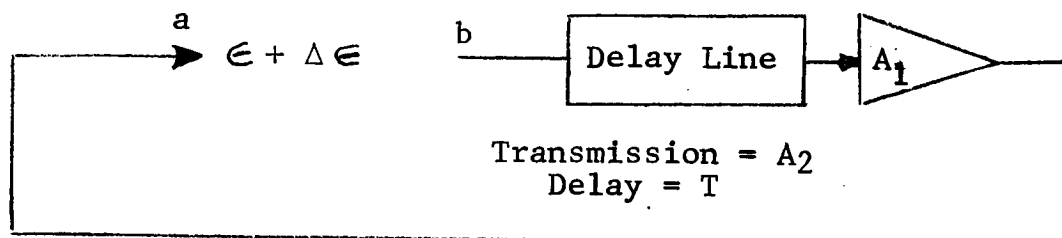
Giannini Controls Corporation

APPENDIX D

BUILDUP OF CARRIER-TYPE DELAY-LINE OSCILLATOR

BUILDUP OF CARRIER-TYPE DELAY-LINE OSCILLATOR

Consider the following circuit:



Frequency of oscillation = f_o .

Figure D-1

Delay-Line Oscillator

If the carrier amplitude is increased in amount $\Delta \epsilon$ by the net gain of the delay line and amplifier combination, then

$$\Delta \epsilon = A_1 A_2 \epsilon - \epsilon = (A_1 A_2 - 1) \epsilon \quad (1)$$

This increment of gain can take place only after the delay time T of the delay line. Thus equation (1) can be written as

$$\frac{\Delta \epsilon}{\text{traverse of delay line}} = (A_1 A_2 - 1) \epsilon \quad (2)$$

assuming that the loop of Figure D-1 is closed, and that the increment $\Delta \epsilon$ is added to the input to the delay line as soon as it is received.

Small Increment Analysis

Consider now the denominator of the left hand side of equation 2. Assuming a non-inverting amplifier A_1 , and integral number n of oscillation wavelengths exist in the delay line at any time. This is the condition for oscillation. The time per cycle of oscillation is given by $1/f_o$. Thus the time per

traverse of the delay line is given by n/f_o . One traverse of the delay line is then given by $\frac{\Delta t}{n/f_o}$ where Δt is the time required for traverse. Substituting into equation (2), this yields

$$\Delta \epsilon \text{ per traverse of the delay line} = \frac{\frac{\Delta \epsilon}{f_o \Delta t}}{\frac{n}{f_o}}$$

$$= (A_1 A_2 - 1) \epsilon$$

or

$$\frac{\Delta}{\Delta t} = \frac{f_o}{n} (A_1 A_2 - 1) \epsilon \quad (3)$$

If we now consider a long time period, in which the number of traverses of the delay line is large, then we can go from the incremental increase in the signal amplitude per traverse as given by equation (3) to the differential or continuous expression

$$\frac{d \epsilon}{d t} = \frac{f_o (A_1 A_2 - 1)}{n} \epsilon \quad (4)$$

The solution of equation (4) is

$$\epsilon = k \exp \left\{ \frac{f_o (A_1 A_2 - 1) t}{n} \right\} \quad (5)$$

where k is the value of ϵ when $t = 0$.

If it is assumed that noise present within the oscillator has an equivalent signal amplitude of 0.01% of the full scale (linear) amplitude of oscillation ϵ_f , then

$$\epsilon = 10^{-4} \epsilon_f \exp \left\{ \frac{F_o (A_1 A_2 - 1) t}{n} \right\} \quad (6)$$

$$\text{or } 10^4 = \exp \frac{f_o (A_1 A_2 - 1) t}{n} \quad (7)$$

$$\text{or } 9.2 = \frac{f_o (A_1 A_2 - 1)t}{n} \quad (8)$$

Now assume $n = 5$ full wavelengths or cycles in the delay line

$$A_1 A_2 = 2, \text{ loop gain}$$

$$f_o = 17500 \text{ cps}$$

Substitution (8) for time yields

$$t = \frac{9.2n}{f_o (A_1 A_2 - 1)} \quad (9)$$

$$\text{or } t = \frac{9.2 (5 \text{ cycles})}{17500 \text{ cycles/sec}(2-1)} = 2.6 \text{ milliseconds}$$

Large Increment Analysis

From Equation (2) we can compute the buildup, assuming step-wise increments in amplitude. Assume that the noise within the oscillator contains a component of 0.001% of the full scale steady state amplitude.*

Also assume $(A_1 A_2 - 1) = 10$, then the following can be written:

	<u>Signal</u>
Initially	10^{-5} f
After 1 transit through the delay line	10^{-4} f
After 2 transits through the delay line	10^{-3} f
After 3 transits through the delay line	10^{-2} f
After 4 transits through the delay line	10^{-1} f
After 5 transits through the delay line	f

Thus it takes 5 traverses through the delay line for the oscillator to build up full amplitude. The time required for this is

$$\frac{5 \text{ traverses } 5 \text{ cycles/traverses}}{17500 \text{ cycles/sec.}} = 1.4 \text{ milliseconds **}$$

* This is assumed lower than in the previous case because of the higher loop gain.

**Note that, even though the initial signal was assumed smaller, the full amplitude is reached in about half the time.

APPENDIX E

TRANSDUCER AND PIPE SECTION

TRANSDUCER AND PIPE SECTION

The following problems have to be solved before a practical design can be developed:

(1) The material selected for the active section of the transducer must retain its electro-mechanical conversion characteristics at $+15^{\circ}\text{K}$. A second constraint on the transducer element is that it have a sufficiently low enough mechanical Q to pass, unattenuated, the 3.5 mc frequency modulated signal.

A deviation of 500 kc means that a mechanical Q of 7.5 must be realized if the transducer is to operate at its mechanical resonant frequency. Of all of the ceramics available, lead zirconate has the lowest mechanical Q , being in the order of 60 to 70. Thus a provision must be made to mechanically load the crystal with an acoustically lossy material. The problem of bonding the material to the crystal face, e.g., thermal coefficient, etc., becomes immense.

A second approach to this problem, and by far the best, is to operate the transducer unloaded and far from either its thickness or radial resonant frequencies. Realizing that much lower electro mechanical coupling is immediately implied by this additional gain, equal to the Q of the crystal, must be provided by the electronics. If lead zirconate is used as the active element of the transducer, the additional gain required is 60.

(2) The method of mounting the transducers to the pipe section must be such as to not materially affect the flow pattern.

If the flow of liquid hydrogen in a perfectly smooth pipe is assumed, the amount of turbulence in the flow can be found by investigating the Reynold's number in the pipe. In general, the Reynold's number is:

$$Rn = \frac{pv l}{u} \quad 1 \quad (1)$$

where

p = Density

v = Velocity

u = Viscosity

l = Diameter of pipe

for liquid hydrogen at 16°K

$$p = 0.0752 \text{ gm/cm}^3 \quad 2$$

$$u = 209 \text{ micro poise} \quad 3$$

Assuming nominal pipe diameter l = 5 inches and a velocity of 160 feet per second. Substituting these values into equation (1):

$$\begin{aligned} Rn &= \frac{.0752 \times 4875 \times 12.7}{209 \times 10^{-6}} \\ &= 21,800,000 \end{aligned}$$

1. Fluid Mechanics, Binder, Prentice-Hall, 1949, p. 81
2. Cryogenic Engineering, Scott, D. Van Nostrand Co., 1959, p. 303
3. Ibid. p. 306

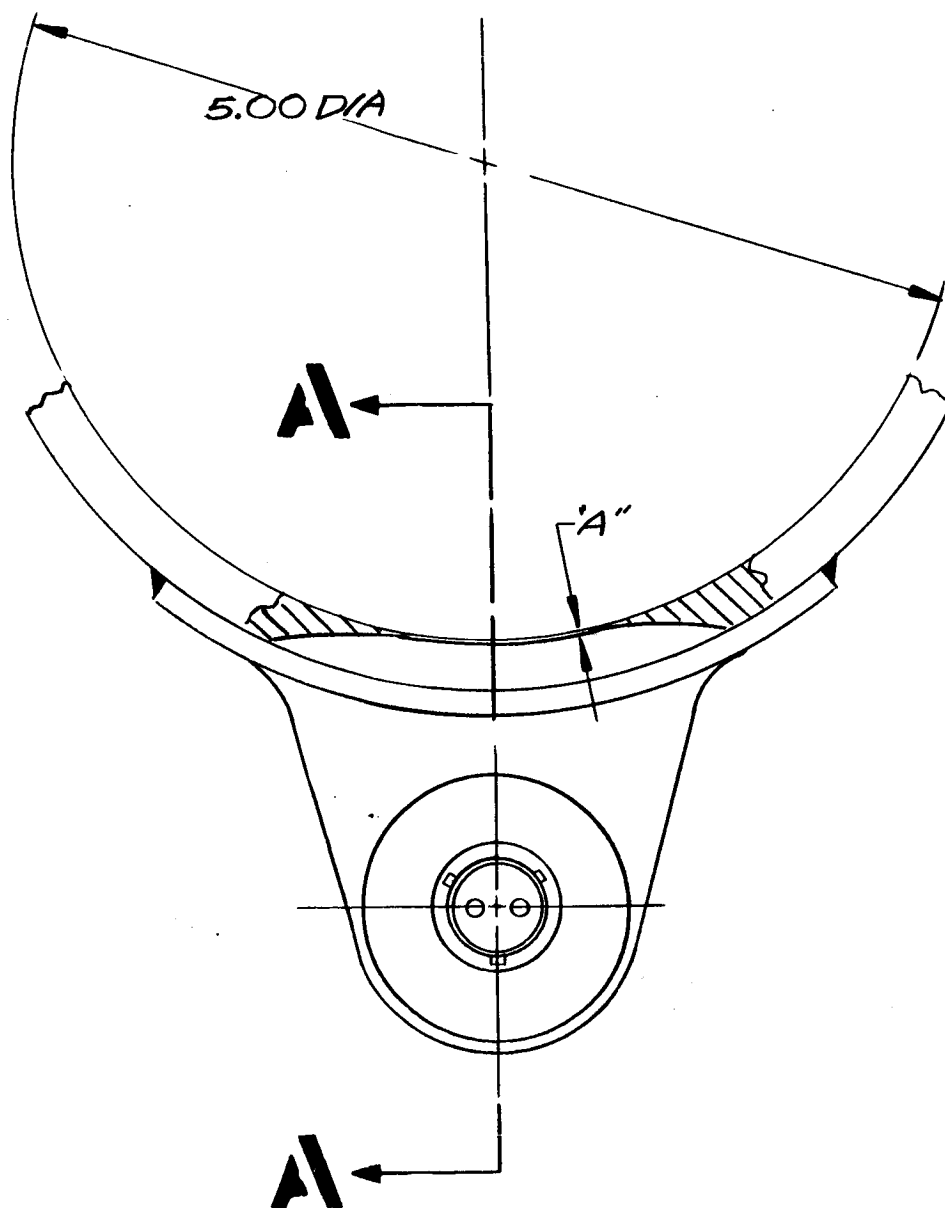


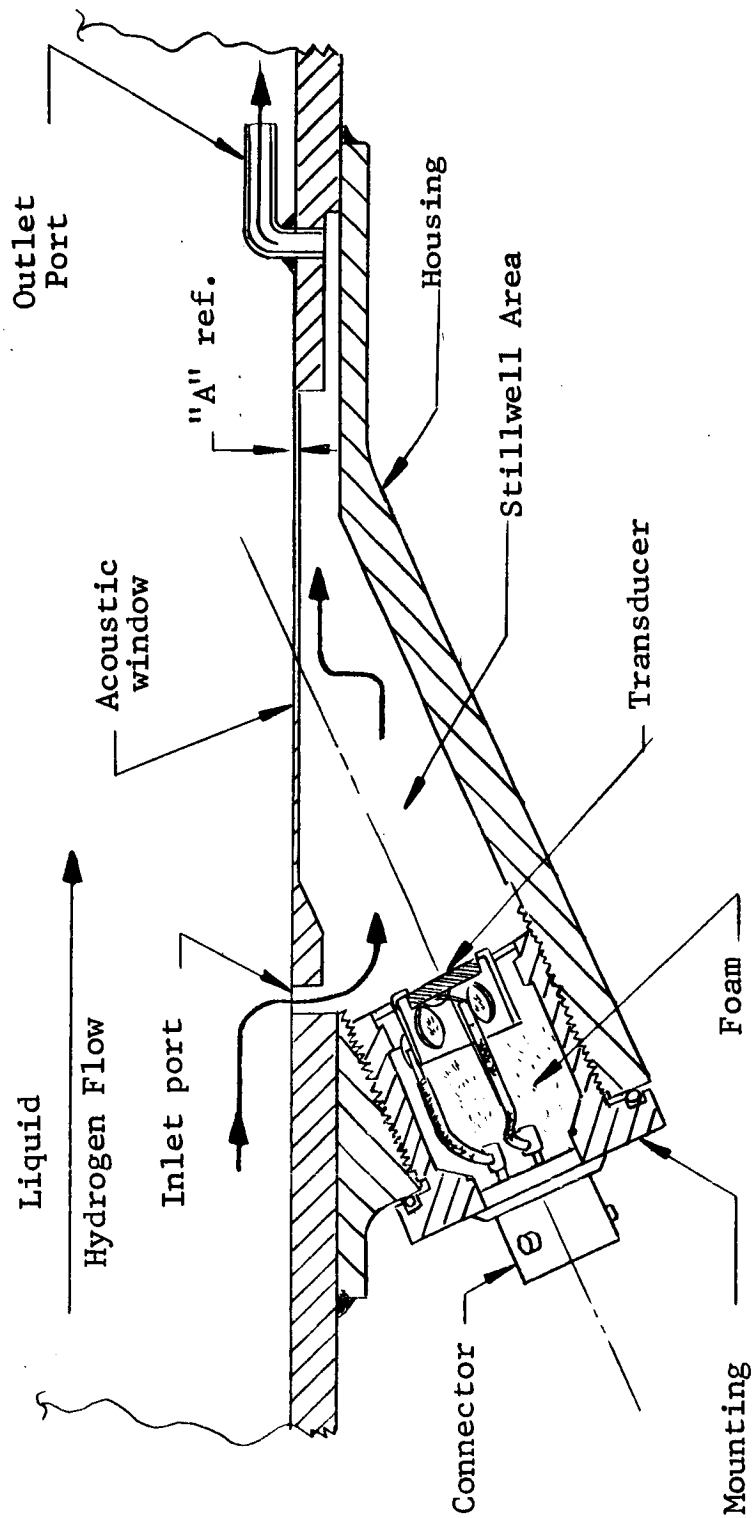
FIG. 1

Appendix E

Thus, it can be seen that even under the best of surface conditions in the pipe, laminar flow of the liquid hydrogen is only mildly possible at high velocities, i.e., 160 ft./sec., but is possible at velocities less than 80 ft./sec. only if extreme care is given to the pipe surface over-all and specifically to the section of the pipe where the transducer is mounted.

To obviate the possibility of any surface discontinuity in the vicinity of the transducer mounting area, the acoustic window, in Figure 2, is placed in the pipe wall (by machining it from the original pipe, for example) in such a manner as to remove any discontinuities in the surface finish. Thus the Reynolds number can be kept to the theoretical minimum.

If the acoustic window is placed as shown in Figure 2, there must be some coupling medium between the transducer face and the acoustic window. If an inlet port is placed before the stillwell area and a shaped outlet port is placed after the stillwell area, a small pressure differential will exist between the inlet port and the outlet port. This will cause a slight flow of liquid hydrogen in the stillwell area and the liquid in the stillwell area will act as the coupling medium between the active portion of the transducer and the acoustic window. The flow turbulence caused by the inlet and outlet ports will be very small as the sizes of these ports will be quite small, since the only criteria is a small pressure differential to keep the stillwell area filled with liquid hydrogen.



SECTION A-A

FIG. 2 APPENDIX-E

(3) The transducer elements must be mounted in a manner which will give complete acoustic isolation between the transducers and the pipe. This is accomplished by holding the transducer crystal with a unicellular foam on its side and rear faces, with only the front face exposed to the liquid hydrogen in the stillwell area. At the very low temperatures the gas entrapped in the foam will solidify but since each cell in the foam is completely closed, the solidified gas will occupy negligible volume when compared to the volume of the cell. Thus the complete acoustic isolation of the transducer is accomplished, even at the cryogenic temperatures.

(4) Due to the very low acoustic loss in liquid hydrogen, direct reflection from transducer to transducer will create a reflected signal comparable in amplitude to the incident signal but varying in phase by any amount from 0 to 360 degrees. For this reason, it is necessary to introduce additional attenuation in the path of the acoustical signal in order that the ratio of the reflected signal to the incident signal is at least 20 db.

This can be accomplished by adjusting the acoustic path through the acoustic window. It can be shown for a perfect conductor of sound, e.g., steel or copper, that an incident signal will be transmitted through a thin sheet with little loss if the sheet thickness is in the order of .1 wavelength. However, it is possible to choose the thickness of this sheet and hence choose the amount of attenuation required to minimize the effects of the reflected waves. As the sheet thickness approaches $1/4$ wavelength, the attenuation of the transmitted

wave is a maximum and when it is $1/2$ wavelength it is a minimum.

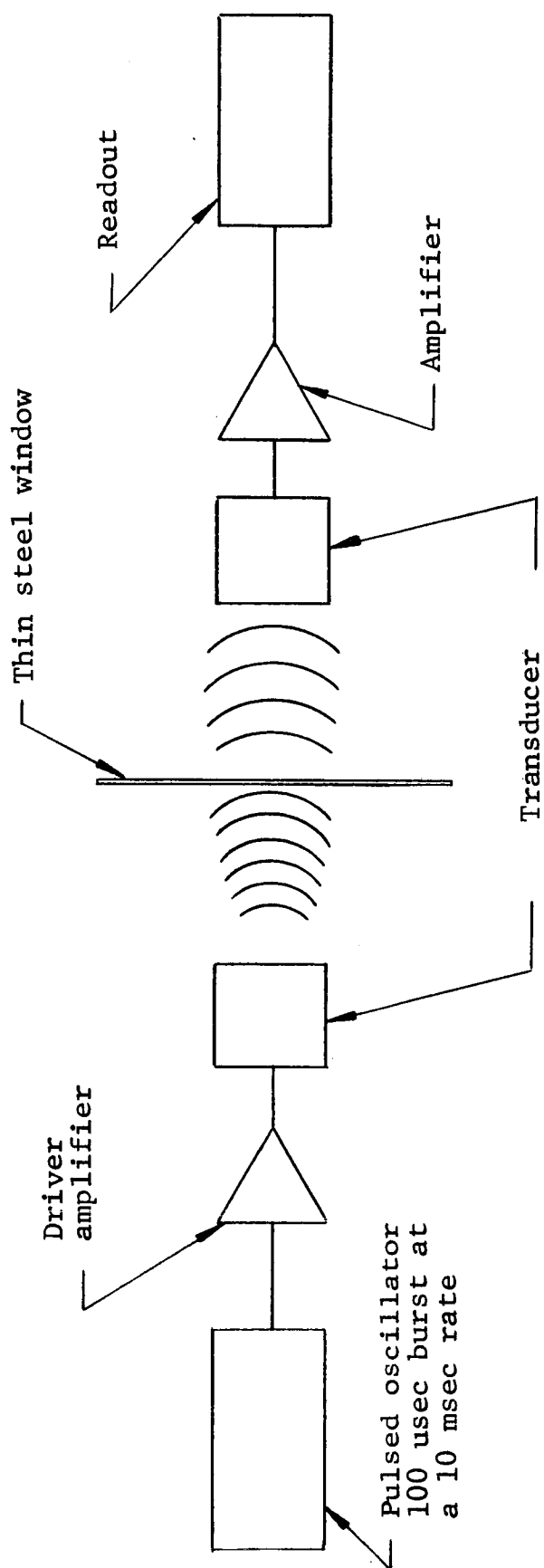
The stress requirement upon the acoustic window is very small. This is due to the fact that the difference between the pressure of the hydrogen inside the stillwell area and the hydrogen outside, it is just large enough to keep the hydrogen inside the stillwell area a liquid. Thus even for a reasonably large window the total forces involved are small.

Experimental evidence as to the validity of the above statements concerning acoustic transmission through a thin steel window were obtained as described below.

A thin sheet of steel (.005" thick) was inserted between the two transducers of Powertron's percent solids indicator. This device is shown in simplified block diagram form in Figure 3. It consists of a pulsed oscillator whose output is a 100 microsecond burst of 3.5 mc sine waves. This burst is then amplified and drives an electrostrictive transducer mounted upon one side of a 4-inch pipe. A similar transducer is placed on the opposite side of the pipe and its output is amplified and then peak detected. The output of the peak detector is then displayed on a DC meter. The coupling medium between the two transducers is water.

The test procedure was as follows:

The sheet of steel was inserted normal to the path of the ultrasound between the two transducers. A reference reading was taken and the sheet was rotated until it was parallel with the transmission path.



BLOCK DIAGRAM OF PERCENT SOLIDS
INDICATOR

The change in attenuation was noted as a function of angle. This angle was then converted to path length.

The results of the test indicated that if the path length, in the steel sheet, was equal to $1/2$ wavelength, the transmission loss was about 6 db.

Thus if the path length in the window is made equal to $\lambda/2$, the ratio of the reflected wave to the incident wave is 24 db. This does not assume any scattering of the signal due to beam width effects.